FOSSIL ENERGY

DOE/BC/15190-4
(OSTI ID: 800798)

3-D RESERVOIR AND STOCHASTIC FRACTURE NETWORK MODELING FOR ENHANCED OIL RECOVERY, CIRCLE RIDGE PHOSPHORIA/TENSLEEP RESERVOIR, WIND RIVER RESERVATION, ARAPAHO AND SHOSHONE TRIBES, WYOMING

Semi-Annual Report
November 1, 2001-April 30, 2002

By:
Paul R. La Pointe[1]
Robert Parney[1]
Thorsten Eiben[1]
Mike Dunleavy[2]
John Whitney[3]

Date Published: September 2002

Work Performed Under Contract No. DE-FG26-00BC15190

Golder Associates, Inc.
Redmond, Washington

National Energy Technology Laboratory
National Petroleum Technology Office
U.S. DEPARTMENT OF ENERGY
Tulsa, Oklahoma

DOE/BC/15190-4
Distribution Category UC-122

3-D Reservoir and Stochastic Fracture Network Modeling for Enhanced Oil Recovery, Circle Ridge Phosphoria/Tensleep Reservoir, Wind River Reservation, Arapaho and Shoshone Tribes, Wyoming

By
Paul R. La Pointe[1]
Robert Parney[1]
Thorsten Eiben[1]
Mike Dunleavy[2]
John Whitney[3]

September 2002

Work Performed Under DE-FG26-00BC15190

Prepared for
U.S. Department of Energy
Assistant Secretary for Fossil Energy

Virginia Weyland, Project Manager
U.S. Department of Energy
National Energy Technology Laboratory
National Petroleum Technology Office
One West Third Street, Suite 1400
Tulsa, OK 74103

Prepared by
[1]Golder Associates Inc.
18300 NE Union Hill Road, Suite 200
Redmond, WA 98052

[2]Marathon Oil Company
Rocky Mountain Region
1501 Stampede Ave.
Cody, WY 82414

[3]Marathon Oil Company
5555 San Felipe
Houston, TX 77056

Table of Contents

List of Graphical Materials

List of Tables

ABSTRACT

This report describes the progress and results made in fulfillment of contract DE-FG26-00BC15190, "3-D Reservoir and Stochastic Fracture Network Modeling for Enhanced Oil Recovery, Circle Ridge Phosphoria/Tensleep Reservoir, Wind River Reservation, Arapaho and Shoshone Tribes, Wyoming" during the fourth 6-month period of the 2-year project. The goal of this project is to improve the recovery of oil from the Circle Ridge Oilfield, located on the Wind River Reservation in Wyoming, through an innovative integration of matrix characterization, structural reconstruction, and the characterization of the fracturing in the reservoir through the use of discrete fracture network models. Progress and results have been obtained during this period for the remaining tasks.

The major achievements for this six-month period consist of the completion and verification of the fracture and fault models for the Field; the preliminary application of the model to re-assess well completions in the overthrust block; calculation of fracture-related reservoir engineering parameter values; and the integration of the matrix data with the fracture and fault models. All subsurface data acquisition and tracer testing was completed during this period, along with analysis of the data and incorporation of the data into the fracture and fault models.

The slight delay in the acquisition of the final subsurface data described in the previous Progress Report due to workover rig availability during the summer of 2001 and delays in permitting the final Na Br tracer experiment impacted the final completion of the project by April 30, 2002. Other than some minor remaining work on the integrated reservoir model, the final reporting and final tribal workshop, all tasks have been completed

1 INTRODUCTION

The first six-month period of this project focused on data collection and preliminary analysis. This included petrophysical analysis and field data collection to support the construction of the 3D palinspastic reconstruction. During the next six-month period, the project's primary focus was the development of a fully three-dimensional structural reconstruction of the Circle Ridge Field. The third six-month period focused on developing and verifying the Discrete Fracture Netowrk (DFN) model and beginning the construction of the integrated 3D fault-matrix-fracture reservoir model. The fourth six-month period described in this report consisted of completion of the model and analysis of the model for use in reservoir planning decisions to improve recovery. In particular, the project focused on:

1) the acquisition, processing and analysis of the bromide tracer test results in the subthrust Phosphoria;
2) the analysis of the image and flow logs fom Shoshone 66-14, a well completed in the Tensleep in the Overthrust block;
3) the integration of the matrix, fault block and reservoir-scale fracture data into a single numerical reservoir model.;
4) the analysis of this model to calculate the compartmentalization/connectivity structure of the fracture network, and to compute the effective reservoir engineering parameters for all structural blocks;
5) the utilization of this model for planning ways to increase recovery; and
6) the submission of journal articles, conference proceedings, workshops and web site updates to help disseminate project results to interested parties.

Throughout this report, reference is made to the "Overthrust Block" and "Subthrust Blocks". In general, this nomenclature is used to distinguish between rock in the hanging wall of the main Red Gully Fault (overthrust) and rock in the footwall (subthrust). The actual structural geology is much more complex, as shown by the reconstruction results, but this terminology has been retained for compatibility with some published references.

The field is further divided into several structural blocks (Figure 1-1), which are referred to in this report by their block number. Block 1 currently contributes most of the production. Most production in the subthrust blocks comes from Blocks 6, 8, 9 and 11.

For reference, the stratigraphic column for the Circle Ridge Field is given in Figure 1-2. Other geological details can be found in La Pointe and Hermanson (2001).

This report follows the outline mandated in Section 4.14 (Guidelines for Organization of Technical Reports (May 1999)) as specified in the contract. The discussion of the experimental work is organized by Task, as are the Results and Discussion section.

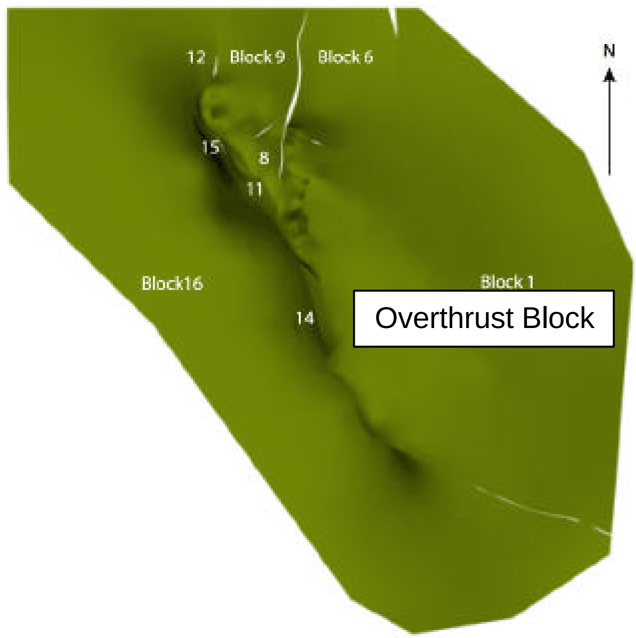

Figure 1-1. Horizontal map view of structural blocks defined for the Phosphoria Formation. Block definitions are very similar for the Tensleep Formation.

The primary reservoir units in the Circle Ridge Field are the Phosphoria, Tensleep and Amsden Formations (Figure 1-2). A large portion of the production comes from the Phosphoria and Tensleep Formations, and the impact of natural fractures is significant in these two younger units, so the project has focused on improving the 3D characterization of these two important reservoir units. Outcrops of Triassic Dinwoody Formation through Cretaceous Cloverly Formation are well exposed throughout much of the Field. Structural reconnaissance (La Pointe and others, 2000) suggests that the Gypsum Springs may act as a detachment horizon in the section, so that deformation patterns, including fracturing, above this unit may not be the same as deformation patterns below the Gypsum Springs.

Era	Period	Unit		Symbol
Mesozoic	Cretaceous	Undifferentiated	Mowry Shale	Ku
			Thermopolis Shale	
		Cloverly Formation		Kcv
	Jurassic	Morrison Formation		Jm
		Sundance Formation		Js
		Gypsum Springs Formation		Jgs
	Triassic	Nugget Sandstone		Jn
		Chugwater Formation	Popo Agie Member	TRpa
			Crow Mountain Member	TRcm
			Red Peak Shale	TRrp
		Dinwoody Formation		TRd
Paleozoic	Permian	Phosphoria Formation		Pp
	Pennsylvanian	Tensleep Sandstone		
	Pennsylvanian / Mississippian	Amsden Formation		
	Mississippian	Madison Limestone		
	Devonian	Darby Formation		
	Ordovician	Bighorn Dolomite		
	Cambrian	Gallatin Limestone		
		Gros Ventre Shale		
		Flathead Sandstone		
PRECAMBRIAN				

Figure 1-2. Stratigraphic column for the Circle Ridge Field (from Smith 2000).

2 EXPERIMENTAL WORK

2.1 Overview

Experimental work during the fourth six-month project period consisted primarily of:

1) the analysis of the image and flow logs from Shoshone 66-14, a well completed in the Tensleep in the Overthrust block;
2) the acquisition, processing and analysis of the bromide tracer test results in the subthrust Phosphoria;
3) the integration of the matrix, fault block and reservoir-scale fracture data into a single numerical reservoir model; and
4) the analysis of the this model to calculate the compartmentalization/connectivity structure of the fracture network, and to compute the effective reservoir engineering parameters for all structural blocks.

.

The sections that follow describe the experimental techniques employed in these tasks.

2.2 Experimental Techniques for Analysis of Subsurface Well Data

La Pointe and Hermanson (2001) have previously described many of the techniques used to acquire and analyze various types of subsurface well information. The subsurface data acquired and used in this project comprise both single well and multiwell tests. Many of these tests provide information that is used for several different purposes.

2.2.1 FRACTURE IMAGE LOGS

Three new fracture image logs were to be acquired as part of this project. Previously, a Fullbore Formation MicroImager™ (FMI - Schlumberger) log was obtained over an open-hole interval in Shoshone 66-07 and a Formation MicroScanner™ (FMS-Schlumberger) in was run in Shoshone 65-37. During the fourth six-month period, the third and final FMS log was obtained on Dec. 12, 2001 in Shoshone 66-14 over the interval 745 ft to 1090 ft (227.1 m to 332.2 m) MD. This interval is located in the Overthrust Block and begins in the Tensleep Marker portion of the Phosphoria Formation and extends into the basal portion of the Tensleep Formation. The logs were interpreted by Marathon and resulted in a summary of fracture and bedding plane information.

2.2.2 DYNAMIC FLOW LOGS

In order to further understand which features provide the flow paths for fluid flow, high-resolution injection profiles were obtained for Shoshone 66-14, the same well in which the final image log was obtained (Section 2.2.1). The flow logging was carried out using a Halliburton spinner tool, and included a temperature log. The depth interval logged extended from 600 ft to 1085 ft (182.88 m to 330.71 m) MD. The log was obtained on Dec. 11, 2001.

2.3 Bromide Tracer Test

Tracer tests can take many different forms. One test has already been carried out, termed the Overthrust Tensleep Nitrogen Test (La Pointe and Hermanson, 2001). During this project period, a second tracer test was initiated to examine the flow properties of the Phosphoria Formation and the possible connection between the Phosphoria and Tensleep Formations. The tracer used was an aqueous sodium-bromide (NaBr) tracer.

This Subthrust Block 6 tracer test was delayed due to permitting issues until November 2001. Permission to inject the tracer was requested from the United States EPA in mid-July 2001, but was not obtained until late October. The tracer test began November 15th

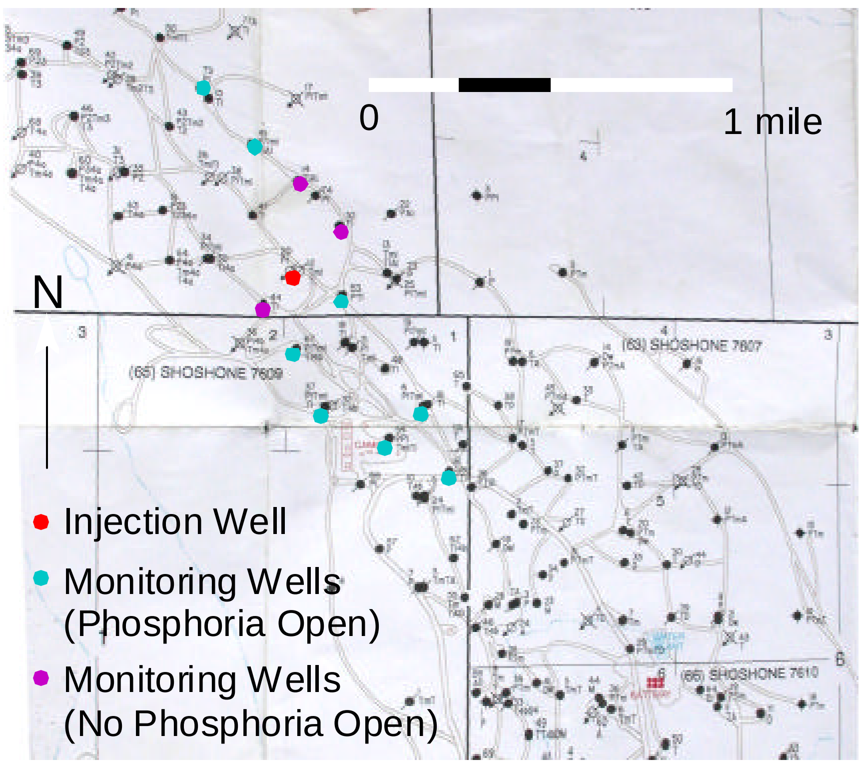

Figure 2-1. Location of injection well (Shoshone 65-20 – colored red) and monitoring wells (colored cyan and purple) used for bromide tracer test in the subthrust Phosphoria.

at the Phosphoria injector, Shoshone 65-20, and surrounding producers in Block 6. The test concluded in mid-December, 2001.

Background water samples from eleven producing wells, offsetting Shoshone 65-20, were collected during late October and early November. The furthest offsets were approximately 0.8 km in horizontal distance from the injector. Analysis, using a high-pressure liquid chromatograph, indicated background bromide concentrations of less than

1 ppm at all offsets. Eight of the wells, Shoshone 65-06, Shoshone 65-37, Shoshone 65-45, Shoshone 65-53, Shoshone 65-54, Shoshone 65-61, Shoshone 65-67, Shoshone 65-73, were completed in only the Phosphoria (Shoshone 66-73) or in both the Phosphoria and Tensleep. The additional wells (Shoshone 65-14, Shoshone 65-44 and Shoshone 65-52) were only open in the Subthrust Block 6 Tensleep Formation or Tensleep and Amsden Formations. Figure 2-1 shows the location on these wells. Note that the wells not containing a completion in the Phosphoria are the wells closest in horizontal distance to the injector.

On November 15, 2001, 41 barrels of 24% NaBr aqueous solution were injected into the Subthrust Block 6 Phosphoria Formation at Shoshone 65-20. This aqueous solution contained 3,339 pounds (1,517.7 kg) of bromine and was gravity fed into the well at a rate of 2,300 barrels per day (365.7 m^3/day). Following injection of the tracer slug, the well was returned to water injection at approximately 175 barrels (27.8 m^3) water injected per day (BWIPD). Monitoring wells were sampled on an approximately daily basis.

2.4 Experimental Techniques For Validation of DFN Model Geometry and Connectivity Using Subsurface Fracture Geometry and Flow Data

There are two levels or types of validation that can be used to assess the quality and usefulness of the palinspastic reconstruction. The first type of validation essentially evaluates the internal consistency of the restoration, and is based on whether various aspects of the model "balance". This type of self-consistency checking guides the sequence and geometrical parameters governing the unfolding and unfaulting of the model. La Pointe and Hermanson (2001) have previously documented the sequence of structural events that provide an internally consistent model.

During this project period, the DFN model was validated not for its internal consistency, but for its usefulness in predicting fracture geometry and flow behavior in the reservoir formations. This was carried out through two series of comparisons:

1) Comparison of predicted fracture orientations and intensity of subsurface image log data; and
2) Comparison of predicted fracture pattern connectivity with subsurface flow results.

Comparison of the predicted and measured fracture geometry relies upon the model developed between strain components and fracturing. This strain/fracture model is applied to the reservoir at the locations where subsurface image log data has been collected. These locations are Shoshone 66-07, a predominantly Overthrust Tensleep section, and Shoshone 65-37, a predominantly subthrust section including both the Tensleep and Phosphoria Formations.

The comparison of subsurface flow data with the connectivity properties of the fracture pattern inferred from the strain pattern is less quantitative. The data that provides the most independent check on the flow properties of the fracture network are the tracer tests. The reason for this is that:

1) Tracer tests involve a number of wells covering a larger area than any single well test, and so reflect the larger scale heterogeneity important for reservoir engineering optimization design involving secondary or tertiary recovery schemes;
2) Tracer tests not only identify areas with very high or low pressure communication, but also identify zones of higher or lower mass transport, which is of importance when designing surfactant injection processes or heat injection processes; and
3) Simulation of single well tests requires specification of fracture permeability and storativity, which can only be derived through calibration against the well tests, and so are not independent checks on the DFN model.

Thus, additional validation is provided by comparing the pattern and timing of tracer breakthrough and pressure interference with the connectivity of the fracture network.

2.5 Assessment of Compartmentalization/Tributary Drainage in Fracture Networks

Compartmentalization refers to the delineation of the spatial extent of portions of the fracture system that form well-connected networks (Figure 2-2). Within these network clusters, fluids can move more easily throughout the fracture system. These networks are isolated or partially isolated from other well-connected networks by regions of much more poorly connected fractures, so that fluid movement between fracture compartments either occurs through the matrix, or is retarded by much more poorly connected fracture systems. Tributary analysis is similar to compartmentalization analysis. It essentially focuses on the extent of fracture connectivity around existing or hypothetical wells.

Figure 2-2 shows the concepts of both fracture network compartmentalization and tributary drainage. The DFN model on the left of the figure shows all of the fractures generated. Circles colored white, red and purple indicate three wells.

While the fractures in the left portion of the model look entirely connected, they are not. The DFN model on the right side of the figure shows the fracture compartments. There are two large compartments, shown in green, and several much smaller compartments, shown in other colors and mainly obscured by the two large compartments.

The amount of tributary drainage is a function of the location and orientation of the well relative to the fracture compartments that develop. The white well appears to access the large northern compartment, while the red and purple wells appear to access the large southern compartment. In fact, neither the white well nor the purple well intersect any of the fractures. Only the red well actually intersects fractures in the large southern compartment.

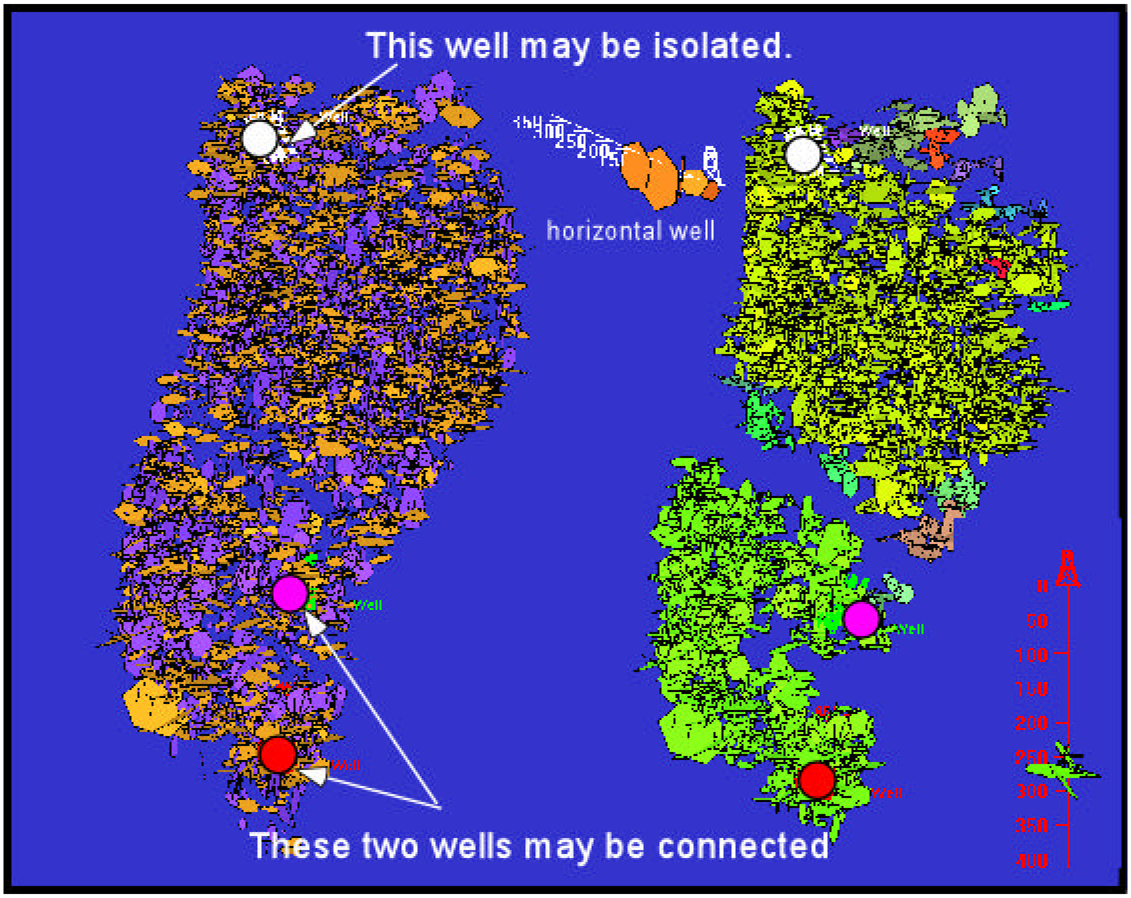

Figure 2-2. DFN model for subthrust block 6, showing fracture compartments formed due to variation in intensity related to folding. The diagram on the left shows all fractures and three vertical well locations. The diagram on the right shows the fracture compartments.

With stimulation, the white and purple vertical wells would probably connect better to the fracture compartments. Or, as shown with the white well, a horizontal completion, rather than a vertical, would intersect a number of fractures and be well-connected to the northern compartment. The tributary drainage volume is the volume of reservoir (matrix) that is potentially accessed by the well through the connected fracture system. Particularly where the fracture permeability is much greater than the matrix permeability, the amount of matrix that can be produced, or subjected to water floods or steam floods is related to the volume of matrix accessed by the compartment that the well connects to. Thus, the red well potentially could access the matrix tributary to the large southern fracture compartment.

The experimental method for determining compartmentalization and tributary drainage is thus a calculation based upon the fracture network connectivity and its spatial extent.

One way to calculate compartmentalization and tributary drainage for a field is to first build a field-wide DFN model, calibrate it to all available data, history match it, and then carry out a connectivity analysis on the DFN model. This alternative requires a full-field history matching simulation, which is not part of the Circle Ridge project's scope, and would also be undesirable, as the only portions of the reservoir that *could* be history matched are the overthrust block and one or two subthrust imbricate blocks. Since there is little or no production in the remaining blocks, these significant potential reservoir additions could not be studied.

Another way to analyze the compartmentalization and tributary drainage is to examine the connectivity geometry as inferred from the palinspastic strain maps, and qualitatively calibrate these strain patterns to the connectivity seen in the nitrogen injection test and the bromide tracer test.

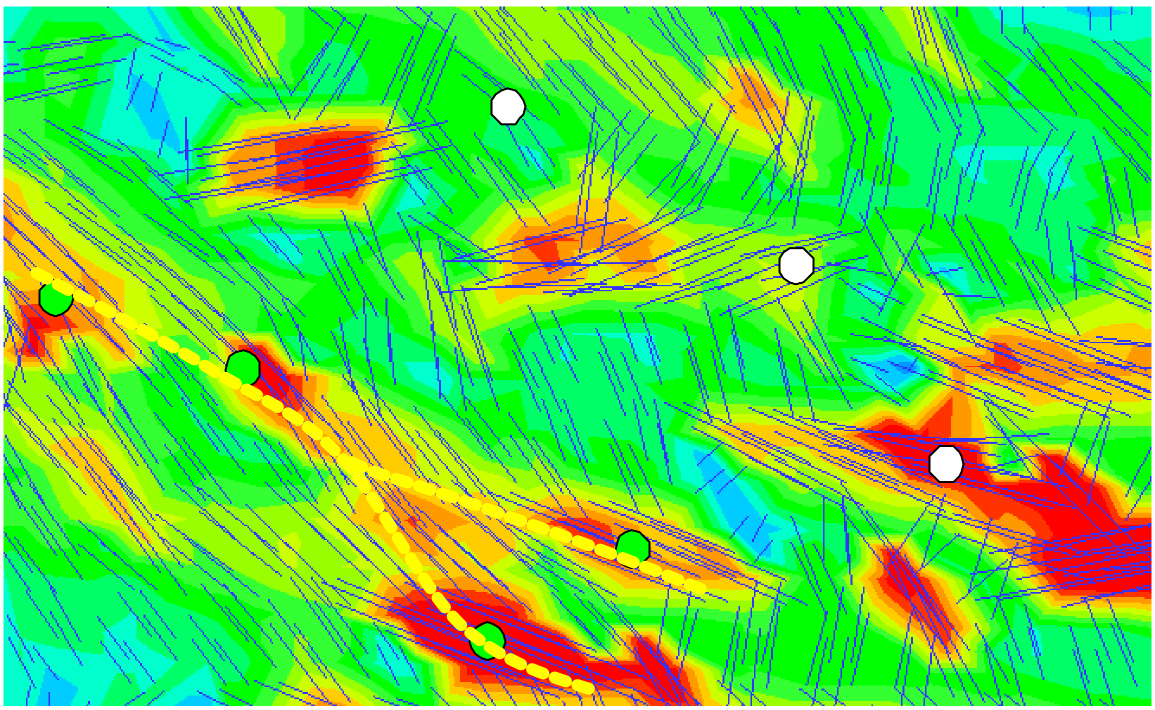

Figure 2-3. Hypothetical example of how strain maps and subsurface tracer data can be related to understand compartmentalization and tributary drainage. Green circle represent wells that appear to have strong pressure or flow connection in a tracer test, while white-shaded circle represent wells that appear disconnected. The contour colors denote the magnitude of strain, while the blue arrows indicate the trend of the dominant extensional fracture set predicted from the strain tensor.

Figure 2-3 shows a hypothetical example of how subsurface tracer breakthrough data can be combined with strain data to delineate the fracture connectivity structure and qualitatively assess the size and shape of fracture network compartments and tributary drainage patterns.

In this hypothetical example, the superimposition of the strain pattern, the dominant extensional fracture strike and the breakthrough pattern in wells can be used to calibrate the strain map and allow it to be interpreted as a connectivity map. High strain regions (shaded red and yellow in Figure 2-3) should represent regions where fracture development is also high. The orientation of the strain field can be used to infer the direction of the dominant extension fracture strike (shown by the blue lines in Figure 2-3). Regions of high strain connected to each other or by fracture corridors should exhibit strong pressure or tracer breakthrough responses. The yellow dotted lines in the figure indicate possible fracture corridors, which are formed by spatially contiguous regions in where the dominant fracture strike is parallel or subparallel. If there are fracture corridors developed in relation to the strain, then wells, such as those shown as green circles in Figure 2-3 should show good communication. Also, wells not connected by fracture corridors, such as those shown as white circles, should show much poorer response. Thus, if there is a geological understanding of why the zones of high strain have occurred, and it can be shown that the strain corridors and orientations and variations in fracture intensity do correspond to fracture orientations as seen in the subsurface from image logs or core, and the pattern of tracer breakthroughs is reasonably well-explained by the strain corridor pattern, then the spatial structure of the strain corridors can be used to quantify the connectivity of the reservoir.

2.6 Calculation of Effective Reservoir Properties

A major goal of this project is to calculate fracture porosity, fracture permeability and the parameters that relate the exchange of fluids between the matrix and the fracture system for the entire Field from the fracture model constructed and validated from the outcrop, well log and well test simulation work. The experimental procedure for carrying out this calculation goes through three stages: derivation of the parameter values needed to create a 3D DFN model of the reservoir; generation of the DFN model; and calculation of parameter values from the DFN model.

2.6.1 CALCULATION OF PARAMETERS FOR THE DFN MODEL

The methodology for calculating the input to the DFN model has largely been covered in previous project semi-annual reports. It is useful to summarize the parameters that are needed, and how they were obtained, as a basis for better understanding of the actual procedure used to generate the DFN models. A DFN model is first baed on identifying individual fracture sets, and then calculating a series of parameter values for each set. Parameters typically are not single numerical values, but are represented as statistical distributions and are related to underlying geological factors.

2.6.1.1 Identification of fracture sets

A fracture set may be interpreted differently depending upon the use. In typical geological usage, a fracture set is a group of fractures with more or less the same orientation. There may also be some additional constraints such as the fractures also formed from the same geological processes and at the same time. Petrophysicists tend to separate fractures based on orientation similarity and also by aperture class: open, partially open, solution enhanced, or filled, because this additional characteristic has implications for fluid flow, which is of primary concern.

For DFN modeling, a slightly different definition is used: a fracture set is a group of fractures that can be characterized and generated stochastically from the same statistical distributions and geological constraints or conditioning functions. While orientation similarity, aperture or filling, and mode of formation all may play a role in defining these sets, they may also be ignored. For example, fractures belonging to the same orientational set that might be classified on an image log as open, partially open or closed, may be combined into a single set with an aperture distribution that reflects all of these class states. Likewise, if there were two fracture populations with similar statistical and geological constraints, except that one portion of the population formed early, and the other during a later event, then there would be no practical reason to treat them as two individual sets from the standpoint of generating the DFN model.

Moreover, the concept of orientation similarity needs care as well, particularly where folding has led to fracture formation, as it has in Circle Ridge. Two fractures may have the same absolute orientation, for example, vertical and striking northeast. Just because these two fractures have an identical orientation does not mean that they are necessarily

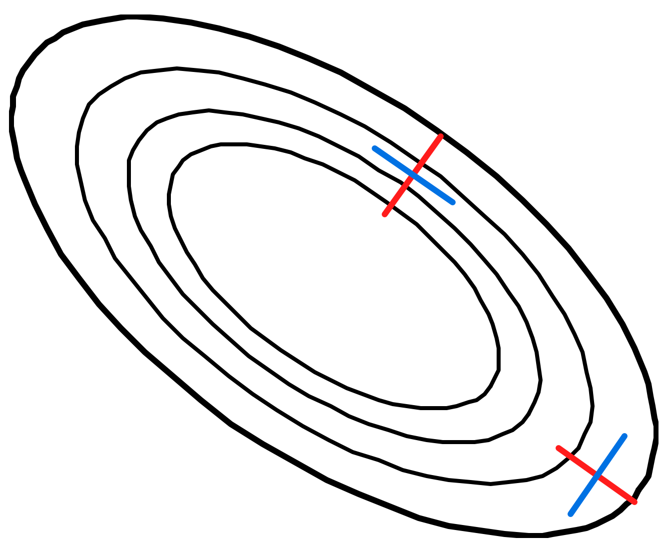

Figure 2-4. Example of fractures of identical orientations belonging to different sets.

part of the same set. If the fold is somewhat more complex, for example, having a double plunge like Circle Ridge, then a northeast striking fracture in one portion of the fold may be dip-parallel, while a northesty striking fracture in another protion may be strike parallel.

Figure 2-4 shows such an example. The red fracture set is always dip parallel (the blacxk lines in the figure denote bedding in this plan-view figure), while the blue fractures are always strike parallel. Typically, the dip parallel fractures have very similar geometrical and fluid flow characteristics, while the strike parallel fractures have internally similar characteristic as well, but characteristics trhat differ from the dip parallel fractures. Blindly combining all northeast fractures into a single set, and all northwest fractures into single set, would obscure these difference and decrease the DFN model's usefulness.

The process for defining sets was based on an iterative analysis of outcrop fracture data, downhole image log data, comparison of outcrop and image log data with extensional strain data calculated from palinspastic reconstruction of the field, inferences drawn from well test modeling, and consideration of nearby outcrop analogs.

The process was to start with the outcrop data at eleven outcrop sites, and define the local orientational groupings at each site. Each set was evaluated in terms of its relation to bedding strike and dip. It was found that there werer typically two sets present, both nearly orthogonal to bedding and to each other. Very often the two sets subparallel bedding strike and dip.

While the process could have been carried out in different order, the next information for delineating sets came from the strain maps calculated from the palinspastic reconstruction of the reservoir formations. The strain components for various stages in the reconstruction (different folding and faulting events) were compared with the outcrop fracture orientations and intensity, and it appeared that the direction of maximum extensional strain produced during the intial folding of the field was a good predictor of the fracture orientations in outcrop.

Image log data from three wells, two in the overthrust Tensleep, one in the subthrust Phosphoria, showed that the fracture sets in the image log had the same relation to the extensional strain as the outcrop fracture pattern. Further comparison of outcrop data in outcrops adjacent to the wellheads for the two overthrust image log wells showed similarity between the outcrop pattern and the subsurface pattern in the reservoir.

Transient well test matching further indicated that a model consisting of two fracture sets, orthogonal to bedding and oriented relative to the strain field, could reproduce the transient well test behavior.

Inspection of Tensleep and Phosphoria outcrops in the Wind River Canyon and in the Bighorn Basin also indicated that there were commonly two sets developed that were orthogonal to bedding and to each other.

Thus, the DFN model defined two fracture sets that were orthogonal to bedding and to each other, and were oriented relative to the direction of maximum extensional strain calculated from the palinspastic reconstruction of the field.

2.6.1.2 Fracture Orientation Variability for Each Set

The orientation variability for each set was based upon data collected from outcrop and from the three image logs. The image log data was further analyzed to determine if variability or orientation changed according to lithology or depth.

Because the fracture sets did not maintain a single global orientation, but varied according to the strain field changes, only the variation of fracture orientation about the mean was used. The local mean orientation was based on the orientation of the calculated extensional strain.

2.6.1.3 Fracture Intensity

Fracture intensity is a term that is often used to describe a number of different measures of how many fractures there are in a particular portion of the reservoir (Dershowitz and Herda, 1992). Most often it refers to the number of fractures per meter of core or image log.

However, fractures are essentially two-dimensional objects in three-dimensional space, and so a three-dimensional measure is needed for constructing a DFN model. A mathematically convenient measure of three-dimensional fracture intensity for DFN models is the total fracture surface area per volume of reservoir, often denoted as P_{32} (Dershowitz and Herda, 1992).

There are several possible approaches to calculating P_{32}. One approach is to estimate the value from the number of fractures per meter, incorporating knowledge of the fracture orientations and the orientation of the wellbore. This approach is a type of non-linear optimization, in which a DFN model is constructed having the correct orientation model and a guess for P_{32}. A well is inserted into the DFN model and used to sample the number of fractures intersected per meter in this synthetic well. This calculation is then compared to the actual number of fractures per meter. The guess for P_{32} is then adjusted up or down accordingly until a close match is achieved.

This guess can also be adjusted for the difference between conductive and non-conductive fractures. With flow meter data or similar logs that distinguish conductive from non-conductive fractures, a ratio of these can be calculated. This same ratio is then applied to the calculated P_{32} value to finally arrive at a conductive P_{32}. for the model.

Another strategy for calculating conductive P_{32} is to derive it from matching transient well tests using DFN models. The intensity for each set is one parameter that can be adjusted to obtain a match. The advantage of this approach is that the intensity calculated is the *conductive* P_{32} itself; it is not necessary to rely upon a ratio inferred from flow meter results.

At Circle Ridge, P_{32} was estimated primarily from transient well test matching. A correlation was established between this value and the value of extensional strain. The value of the local P_{32} intensity was thus based upon the local extensional folding strain magnitude and the correlation function.

2.6.1.4 Fracture Size

Fracture may be estimated from fracture trace length statistics, by matching the "pad intersection" percentages, from image logs, or from well test matching DFN simulations where size is treated as a "free" parameter in the matching (La Pointe and others, 1993).

The matching of trace lengths to estimate fracture sizes relies upon DFN simulation. In this approach, fractures are realized as circular discs with a radius distribution drawn from some assumed statistical distribution, such as lognormal with mean equal to 50 m and standard deviation equal to 27 m. An outcrop, represented by a plane, is inserted into the model and the resulting trace length distribution on the plane is converted to a trace length frequency distribution. This distribution is then compared to the measured trace length frequency distribution. The parameters of the DFN mode are adjusted in order to achieve a statistically significant match either through manual adjustment or through nonlinear optimization.

The procedure to estimate size from image log data follows a similar approach. FMI and other facture imaging tools use from 4 to 8 pads to image the fractures. Many, if not most, of the fractures are imaged on all pads. Some fractures appear on fewer than all of the pads. One reason for a fracture to appear on fewer than all of the pads is related to fracture size. If a fracture were a kilometer in radius and intersected a wellbore, the probability that it would cut entirely through the wellbore is very high. If the fracture is very small, on the order of centimeters, then the probability that it would cut entirely through the wellbore and appear on all pads is much, much lower. Using this principle, a DFN model for each set is made with the already calculated fracture orientation model and intensity, but with a guess as to the size distribution of the fracture set. This model is sampled with a synthetic wellbore, and how many pads each intersecting fracture would have appeared on is recorded automatically. The percentages of fractures appearing on all of the pads, some of the pads or only a few of the pads are then compared to the actual pad intersection percentages. The fracture size parameters are then adjusted by hand or through a nonlinear optimization procedure to achieve a statistically significant match. This is done for each set and each well separately.

As in the case of fracture intensity, estimation of fracture sizes from image logs or traces in outcrop produces an estimate of the size distribution of both non-conductive and conductive fractures together. Estimation from well test simulation, on the other hand, produces an estimate that probably better characterizes the size distribution of the conductive fractures that play an important role in the reservoir-scale flow processes.

Essentially, fracture size is treated as a free parameter to be adjusted when matching transient well tests. The only constraints on the results of this approach are that the resulting conductive fracture sizes should be at least as large as the non-conductive; and the statistical distribution calculated should not produce fractures that strech geological credibility or available outcrop analogs. The important portion of the transient well test curve to match is the longer time portion, as this best captures how larger volumes of the reservoir away from the immediate wellbore are responding.

At Circle Ridge, image log data did not produce enough fractures to compute robust pad intersection statistics. The outcrop data was not used because (1) it was in the Crow Mountain and Red Peak Members of the Chugwater Formation, not the Tensleep or Phosphoria Formations, and could thus be different; and (2) the trace length data in the outcrops was heavily censored, making the trace length matching calculation highly non-unique. Thus, the size distribution was derived from well test matching and checked against outcrops of the Tensleep and Phosphoria Formations in the Wind River Basin.

2.6.1.5 Fluid Flow Properties for Individual Fractures

A DFN model is composed of individual fractures, and each of these individual fractures must have a value of transmissivity and storage (or alternatively permeability and compressibility) assigned to it. These parameters cannot be measured directly in situ. They are derived by treating them as free parameters in well test matching or other types of subsurface flow and transport modeling, such as tracer test simulations. For Circle Ridge, these parameters were estimated through matching aspects of the Nitrogen Injection tracer test results.

2.6.2 GENERATION OF THE DFN MODELS

The method used to generate the DFN models for the Circle Ridge Field relied upon the Golder's commercial FRED fractured reservoir characterization and simulation software. The steps in the process are as follows:

1) Specify the input parameters for each fracture set described in 2.6.1 (Figure 2-5).
2) Generate or "realize" each set (Figure 2-6). This is done for each structural block and reservoir formation separately.
3) Clip the fractures against formation boundaries (Figure 2-7)
4) Save each set (Figure 2-8)
5) Combine data sets for different structural blocks and formations into a single model (Figure 2-9).

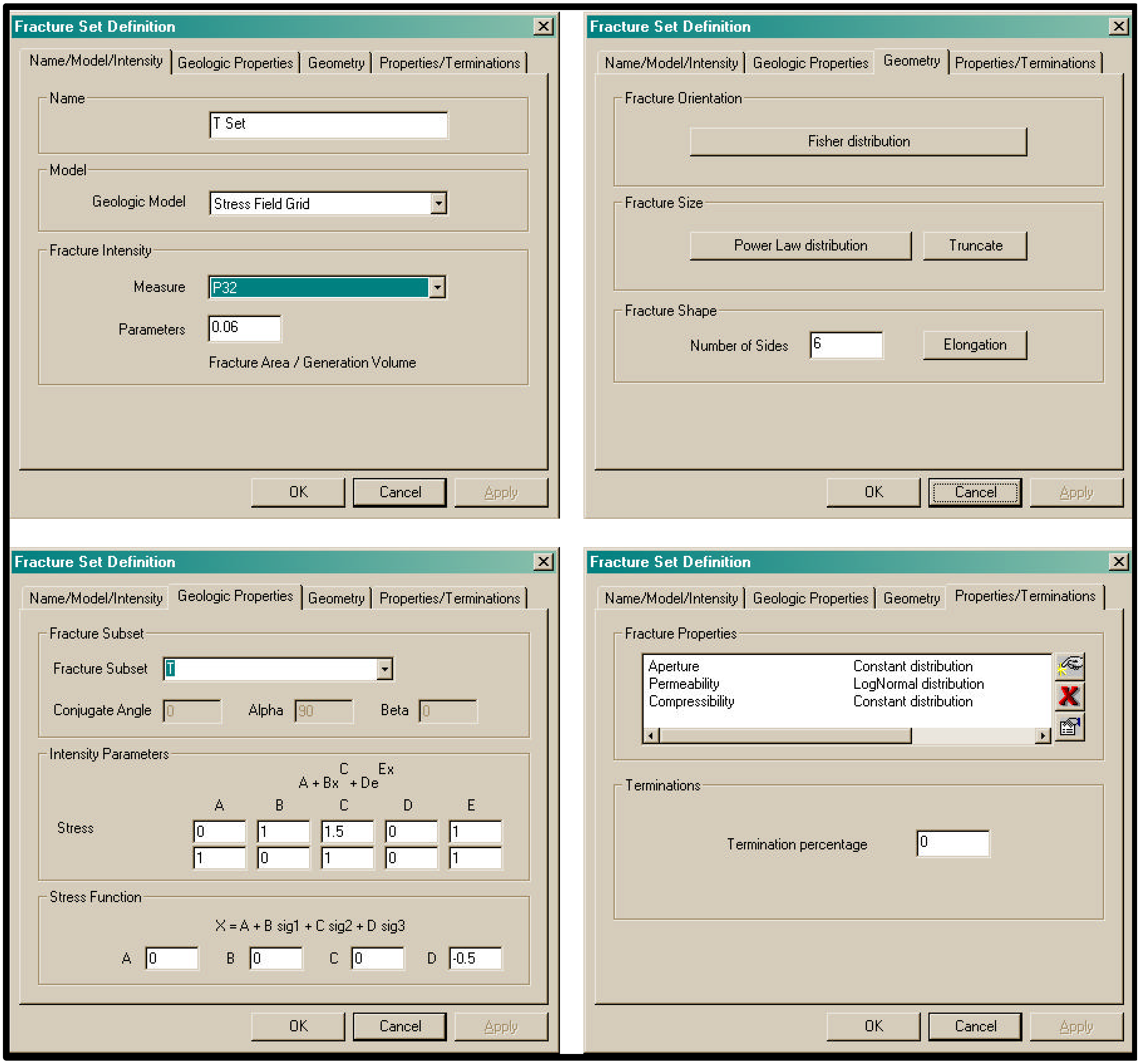

Figure 2-5. Example of data being entered into FRED for generation of a fracture set.

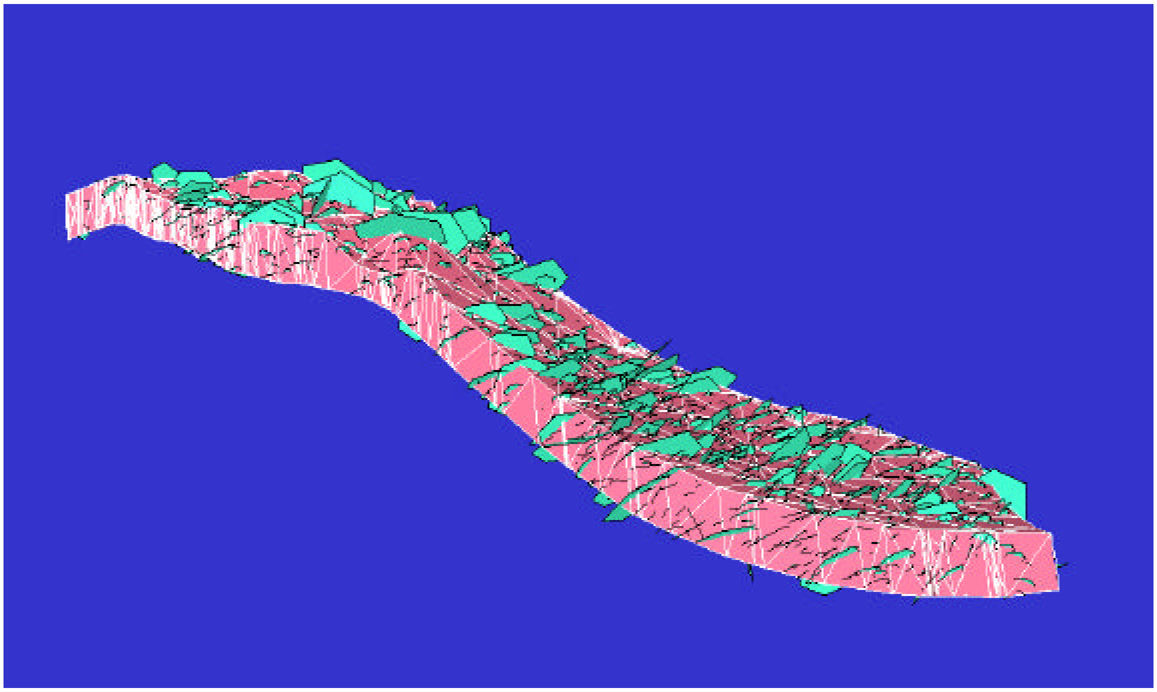

Figure 2-6. Generation of one fracture set in a DFN model. The block shown is Block 6, Tensleep Formation, viewed from east to west. The grid shown is the tetrahedral grid containing extensional strain values and orientations produced in the palinspastic reconstruction of the field.

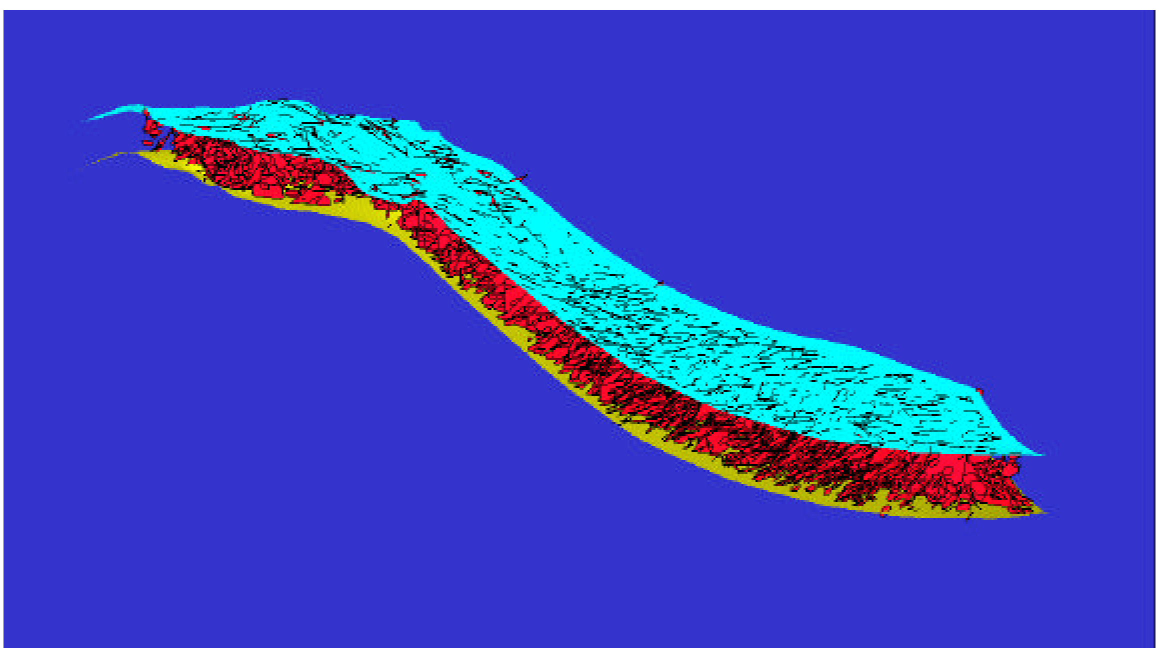

Figure 2-7. Example of fracture set clipped against upper and lower boundaries of Tensleep Formation, Block 6.

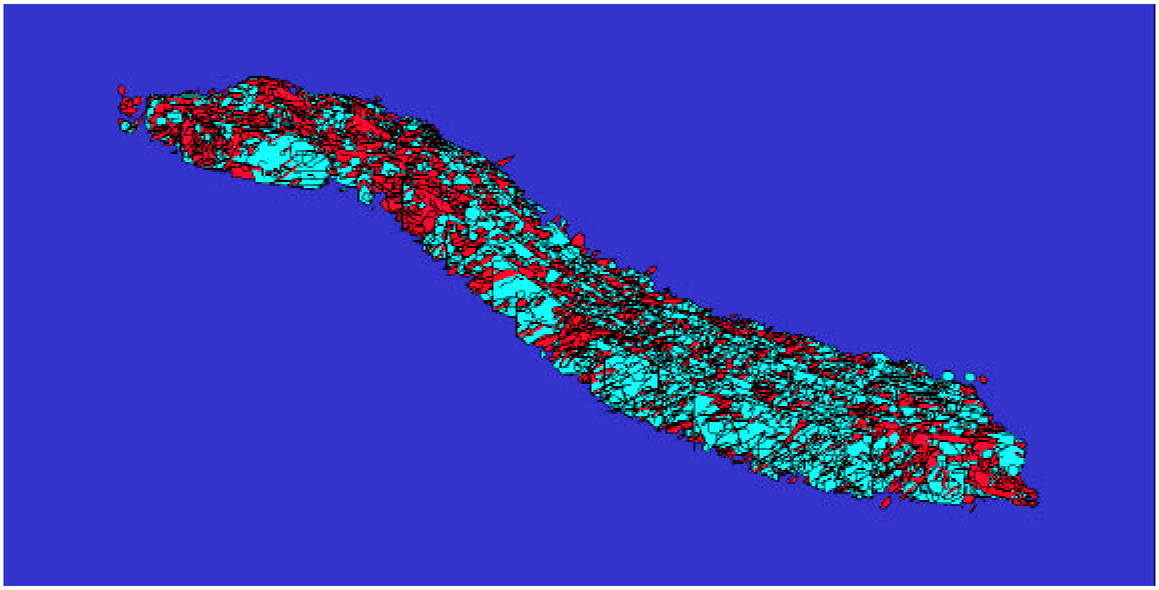

Figure 2-8. Final DFN model for Tensleep Formation, Block 6, including both major fracture sets clipped against the upper and lower boundaries of the Tensleep Formation.

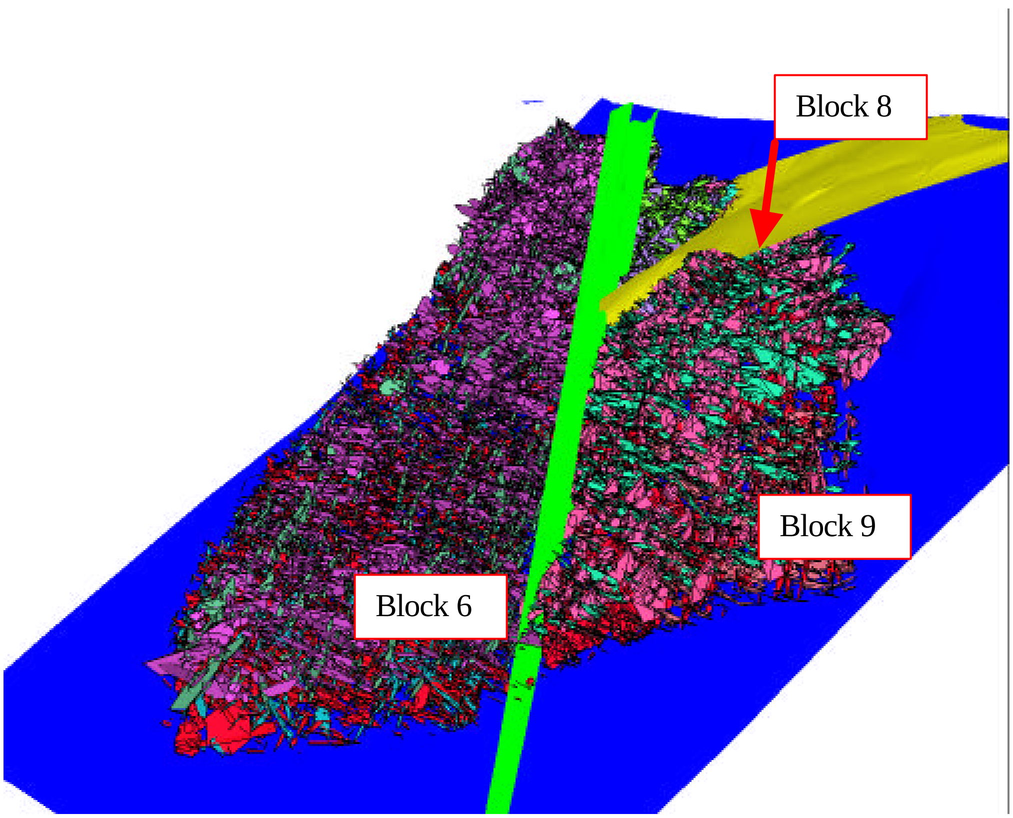

Figure 2-9. DFN model of structural blocks 6, 8 and 9 for both Tensleep and Phosphoria Formations. Also shown are the Green Valley, Yellow Flats and Blue Wash Faults.

2.6.3 CALCULATION OF EFFECTIVE RESERVOIR PROPERTIES

Once the DFN model has been generated for the entire reservoir, the next step is to calculate effective fracture properties from the DFN model. The properties of interest are fracture porosity, fracture intensity, directional fracture permeability, and sigma factor, a parameter that is used in many reservoir simulators to approximate how fluids move between the matrix and the fracture systems under a pressure gradient. By there very nature, these properties encompass a volume of reservoir, and therefore must be calculated over reservoir volumes.

If a reservoir simulation grid has been defined for the reservoir, then this is the most desirable assemblage of subvolumes (the simulator grid cells) over which to calculate the effective properties. In practice any grid can be used. Because a field-wide reservoir simulation grid has not been prepared for the Circle Ridge Field, grids were generated individually for each formation and structural block. The number of grid cells in each block and formation was specified so that the mean horizontal dimensions of each grid cell were on the order of 50 m, and the mean thickness of each grid cell was on the order of 25 m. These values were chosen as they are on the order of size of typical reservoir simulation grid cells, and they are large enough that each cell contains a number of fractures. Where the reservoir layer thins appreciably over the structural block, the vertical thickness of the cell may be less than the target 25 m since the number of grid layers is always preserved. Figure 2-10 shows an example of such a grid. The grid in this figure was generated for the Tensleep Formation in Block 6.

The calculation of the effective fracture properties in an individual grid cell (Dershowitz and others, 2000) is based on the actual fractures found in each cell. An example of calculation results for an entire grid is shown in Figure 2-11. The cells are colored coded according to the value of vertical permeability calculated for each grid cell. The FRED software carries out these calculations for all of the grids for every structural block and reservoir formation, and outputs the values as ASCII files containing the centroid location of each grid cell, its dimensions and orientation, and the effective properties. The effective properties consist of:

- fracture count;
- P_{32} fracture intensity;
- Fracture porosity;
- the full permeability tensor such that the Pxx, Pyy and Pzz components are aligned with
- the global (X, Y and Z) coordinate system;
- the full permeability tensor such that the Pxx, Pyy and Pzz components are aligned with
- the local (I, J, K) coordinate system; and
- sigma factor

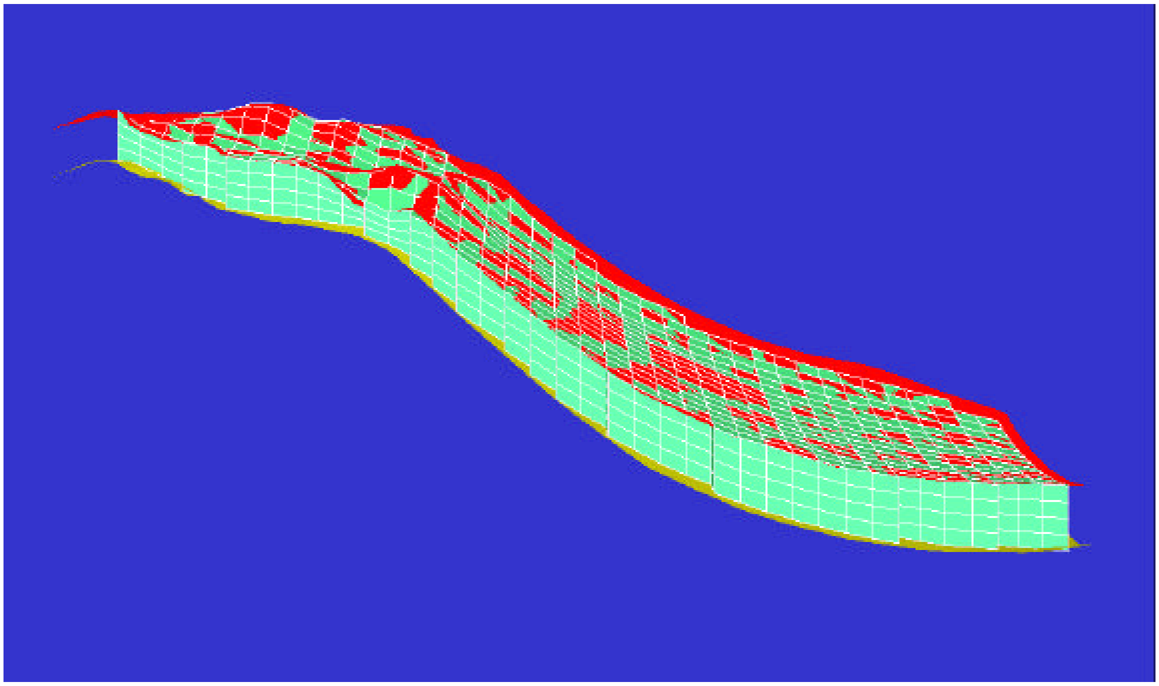

Figure 2-10. Example of a grid (cyan) generated between the upper (red) and lower (green) Tensleep boundaries for Block 6.

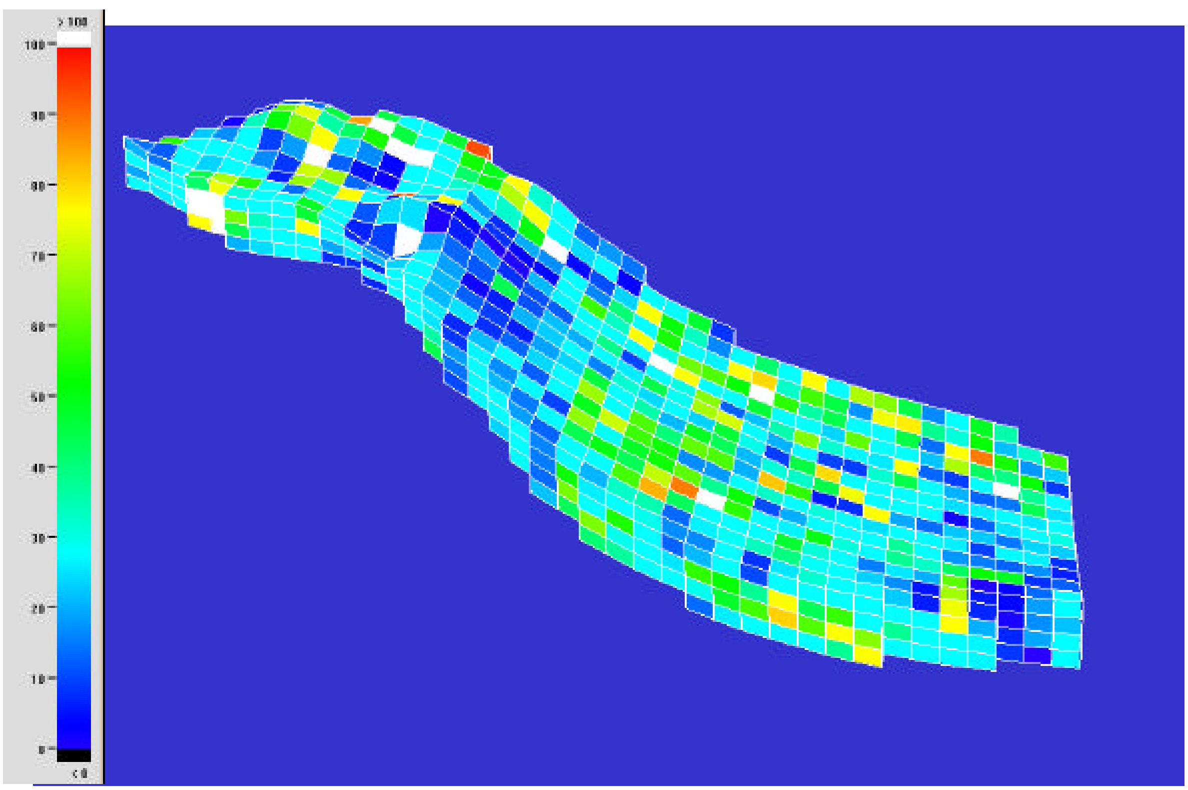

Figure 2-11. Values of vertical permeability calculated for grid shown in Figure 2-10. Values are in mD.

2.7 Integration of the Matrix and Fault Block Architecture Into a Single Numerical Reservoir Model

An important aspect of this project is the creation of an integrated matrix/fault block/fracture numerical model. This model will allow the visualization of the fractures in 3-D and their relation with other parameters, and will provide the numerical parameter values to reservoir simulations or other calculations to design and evaluate options to enhance production.

The Circle Ridge Field is encompassed within a complex structural sitting. The basic structure that defines the field is an anticline. The complexity enters due to the faulting of the anticline structure. This complexity is not just due to the number of the faults observed and modeled, but also the type of faulting in the Field. Many faults intersect other faults, cross other faults, or die out. The Circle Ridge Field has not only nearly vertical faulting which is fairly simple to model, but also shallowly dipping faults and in particular, shallowly dipping reverse faults. This last type of fault is difficult to incorporate in many 3D modeling software systems.

Of the modeling software packages that can handle the complex types of faulting that occur at Circle Ridge, further classification of the software can be made in their ability to upscale the geo-cellular model to reservoir simulation models. This process of upscaling has been addressed in some of the software so that directly readable grid files are written that can be read by the reservoir simulation software. This becomes important in order to allow the operator of the field a method of evaluating the best economic methods of extracting the most reserves from the field. The ability of geo-cellular models to easily output simulation modeling grids is an important point to consider in picking the geologic modeling software. With these considerations, the software system that proved most useful was GoCad®(http://www.ensg.u-nancy.fr/GOCAD/).

The data used to create the model derives from the four main project tasks. The matrix data is derived from interpretations made from well logs. Task 1 of this project supplemented the existing interpretations made from modern well logging suites with data derived by calibrating logs from 113 older wells. This provided for a data set on matrix properties for the Tensleep and Phosphoria Formations for the Overthrust Block and most of the imbricate blocks lying in the footwall of the Red Gully Fault. The well data was interpolated between well control using the geostatistical algorithms available in GoCad.

The second component of the integrated reservoir model are the major faults: the Red Gully Fault, Green Valley, Yellow Flats, Blue Draw, Grey Wash, Orange Canyon and Purple Sage faults. Prior to this project, the geometry of the faults at depth was poorly constrained. Through the 3D palinspastic reconstruction based on the additional well control also provided by the well log recalibration, and the three new cross sections, it was possible to greatly improve the constraints on fault surface geometry of these seven major faults. The faults themselves were exported from the palinspastic reconstruction software, and converted into triangular meshes that could then be reformatted into native

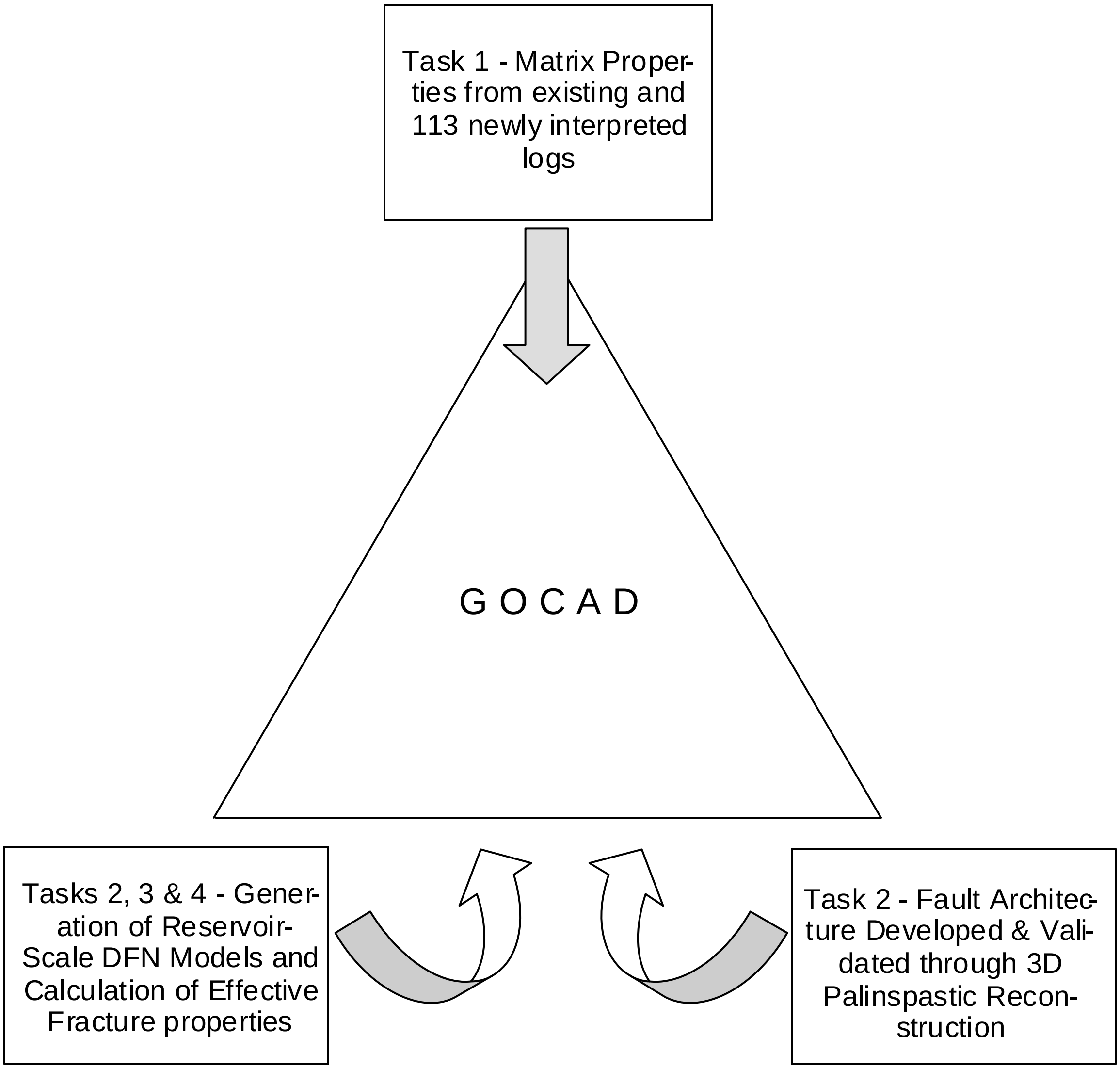

Figure 2-12. Data flow from project tasks into the integrated reservoir model.

GoCad surface files.

The reservoir-scale fractures themselves are not explicitly represented as individual object sin the final integrated reservoir model. Rather, the effective fracture parameter values derived from them are incorporated into model.

Field work on outcrops, fracture image logs from three wells, well tests and tracer tests were all used to generate a validated discrete fracture network model for the Tensleep and Phosphoria Formations for all structural blocks making up the Circle Ridge Field. As described in Section 2.6, the formations were gridded and the effective fracture properties calculated for each grid cell. The values for each parameter were then imported into the integrated reservoir model.

3 RESULTS AND DISCUSSION

3.1 Overview

This section discusses the results of the active subtasks that were the focus of work during the 4^{th} six-month project period. These tasks comprise the development of a procedure to populate the reservoir model with fractures based upon the strain calculated in the 3D palinspastic reconstruction; the validation of this model; the derivation of flow parameters for the fracture model from the analyses of the subsurface tests; the development of the integrated 3D fault block and matrix model; the preliminary use of the model to develop plans for reservoir enhancement; and technology transfer.

3.2 Task 4.1 – Compartmentalization/Tributary Analysis

3.2.1 PURPOSE OF TASK

The purpose of this Task is to develop a predictive understanding of the connectivity structure of the Tensleep and Phosphoria reservoirs, so that it can be used to help site new wells, orient horizontal completions and be used for assessing the potential suitability and subsequent design of secondary or tertiary recovery processes.

3.2.2 ANALYSIS OF SHOSHONE 66-14

3.2.2.1 Orientations & Intensity

During the six-month period of the project covered by this report, image log and flowmeter data were obtained and analyzed for the third and final well for this project. The well logged was Shoshone 66-14, located in the Overthrust Block (Structural Block 1) in the southeastern end of the Circle Ridge Field (Figure 3-1). The interval logged extended from measured depths of 745 ft (227.08 m) to 1090 ft (332.23 m). This interval begins in the Tensleep Marker portion of the Phosphoria and extends to the base of the Tensleep Formation. The spinner log was run over a measured depth of 580 ft (176.78 m) to 1080 ft (329.18 m).

Figure 3-2 and Figure 3-3 show how fracture and bedding orientations and intensity vary over the logged interval.

Bedding orientation (shown by the purple and dark blue symbols in difference above 840 ft (256.03 m) MD,Figure 3-2) is quite consistent throughout, although there does seem to be a minor difference from the bedding orientation below. Bedding orientations in terms of both dip and dip azimuth are less variable above 840 ft 256.03 m) MD than below,

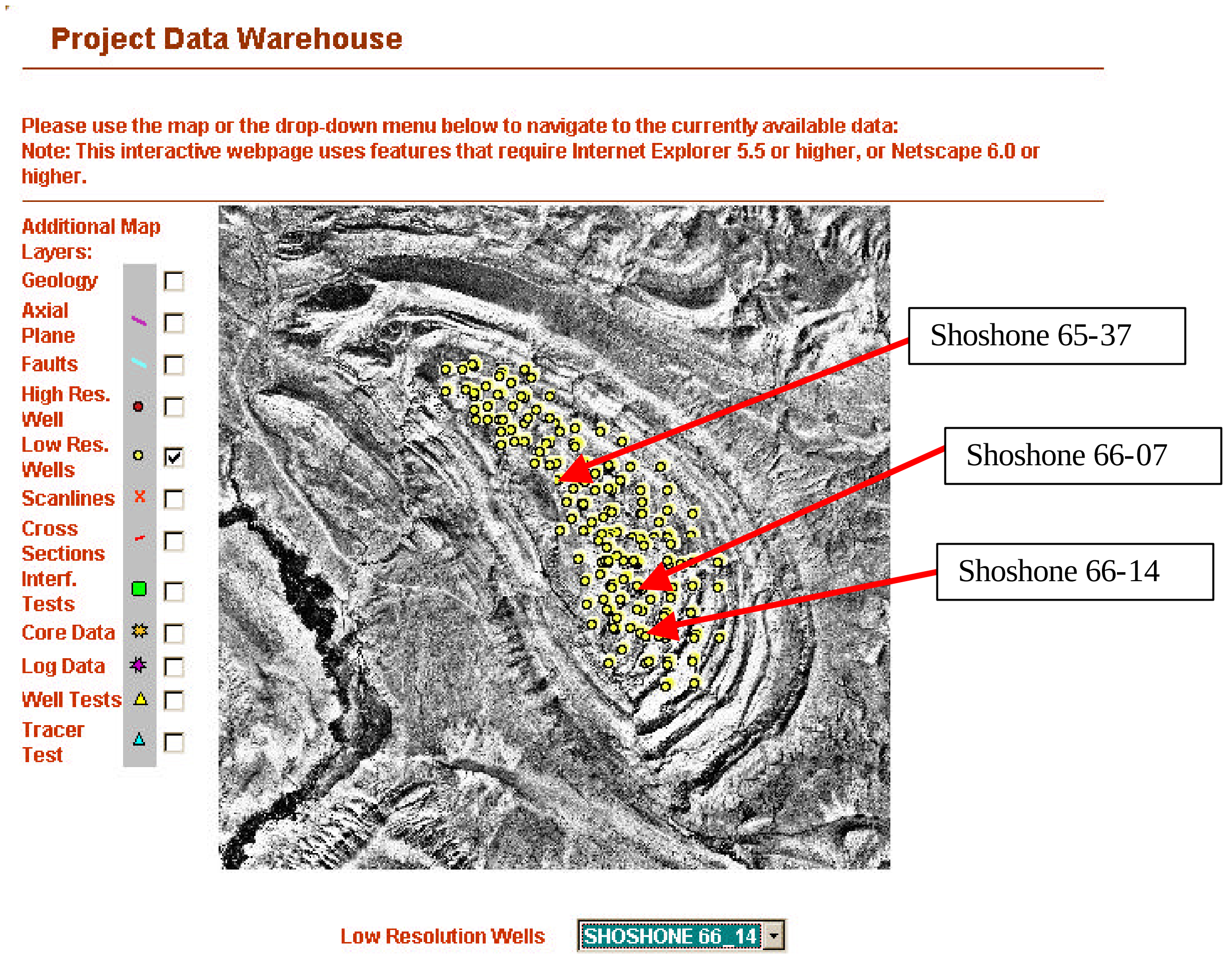

Figure 3-1. Location of wells in which image logs and flowmeter logs were obtained. Shoshone 66-14 was logged and interpreted during the most recent 6-month project period. The display of the well locations is taken from the project web page, http://www.fracturedreservoirs.com.

and have a slightly different orientation. Bedding dip azimuths are around 140° to 160° and the bedding dips from 10° to 20° above 840 ft (256.03 m) MD and about ten degrees more below that depth. Bedding dip azimuth also rotates 10° to 20° in a clockwise manner going from the upper zone to the lower zone. Fracture dip azimuths fall largely into one of three orientations: 25° to 30°; 160°; and 340° to 350°. There appear to be no differences between 4-pad fractures and 3-pad fractures in terms of orientations. The 340° orientation is 180° opposite the bedding dip azimuth, and the dip angles are about 90° different. This means that the fractures whose dip azimuth is around the 340° are orthogonal to bedding and parallel or nearly parallel to bedding strike. This is an orientation that would be expected if fractures formed during the folding of the rock. The group of fractures whose azimuths are near 150° also strike parallel to bedding, but dip about 30° more steeply than bedding and in the same direction as bedding dip. The fractures whose dip azimuths are in the 25° to 35° range dip steeply and are about 20° from being subparallel to bedding dip, although they are nearly orthogonal to bedding.

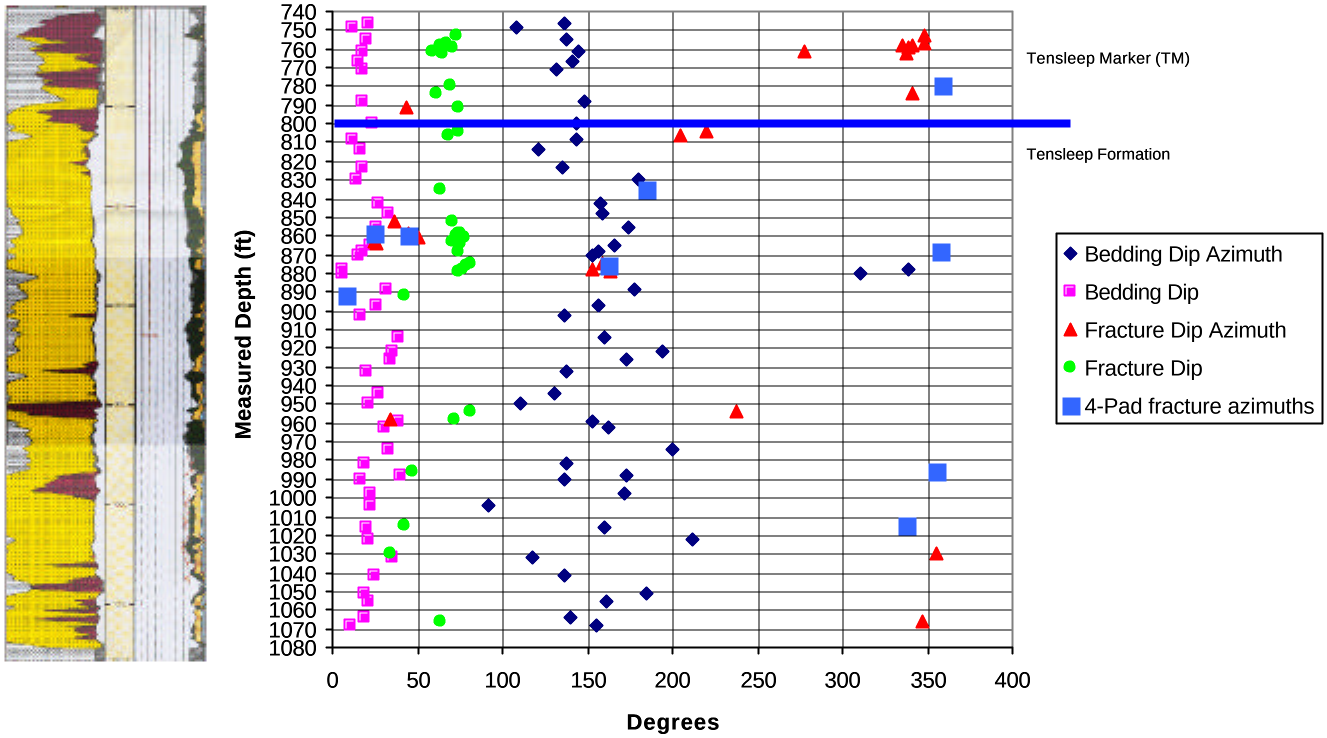

Figure 3-2. Orientation of fractures and bedding in Shoshone 66-14 interpreted from image logs. The top of the Tensleep Formation is shown by the solid blue line.

The largest visual change in the pattern of orientations does not appear to correspond to the boundary between the Tensleep Marker and the top of the Tensleep; rather, the most noticeable change, although a small one, occurs at about 840 ft (256.03 m). This is located somewhere in the T2A unit of the Tensleep, and is not a major stratigraphic boundary.

Figure 3-3, which is the plot of the cumulative fracture count, shows a similar break at this point. The slope of the line on this figure is inversely related to fracture intensity: the shallower the slope, the higher the intensity. There appear to be two zones of higher fracture intensity, and two zones of lower intensity. There may be some minor increases in fracture intensity at the top of the Tensleep and at the top of the T3 unit (952 ft or 290.17 m) MD. Within each of the four zones, the fracture intensity (slope) is relatively constant. The major zone boundaries, however, don't necessarily correspond with the stratigraphic unit boundaries, nor do they seem to be consistently associated with particular lithologies. For example, the top of the T3 is associated with a more highly fractured dolomitic unit, as is the top of the T2A unit and the more dolomitic rich portion of the TM above 765 ft (233.17 m). However, the zone of highest fracture intensity from about 855 ft to 880 ft (260.60 m to 268.22 m) is devoid of dolomite. The presence of dolomite below the top of T3 appears to have no relation to increased fracture intensity.

What does cause the variations in fracture intensity with depth? Another possibility is bed thickness. In many layered rocks, fracture spacing is proportional to bed thickness: the thinner the beds, the shorter the fracture spacing of fractures orthogonal to the beds.

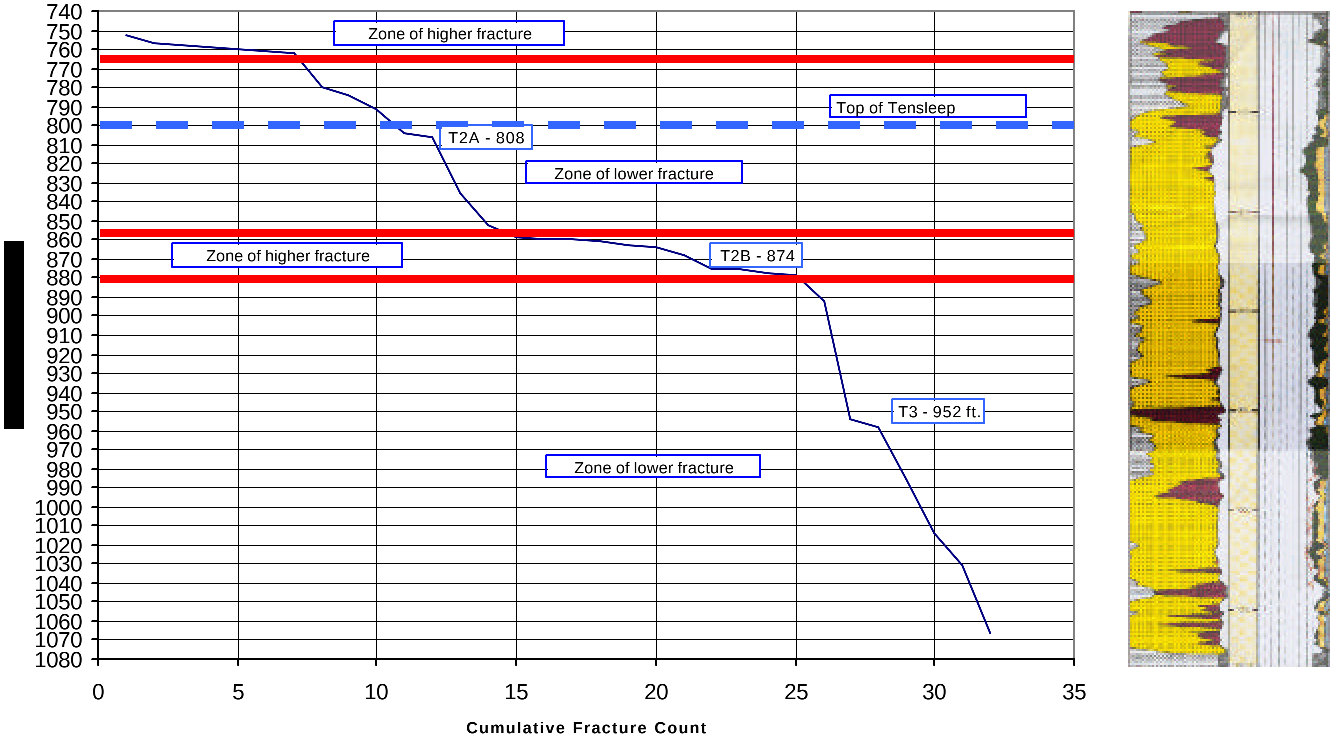

Figure 3-3. Cumulative fracture count for Shoshone 66-14 for fractures interpreted from image log. Red solid lines indicate alternating zones of higher and lower fracture intensity. Dashed blue line indicates the approximate top of the Tensleep Formation.

Figure 3-4 compares bedding intensity with fracture intensity. In this plot, the number of beds or fractures was counted over 15 ft (4.572 m) windows. This figure shows that there does appear to be a visual correspondence between bedding plane intensity and fracture intensity. A Wilcoxon signed-rank test was significant at $\alpha = 0.06$, which suggests that bedding thickness does influence fracture intensity. The variations in bedding plane intensity do not show any obvious visual correspondence with variations in the three principal lithologies: sandstone, shale and dolomite (Figure 3-4). It is important to note that the higher intensity does not necessarily indicate that the fractures are larger or that the overall fracture surface area per volume of rock is greater. Thus, the relation between fracture intensity and formation productivity is not resolved until the intensity is compared to productivity.

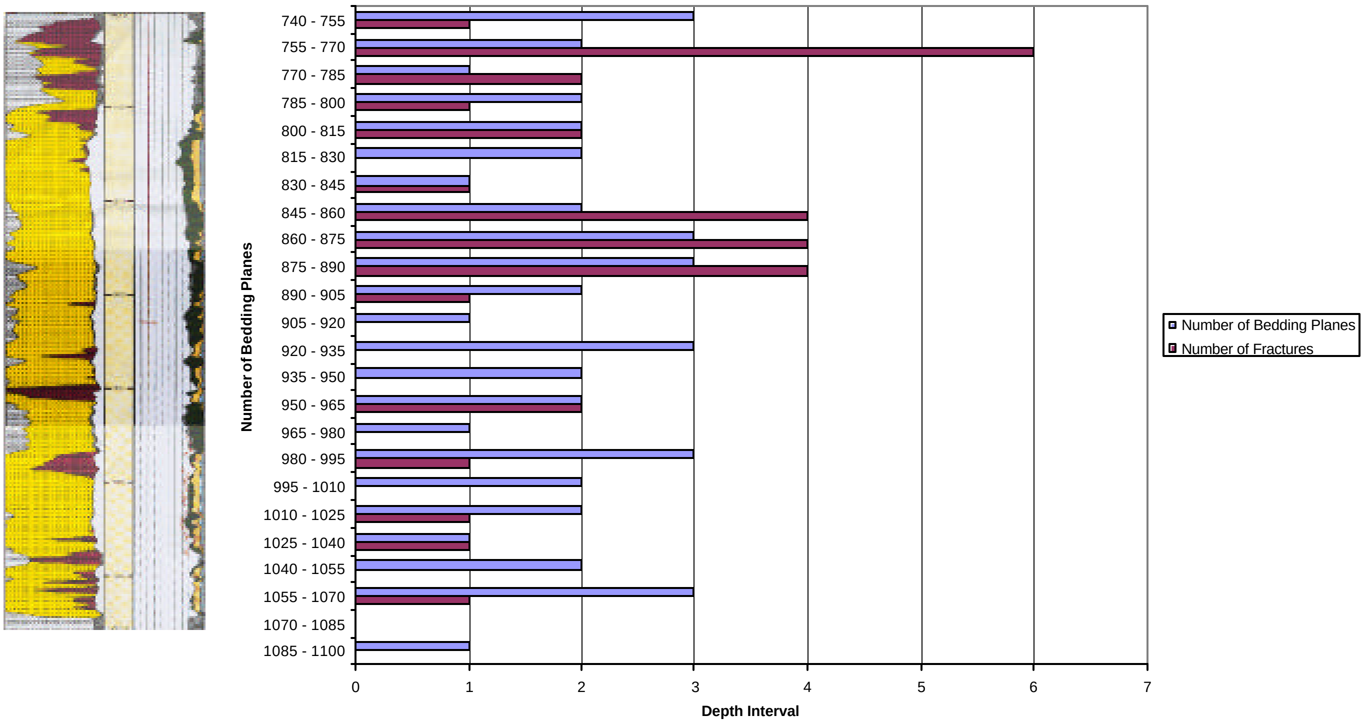

Figure 3-4. Correspondence of bedding intensity and fracture intensity. Intensity is calculated over 15 ft (4.572 m) non-overlapping windows.

3.2.2.2 Productivity

A spinner log survey was carried out in Shoshone 66-14 on Dec. 12, 2001. The results of the cumulative production are shown in Figure 3-5. As in many, if not most, fractured reservoirs, the majority of major flow anomalies coincide with the location of open fractures, but most of the open fractures do not coincide with major flow anomalies.

It is interesting to plot the cumulative intensity of open fractures and the cumulative production over the same interval (Figure 3-5). The cumulative production and the cumulative fracture intensity have been normalized to a range of 0% to 100% in order to commensurate them.

The comparison of these two cumulative plots shows that the increases in production generally follow increases in open fracture intensity. The flow anomaly at 810 ft (246.89 m) corresponds to the small zone of high fracture intensity at the top of the T2A unit. The anomaly at 802 ft (244.45 m) is close to the top of the T1 unit. The anomalies at 748 ft and 752 ft (227.99 m and 229.21 m) are in the higher fracture intensity zone at the top of the Tensleep Marker zone. The flow anomaly at 788 ft (240.18 m) corresponds to neither a stratigraphic boundary nor to a fracture intensity zone boundary, nor were there

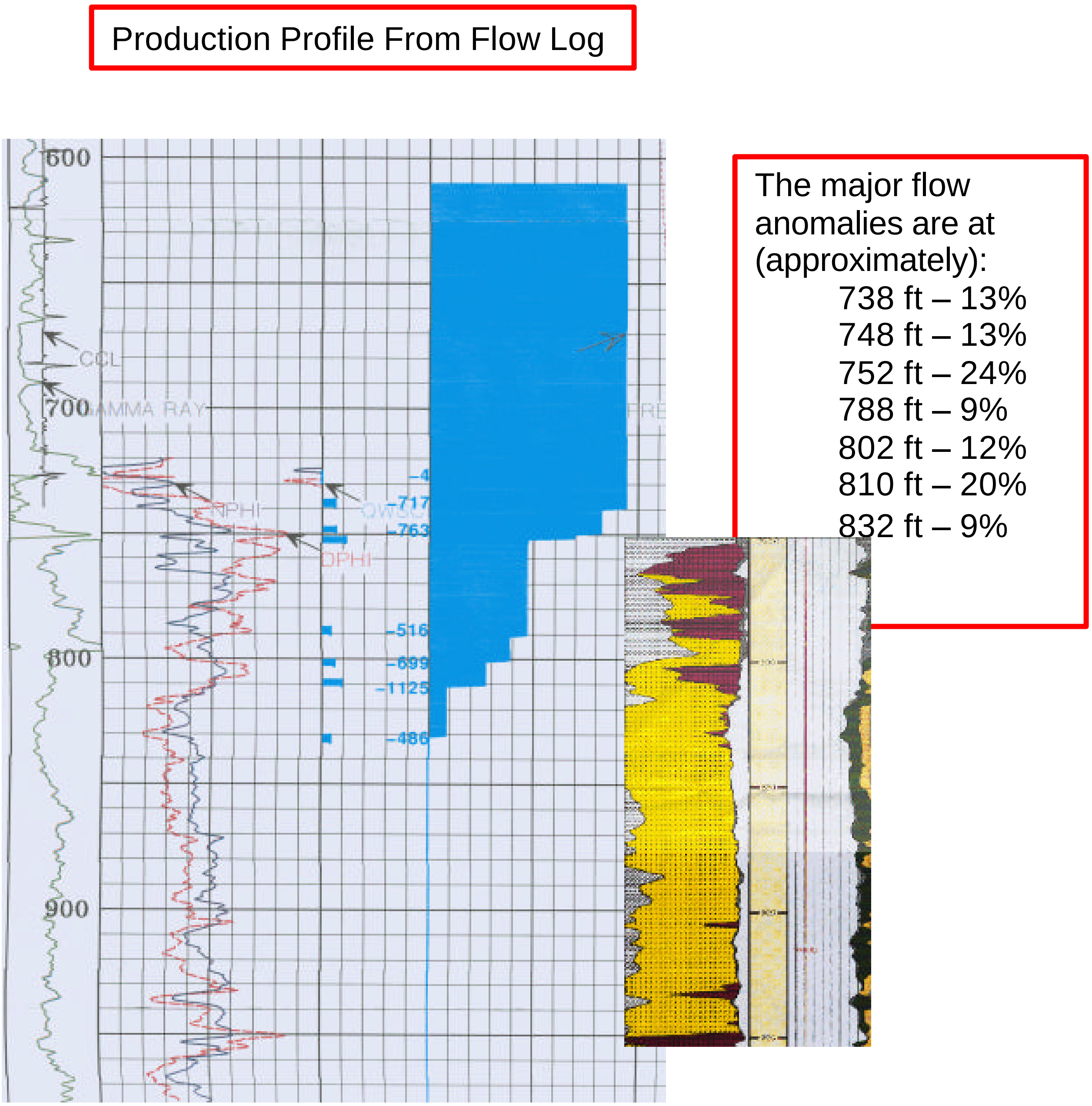

Figure 3-5. Cumulative production profile for Shoshone 66-14.

fractures found in that interval. The remainder of the flow anomalies were above the fracture image log, and so their correspondence could not be ascertained

Figure 3-6 compares the cumulative production to the cumulative fracture intensity normalized to vary from 0% to 100) over the interval that was logged for flow and starting at 0% at the bottom of the flow-logged interval. The cumulative fracture intensity and cumulative production follow one another fairly closely. One interpretation of the fact that flow anomalies generally track open fracture intensity, but may or may not correspond to the presence or absences of individual fractures, is that it is the general strain in the rock that matters, not how that strain is locally connected to the wellbore. If a zone is highly strained, it has a much higher fracture permeability, and whether that permeability is connected to the wellbore by one fracture or some small fractures or by the matrix may be less important. This suggests that the strain anomalies calculated through the palinspastic reconstruction may be good predictors of reservoir-scale subsurface fluid movement, while at the same time not necessarily predicting local scale well behavior with the same level of utility.

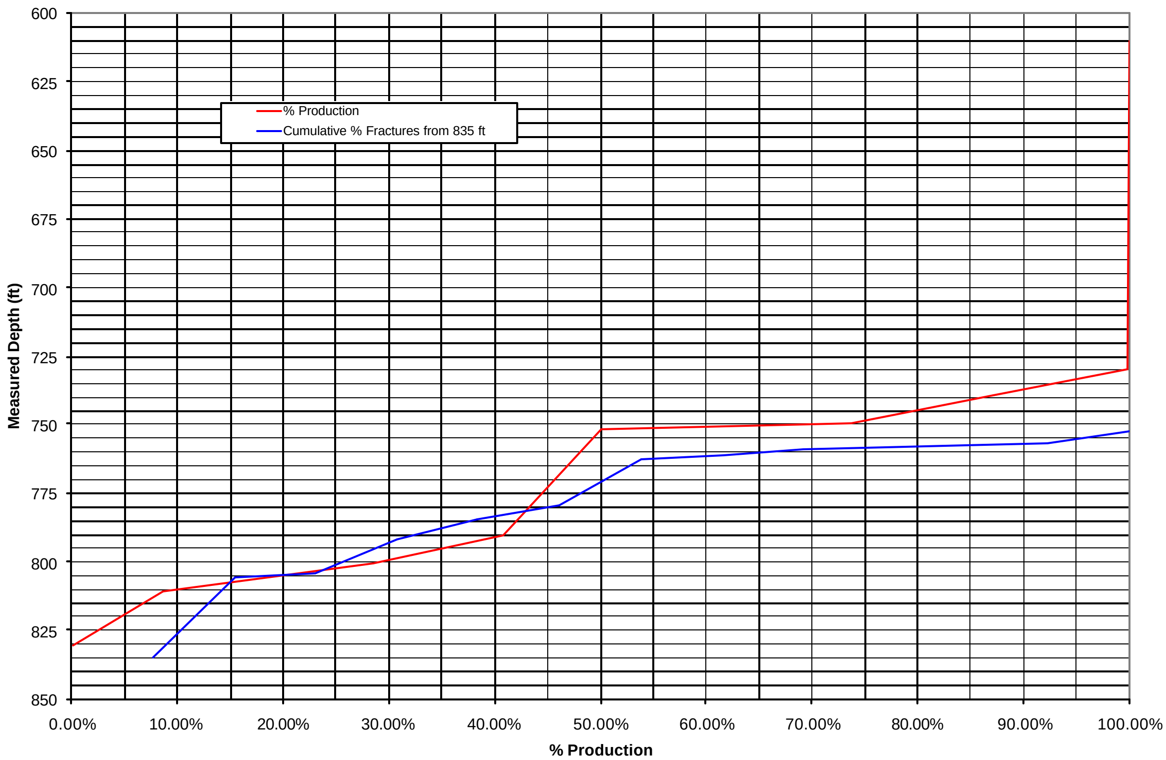

Figure 3-6. Comparison of cumulative fracture intensity and cumulative production from Shoshone 66-14. The red line is the % production from the spinner survey data. The blue line is the cumulative percent of fractures starting at a depth of 835 ft. (there were not enough 4-pad fractures to plot this component separately).

3.2.2.3 Further Considerations Concerning Stratigraphic Differences in Fracturing

The plot of fracture dip azimuths in Figure 3-2 suggests that there may be some differences between the fractures in the Tensleep Marker interval and those in the top of the Tensleep. Figure 3-7 and Figure 3-8 show the orientations of fractures in these two zones.

It is interesting to note that about 60% to 70% of the cumulative production comes from 3 or 4 zones in the Tensleep marker interval, while only 30% to 40% of the production comes from 2 or 3 zones in the top of the Tensleep Formation. The stereoplots in Figure 3-7 and Figure 3-8 suggest one reason why the upper TM zone might be more productive: multiple sets in the TM vs. a single set below. Figure 3-7 shows that there are three orientations of fractures in the TM. On the other had, Figure 3-8 shows only

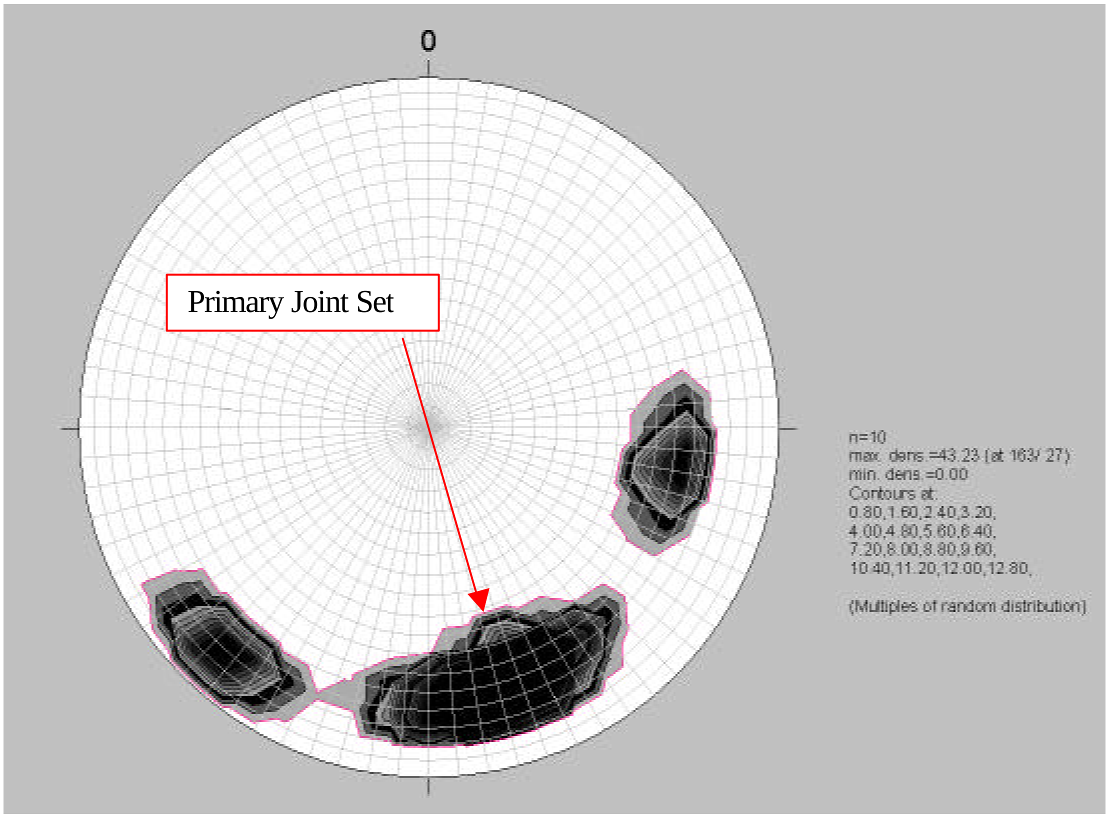

Figure 3-7. Fractures in the Tensleep Marker interval of Shoshone 66-14.

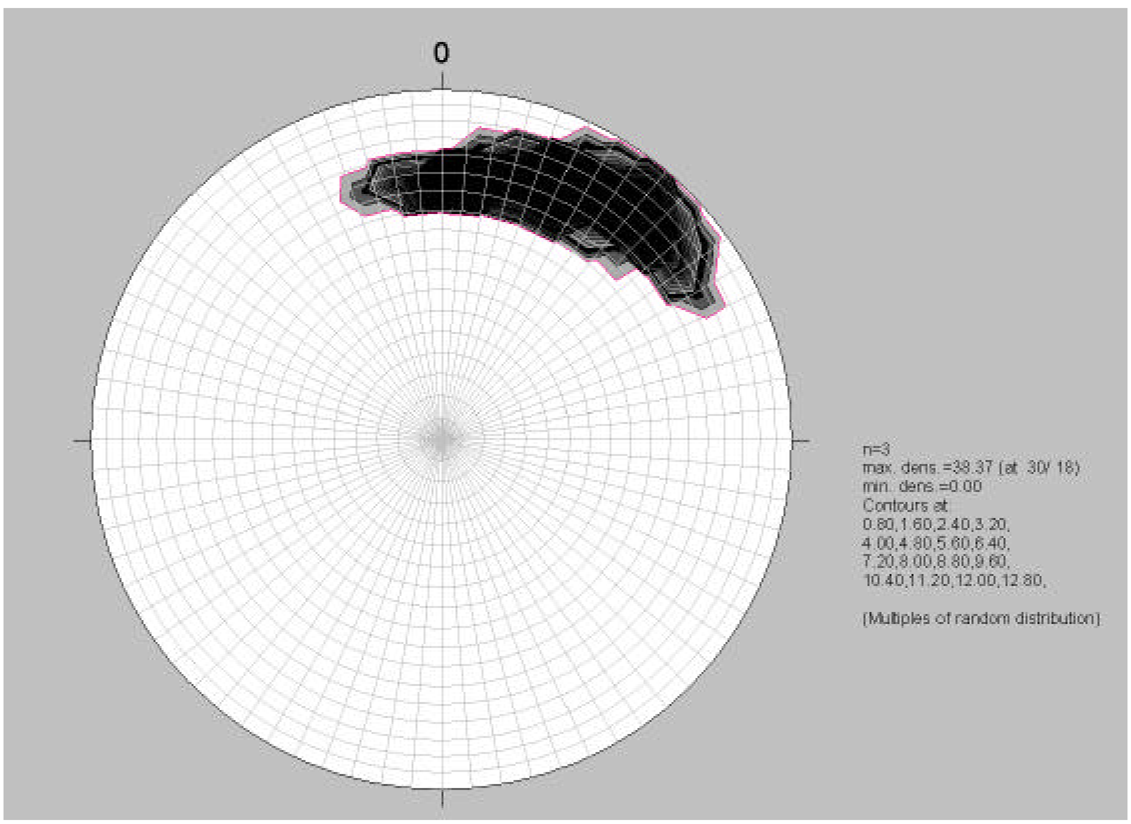

Figure 3-8. Fractures in the T1 and T2A intervals of the Tensleep Formation, Shoshone 66-14.

one dominant orientation. It is difficult to have regional fracture permeability if there is only one orientation of fractures. Connectivity is greatly enhanced when there are two or more orientations.

The dominant orientation of fracturing in the TM portion of Shoshone 66-14 conforms reasonably well with the primary extension fracture set predicted from the palinspastic reconstruction (Figure 3-9). The primary set strikes northeast to east-northeast. This is the dominant direction in the vicinity of the well, shown as a red filled circle in Figure 3-9. This figure also indicates that there should be a fracture set striking north-south to north-northeast as well, which is the same strike orientation as one of the secondary sets in the TM interval. The northwesterly striking secondary set is not parallel to a predicted extensional strain direction, but it is approximately perpendicular to the north easterly striking set, and so is consistent with previous measurements and models of fractures formed during folding (La Pointe and others, 2001).

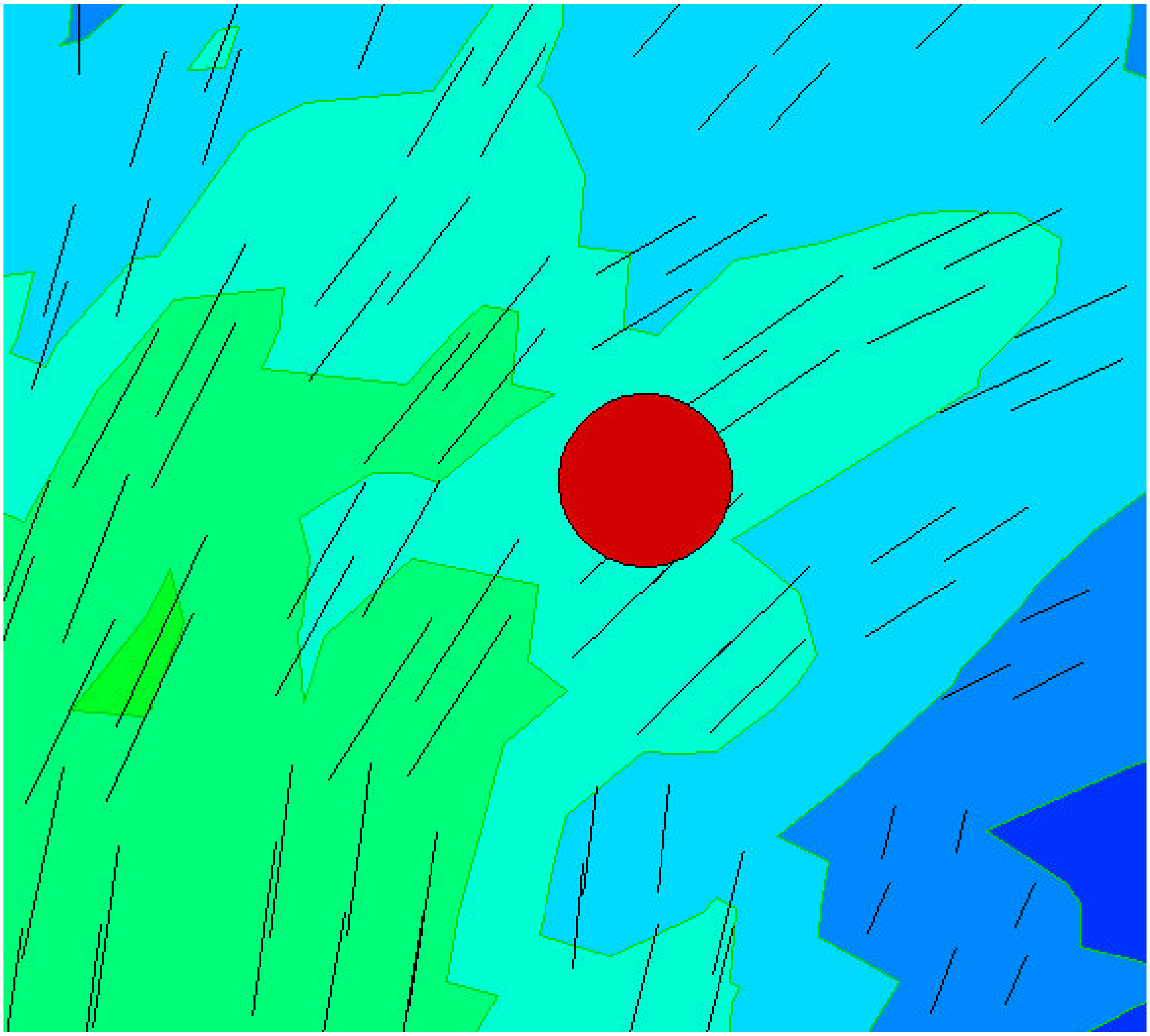

Figure 3-9. Predicted direction of primary extension fracture set for Shoshone 66-14 based upon palinspastic strain reconstruction. Black lines should predicted strike of primary extension set. Contours indicate magnitude of extensional strain

The fracture orientations in the Upper Tensleep portion below the TM (Figure 3-8) are not parallel to the direction predicted from the palinspastic strain orientations. Rather, they strike sub-perpendicular, like one of the secondary sets in the TM portion. Current compressive stress inferred from breakout data (La Pointe and Hermanson, 2001) is in the northeast-southwest direction, and so these northwesterly striking fractures may not be as well oriented with respect to the in situ stresses as the northeasterly striking fractures. This may also play a role in explaining why the TM portion seems to have more productive fracture networks than the Upper Tensleep portion.

Figure 3-10 shows the fractures in the Tensleep Marker and Upper Tensleep portion of Shoshone 66-14 that are encompassed by the flow anomalies. Note that the dominant fracture orientation in this interval is orthogonal to bedding (shown by the contour concentrations at the edge of the diagram). Interestingly, the greatest concentration is for orientations that would be about 23° oblique to being strike parallel, as shown.

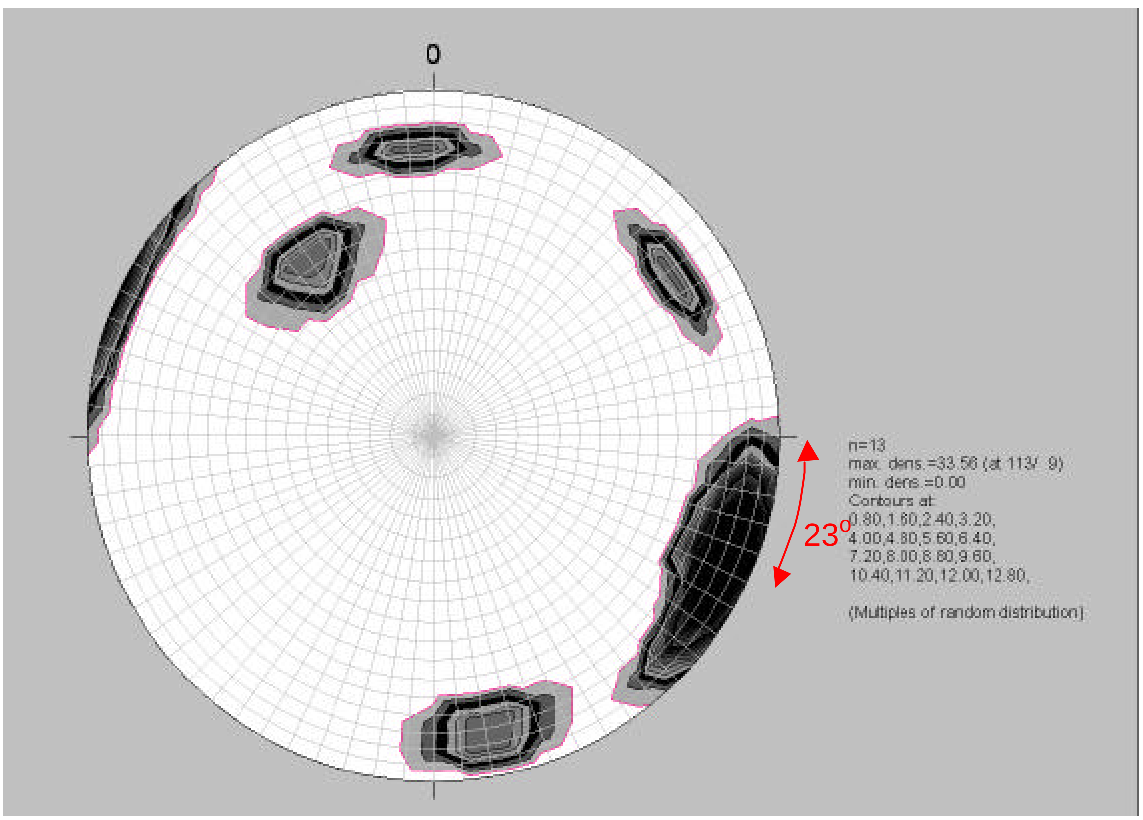

Figure 3-10. Fractures in the productive TM and upper Tensleep intervals, rotated into the plane of bedding (bedding strike north).

In this rotated orientation, the maximum compressive in situ stress would be approximately north-south, so it would be oblique to the dominant extensional joint set.

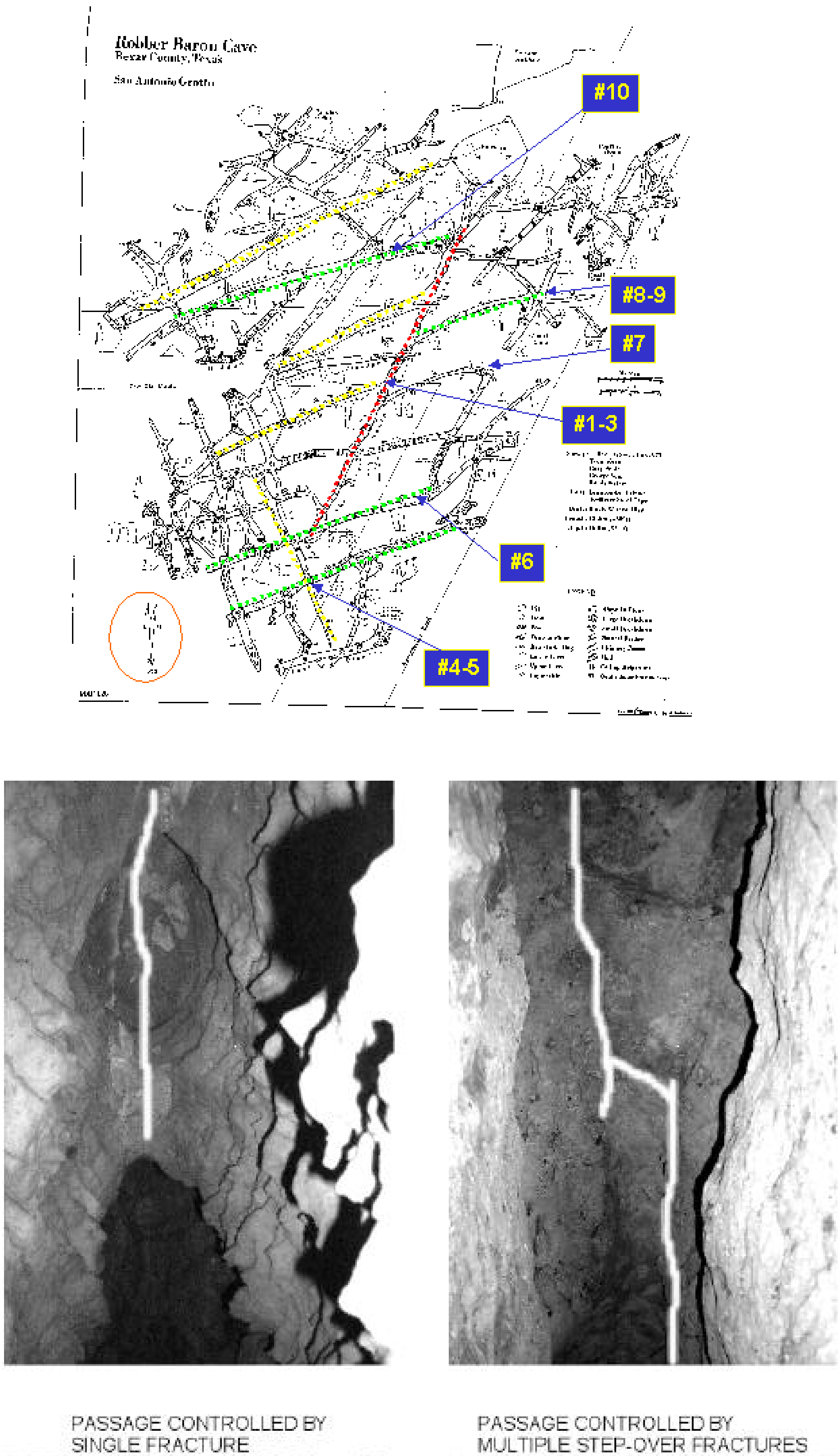

Figure 3-11. Example of shearing in the Austin Chalk Formation leading to enhanced dissolution. Photographs and map courtesy of L. Thompson.

Figure 3-11 shows an example of permeability enhancement in oblique fracture systems. This figure shows the Robber Barron Cave in San Antonio, TX. The primary extension direction is to the southeast, and the maximum compressive direction is northeast-southwest. Fractures have formed orthogonal to bedding and parallel and perpendicular to the maximum extension (and compression) directions. These cave systems are shown by yellow-colored passages in the upper portion of the figure, and the highlighted photograph in the lower left corner shows how these vases are developed along a single extension fracture (white highlighted line). Conversely, in the green-colored oblique passages, the cave passages are not developed along a single fracture, but along of consistently offsetting extension fractures that step periodically to the next fracture. The reason this occurs is because there is a shear component in the rock that caused these extension fracture to link up and create oblique cave passages. These green oblique cave passages are much more solution enhanced than the yellow ones.

While the mechanism of fracture development differs in the Austin Chalk, and the fractures developed in a very different tectonic setting, the caves do show how an orientation that is ten to twenty degrees promotes shear. Mild shear, on the other hand, generally enhances fracture permeability unless it produces a fault gouge that may then reduce permeability.

3.2.2.4 Relation of Fracture Orientations in Image Logs to Surface Outcrop Fracturing

Shoshone 66-14 presents an opportunity to evaluate directly whether the fracture orientations found in the image logs for the Tensleep are similar or not to the fracture orientations in the Red Peak and Crow Mountain outcrops that formed the basis for the outcrop studies. While the structural reconstruction and field reconnaissance work strongly suggests that the reservoir formations and these two Members of the Chugwater Formation have undergone very similar deformational histories, this was not explicitly tested, since the image logs were obtained subsequent to the outcrop work. There were no outcrops in the immediate vicinity of Shoshone 66-14 that would be of sufficient quality for the detailed scanline studies reported in La Pointe and Hermanson (2001), but there are some outcrops near to the wellhead on which qualitative fracture orientation observations could be made. Recent field work in the Circle Ridge Field undertaken during the fourth six-month period made it possible to check the fracture orientations in outcrop for both Shoshone 66-14 and Shoshone 66-07.

Figure 3-12 shows the orientations of fractures in an outcrop of Red Peak a few tens of meters from the wellhead of Shoshone 66-14. In the rosette diagrams to the left of the photograph. ths trike orientations of open (red), partially open (yellow) and solution enhanced (green) fractures are shown. The dominant orientations are east-west and northwest-southeast. In the outcrop, the dominant direction is east-west (yellow dotted lines) and northwest (red dotted lines). The strike orientations for fractures in the Red Peak closely match those found in the Tensleep at depth.

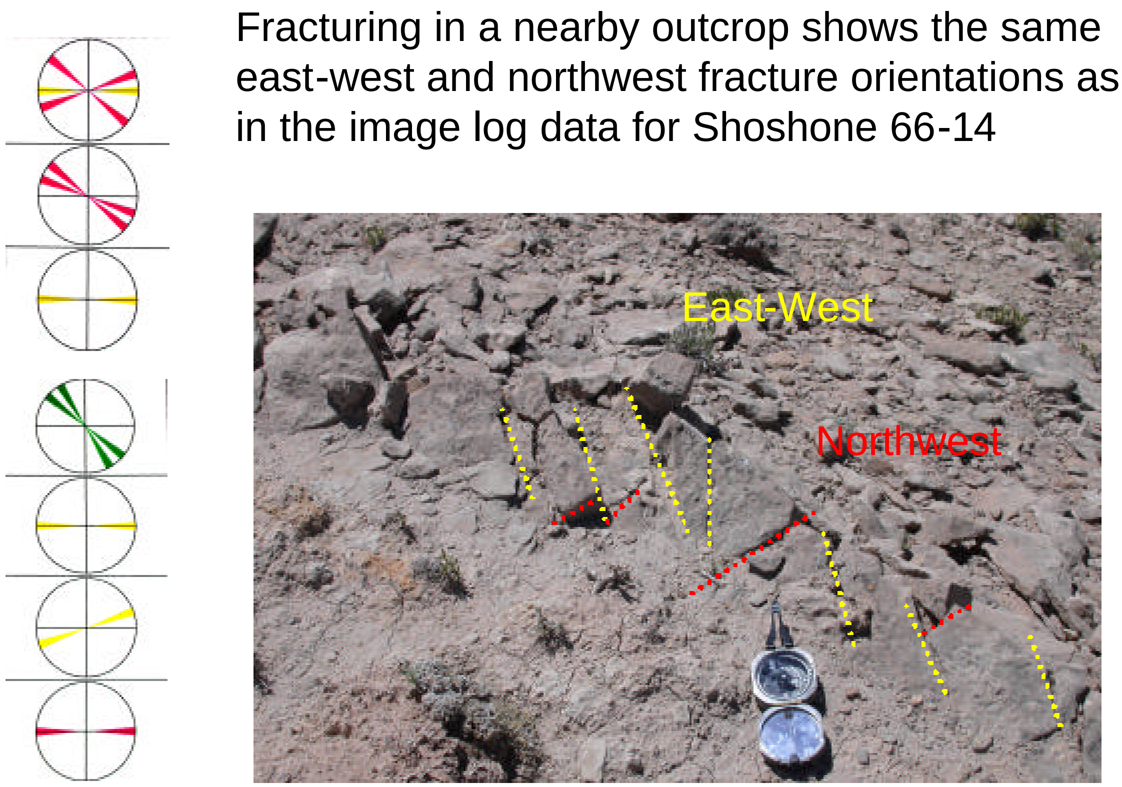

Figure 3-12. Orientations of fractures in the Red Peak Formation near the wellhead for Shoshone 66-14. Compass points approximately west. Strikes of fractures from image log are shown in rosette diagrams to left of photograph.

It was also possible to test the image log fracturing and the overlying fracturing in outcrop for Shoshone 66-07. Figure 3-13 shows a plot os fracture strikes for the Tensleep obtained from image log data, as well as fracturing in the Red Peak Member in an outcrop about 20 m south from the Shoshone 66-07 wellhead. The image log data shows that the dominant open fractures (the red colored rosettes) strike approximately east-west or northwest-southeast, while the strikes of partially open fractures (yellow rosettes) strike in similar directions as well. The outcrop photo shown to the right of the rosette has a red line indicating a prominent northwest set's strike found in the outcrop, while the yellow line indicates an equally prominent east-west set found in outcrop. It is interesting to note that the valley formed to the immediate west of the outcrop (demarcated bu the yellow line) trends in virtually the same orientations as the dominant east-west set (shown in the enlarged portion of the outcrop at bottom).

It was not possible to test the relation between Chugwater fracturing and the fracturing in the subthrust Phosphoria in Shoshone 65-37 since there are no nearby outcrops.

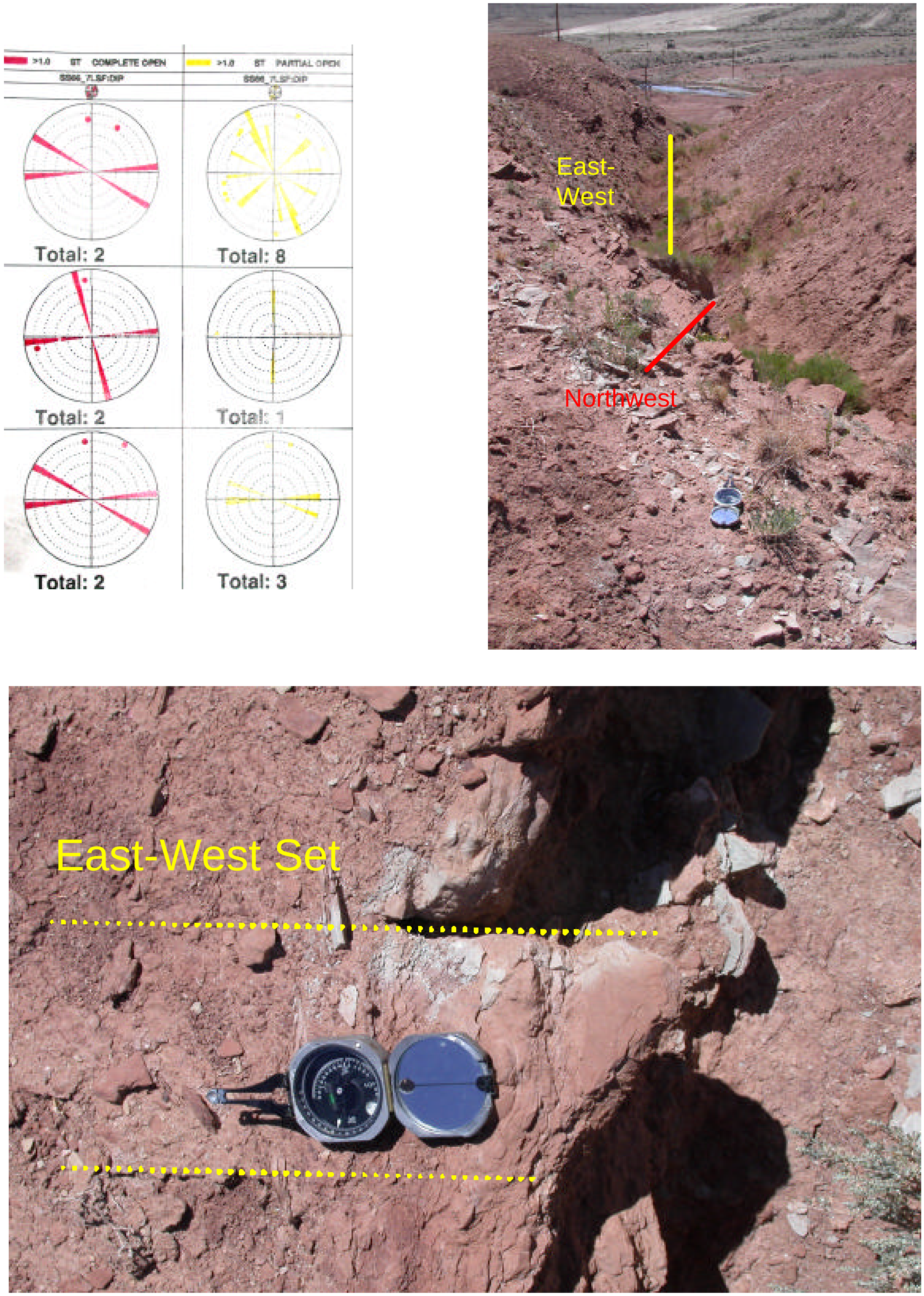

Figure 3-13. Fracture orientations in image logs and outcrops of Red Peak for Shoshone 66-07.

3.2.2.5 Summary of Findings Regarding Shoshone 66-14

Analysis of fracturing, lithology and flow logs for Shoshone 66-14 suggests that the dominant permeable fracturing is consistent with the orientation predicted from the palinspastic reconstruction, as were the previous two wells (La Pointe and others, 2001) and the outcrop data (La Pointe and Hermanson, 2001). Fracture intensity correlates with bedding thickness: the thinner the beds, the higher the measured fracture intensity, but it is important to note that fracture intensity at the wellbore alone may or may not be a good predictor of cumulative flow. Consideration of the fracture orientations suggests that the presence of multiple orientations, capable of forming networks, and a favorable orientation with respect to in situ stresses, may be very important. Analyses of Shoshone 66-14 and the two previous wells (La Pointe and others, 2001) suggests that a more general increase in the intensity of favorably oriented fractures (usually this is the orientation predicted by the palinspastic strain) is probably a more accurate predictor of the probability of finding a conductive fracture and of that fracture's productivity. Lithology, at least in terms of the relative percent of sandstone, dolomite and shale, does not seem to play a primary role in delineating fracture prone from non-fracture prone zones of the Tensleep and Tensleep Marker, although it may play a secondary role when there are abrupt transitions between sandstone and dolomite.

The comparison of fracturing in outcrops and image logs for Shoshone 66-14 and Shoshone 66-07 further validate the usefulness of the outcrop from the Red Peak and Crow Mountain Members obtained and analyzed in La Pointe and Hermanson (2001) and La Pointe and others (2001).

3.2.3 ANALYSIS OF BROMIDE TRACER EXPERIMENT

The bromide tracer experiment had several purposes: to test the connectivity between the Tensleep and Phosphoria Formations; to delineate the geometry of major flow conduits; to provide a basis for ascertaining whether the large scale fracture connectivity structure deduced from the palinspastic reconstructions and implied fracture patterns are consistent with the flow conduits or in fact could have been used to predict them; and to develop additional fluid flow properties for the DFN model.

The bromide tracer experiment involved a number of wells completed in the Tensleep and/or Phosphoria in imbricate blocks 6, 8 and 9 (Figure 3-14). Table 3-1 presents the data obtained at the injector and the monitoring wells over the course of the experiment. This raw data was converted to time vs. concentration plots (Figure 3-15). This graph shows the rapid breakthrough seen in Shoshone 65-53, the later breakthroughs in Shoshone 65-37 and Shoshone 65-73, and the lack of tracer breakthrough in the remaining monitored wells. Table 3-2 summarizes the time between injection and the highest measured bromide concentration in each monitoring well.

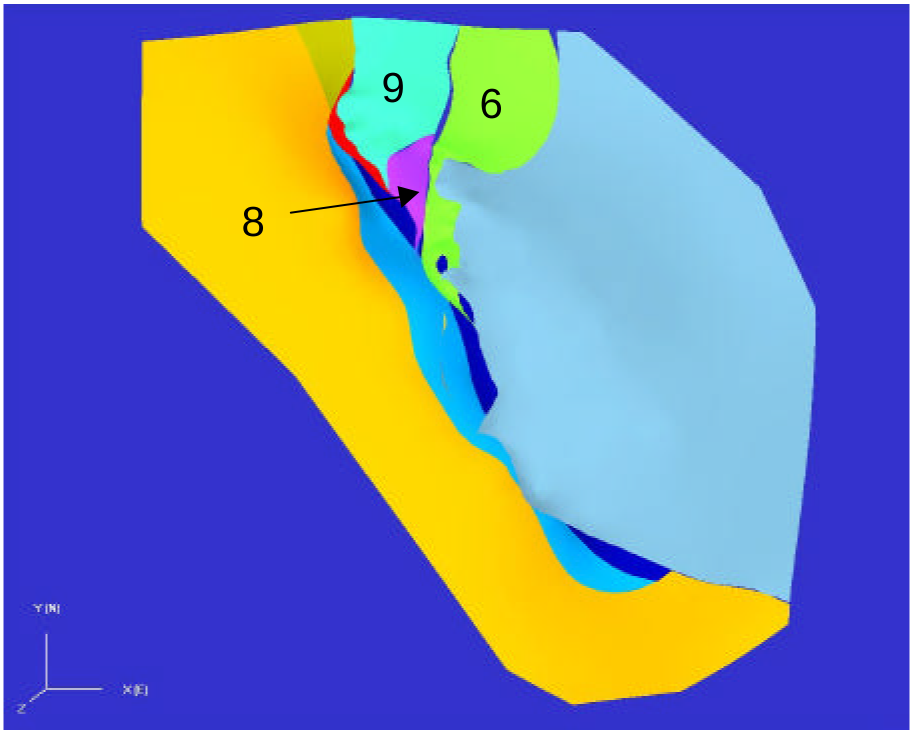

Figure 3-14. Structural blocks involved in the Bromide Tracer experiment in the Phosphoria Formation. Blocks 6, 8 and 9 are the uppermost imbricate fault blocks.

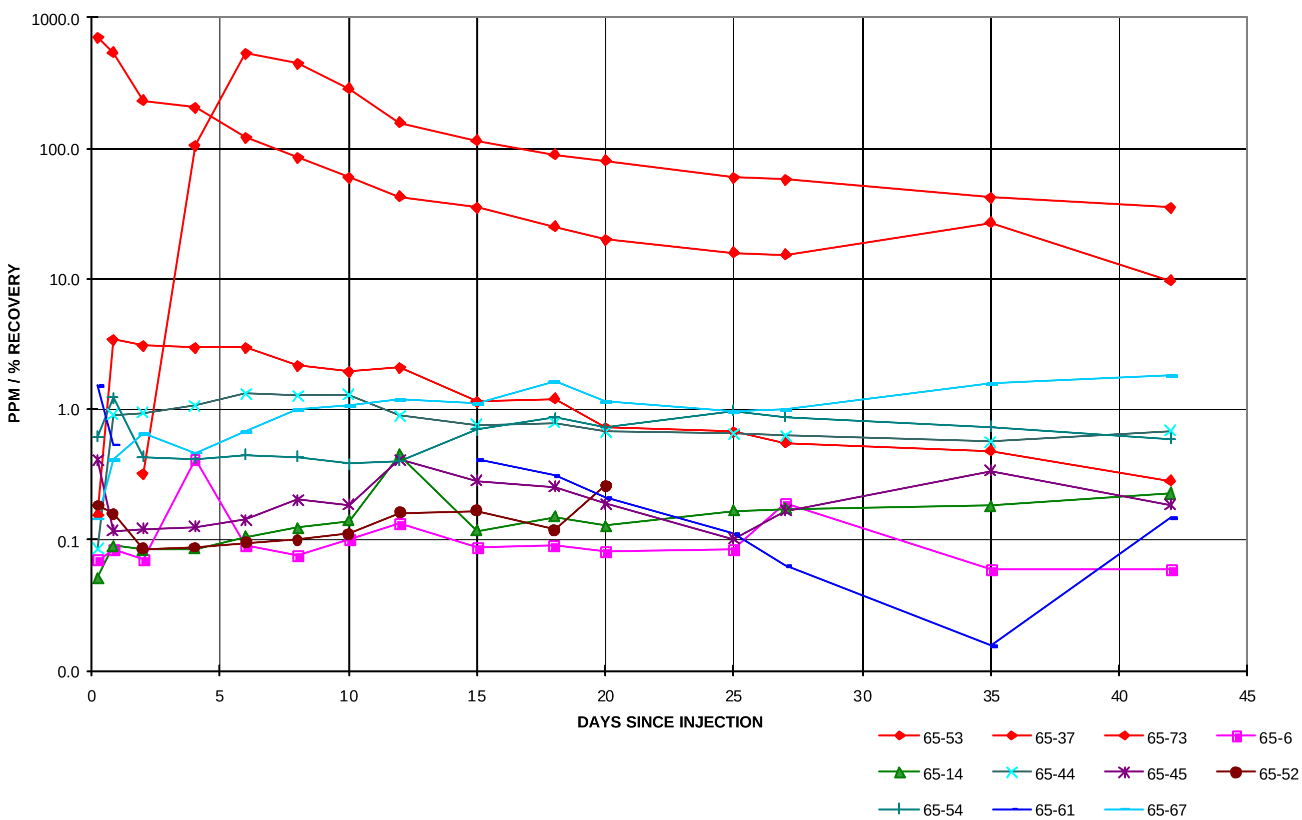

Figure 3-15. Time vs. bromide concentration for the bromide tracer test monitoring wells.

			Bromide Results for Offsets on:								SHOSHONE 65-20 P				
	10/26	10/29	11/02	11/05	11/06	11/15	11/15	11/16	11/17	11/19	11/21	11/23	11/25	11/27	11/30
INJECTOR DATA															
# BROMIDE INJECTED						3339									
CONC. SODIUM BROMIDE %						24									
INJECTION RATE BPD						400	175	206	350	390	425	573	573	573	538
DAYS SINCE INJECT.							0.229	0.840	2	4	6	8	10	12	15
DISPLACEMENT BBLS.							40	166	572	1352	2202	3348	4494	5640	7253
OFFSET DATA															
Shoshone 65-6															
BROMIDE, PPM	0.18	0.08	0.08	0.11	0.06		0.07	0.08	0.07	0.41	0.09	0.08	0.10	0.14	0.09
BR-BGRD, PPM							0.00	0.00	0.00	0.31	0.00	0.00	0.00	0.03	0.00
BWPD							303	303	303	303	303	303	303	303	303
# BR PROD.							0.00	0.00	0.00	0.03	0.00	0.00	0.00	0.00	0.00
CUM # BR PROD.							0.00	0.00	0.00	0.03	0.07	0.07	0.07	0.07	0.07
% RECOVERY							0.00	0.00	0.00	0.00	0.00	0.00	0.00	0.00	0.00
NOTES															
Shoshone 65 14TA															
BROMIDE, PPM	0.07	0.06	0.01	0.10	0.08		0.05	0.09	0.09	0.09	0.11	0.13	0.14	0.45	0.12
BR-BGRD, PPM							0.00	0.03	0.02	0.02	0.04	0.06	0.08	0.39	0.06
BWPD							98	98	98	98	98	98	98	98	98
# BR PROD.							0.00	0.00	0.00	0.00	0.00	0.00	0.00	0.01	0.00
CUM # BR PROD.							0.00	0.00	0.00	0.00	0.01	0.01	0.01	0.03	0.05
% RECOVERY							0.00	0.00	0.00	0.00	0.00	0.00	0.00	0.00	0.00
NOTES															
Shoshone 65 37PT															
BROMIDE, PPM	0.15	0.22	0.14	0.21	0.13		Down	Down	0.50	105.69	532.54	448.01	288.85	157.10	115.14
BR-BGRD, PPM							0.00	0.00	0.32	105.52	532.37	447.84	288.67	156.93	114.97
BWPD							14	14	14	14	14	14	14	14	14
# BR PROD.							0.00	0.00	0.00	0.50	2.52	2.12	1.36	0.74	0.54
CUM # BR PROD.							0.00	0.00	0.00	0.50	3.51	8.15	11.63	13.73	15.66
% RECOVERY							0.00	0.00	0.00	0.02	0.11	0.24	0.35	0.41	0.47
NOTES															
Shoshone 65 44T															
BROMIDE, PPM	0.06	0.09	0.10	0.00	0.00		0.09	0.91	0.94	1.07	1.33	1.27	1.30	0.89	0.76
BR-BGRD, PPM							0.04	0.86	0.89	1.02	1.28	1.22	1.25	0.84	0.71
BWPD							227	227	227	227	227	227	227	227	227
# BR PROD.							0.00	0.07	0.07	0.08	0.10	0.10	0.10	0.07	0.06
CUM # BR PROD.							0.00	0.02	0.10	0.26	0.44	0.64	0.83	1.00	1.18
% RECOVERY							0.00	0.00	0.00	0.01	0.01	0.02	0.02	0.03	0.04
NOTES															
Shoshone 65-45PTA															
BROMIDE, PPM	0.12	0.03	0.12	0.10	0.11		0.41	0.12	0.12	0.13	0.14	0.21	0.19	0.41	0.28
BR-BGRD, PPM							0.31	0.02	0.03	0.03	0.05	0.11	0.09	0.32	0.19
BWPD							144	144	144	144	144	144	144	144	144
# BR PROD.							0.02	0.00	0.00	0.00	0.00	0.01	0.00	0.02	0.01
CUM # BR PROD.							0.00	0.01	0.01	0.01	0.02	0.02	0.03	0.06	0.09
% RECOVERY							0.00	0.00	0.00	0.00	0.00	0.00	0.00	0.00	0.00
NOTES															
Shoshone 65-52T															
BROMIDE, PPM	0.00	0.00	0.00	0.00	0.00		0.18	0.16	0.09	0.09	0.10	0.10	0.11	0.16	0.17
BR-BGRD, PPM							0.18	0.16	0.09	0.09	0.10	0.10	0.11	0.16	0.17
BWPD							638	638	638	638	638	638	638	638	638
# BR PROD.							0.04	0.04	0.02	0.02	0.02	0.02	0.02	0.04	0.04
CUM # BR PROD.							0.01	0.03	0.06	0.10	0.14	0.19	0.24	0.30	0.41
% RECOVERY							0.00	0.00	0.00	0.00	0.00	0.01	0.01	0.01	0.01
NOTES															
Shoshone 65-53PT															
BROMIDE, PPM	0.00	0.00	0.00	0.00	0.00		703.73	543.19	231.40	203.32	121.07	85.18	59.20	42.43	38.00
BR-BGRD, PPM							703.73	543.19	231.40	203.32	121.07	85.18	59.20	42.43	35.00
BWPD							1564	1564	1564	1564	1564	1564	1564	1564	1564
# BR PROD.							385.22	297.34	126.67	111.30	66.27	46.63	32.40	23.23	19.16
CUM # BR PROD.							88.22	296.74	542.67	780.63	958.20	1071.10	1150.13	1205.76	1269.34
% RECOVERY							2.64	8.89	16.25	23.38	28.70	32.08	34.45	36.11	38.02
NOTES															
Shoshone 65-54PT															
BROMIDE, PPM	0.84	0.83	0.44	0.39	0.44		0.62	1.23	0.44	0.42	0.45	0.44	0.38	0.41	0.70
BR-BGRD, PPM							0.03	0.64	0.00	0.00	0.00	0.00	0.00	0.00	0.12
BWPD							8	8	8	8	8	8	8	8	8
# BR PROD.							0.00	0.00	0.00	0.00	0.00	0.00	0.00	0.00	0.00
CUM # BR PROD.							0.00	0.00	0.00	0.00	0.00	0.00	0.00	0.00	0.00
% RECOVERY							0.00	0.00	0.00	0.00	0.00	0.00	0.00	0.00	0.00
NOTES															
Shoshone 65-61PT															
BROMIDE, PPM	0.22	0.11	0.09	0.27	0.24		1.72	0.73	0.12	0.12	0.11	0.12	0.13	0.09	0.60
BR-BGRD, PPM							1.54	0.54	0.00	0.00	0.00	0.00	0.00	0.00	0.42
BWPD							308	308	308	308	308	308	308	308	308
# BR PROD.							0.17	0.06	0.00	0.00	0.00	0.00	0.00	0.00	0.05
CUM # BR PROD.							0.04	0.11	0.14	0.14	0.14	0.14	0.14	0.14	0.21
% RECOVERY							0.00	0.00	0.00	0.00	0.00	0.00	0.00	0.00	0.01
NOTES															
Shoshone 65-67PT															
BROMIDE, PPM	0.21	0.19	0.07	0.22	0.20		0.15	0.42	0.66	0.47	0.68	1.01	1.08	1.19	1.12
BR-BGRD, PPM							0.00	0.24	0.49	0.29	0.50	0.84	0.90	1.01	0.94
BWPD							612	612	612	612	612	612	612	612	612
# BR PROD.							0.00	0.05	0.10	0.06	0.11	0.18	0.19	0.22	0.20
CUM # BR PROD.							0.00	0.02	0.11	0.27	0.44	0.73	1.10	1.51	2.14
% RECOVERY							0.00	0.00	0.00	0.01	0.01	0.02	0.03	0.05	0.06
NOTES															
Shoshone 65-73P															
BROMIDE, PPM	0.09	0.09	0.07	0.22	0.26		0.30	3.57	3.21	3.14	3.11	2.30	2.11	2.25	1.30
BR-BGRD, PPM							0.16	3.42	3.06	2.99	2.96	2.15	1.96	2.10	1.15
BWPD							250	250	250	250	250	250	250	250	250
# BR PROD.							0.01	0.30	0.27	0.26	0.26	0.19	0.17	0.18	0.10
CUM # BR PROD.							0.00	0.10	0.43	0.96	1.48	1.93	2.29	2.64	3.07
% RECOVERY							0.00	0.00	0.01	0.03	0.04	0.06	0.07	0.08	0.09
NOTES															
ALL OFFSETS															
# BR PROD.							385.46	297.86	127.13	112.26	69.28	49.24	34.27	24.50	20.16
CUM # BR PROD.							88.27	297.03	543.52	782.91	964.45	1082.97	1166.47	1225.24	1292.23
% RECOVERY							2.64	8.90	16.28	23.45	28.88	32.43	34.93	36.69	38.70

Table 3-1. Raw data obtained in injection and monitoring wells during the bromide tracer experiment.

Well	Time (days)	
	Peak	First Break
65-53	Instant	
65-73	0.84	
65-37	4.00	
65-67	2.00	
65-06	4.00	
65-14	12.00	0.84
65-44	0.84	
65-45	12.00	
65-52	12.00	0.18
65-54	15.00	0.84
65-61	15.00	

Table 3-2. Summary of time to maximum measured bromide concentration. Values for wells shaded yellow represent maximum measured concentrations, but do not correspond to obvious breakthroughs, and may be more due to random fluctuations in bromide levels, measurement precision, minor breakthroughs, or some combination of these factors.

Figure 3-16 shows that breakthrough did not occur in the three wells completed in the Tensleep but not the Phosphoria (Shoshone 65-14, 65-44 and 65-52). This may indicate a decoupling of the fracture system in the upper Tensleep and the lower Phosphoria. There is field evidence for this decoupling in outcrops of the upper Tensleep at Zeisman Dome on the west flank of the Bighorn Basin between Manderson and Worland, WY (Figure 3-17). The cliff in the upper portion of this figure shows a number of joints that are subvertical and cut through the entire cross-bedded dune sequence making up most of the visible rock in the photo. A closer examination of the contact between these dunes and the underlying interdune sequence shows how these large, dramatic joints typically terminate against this depositional boundary. Inspection of the contact along the entire exposed sequence boundary revealed no fractures the encompassed both the dune and interdune portions of the Tensleep. While the upper contact with the Phosphoria was not observed the lower termination suggests that the large jointing is very much confined to the dune sequence.

The remaining eight monitoring wells were completed in the Phosphoria and also may have completions in the Tensleep. The strain contours are consistent with many, but not all, of the responses.

Figure 3-18 shows as display of the wells, the strain field and the inferred strike direction of the dominant extensional fracture set that would be expected to develop consistent with the strain field. Under the assumption that fluids would be more likely to follow paths defined by corridors of intense fracturing, and in the direction of the dominant fracture set, this figure explains of almost all Phosphoria completion wells except Shoshone 65-44.

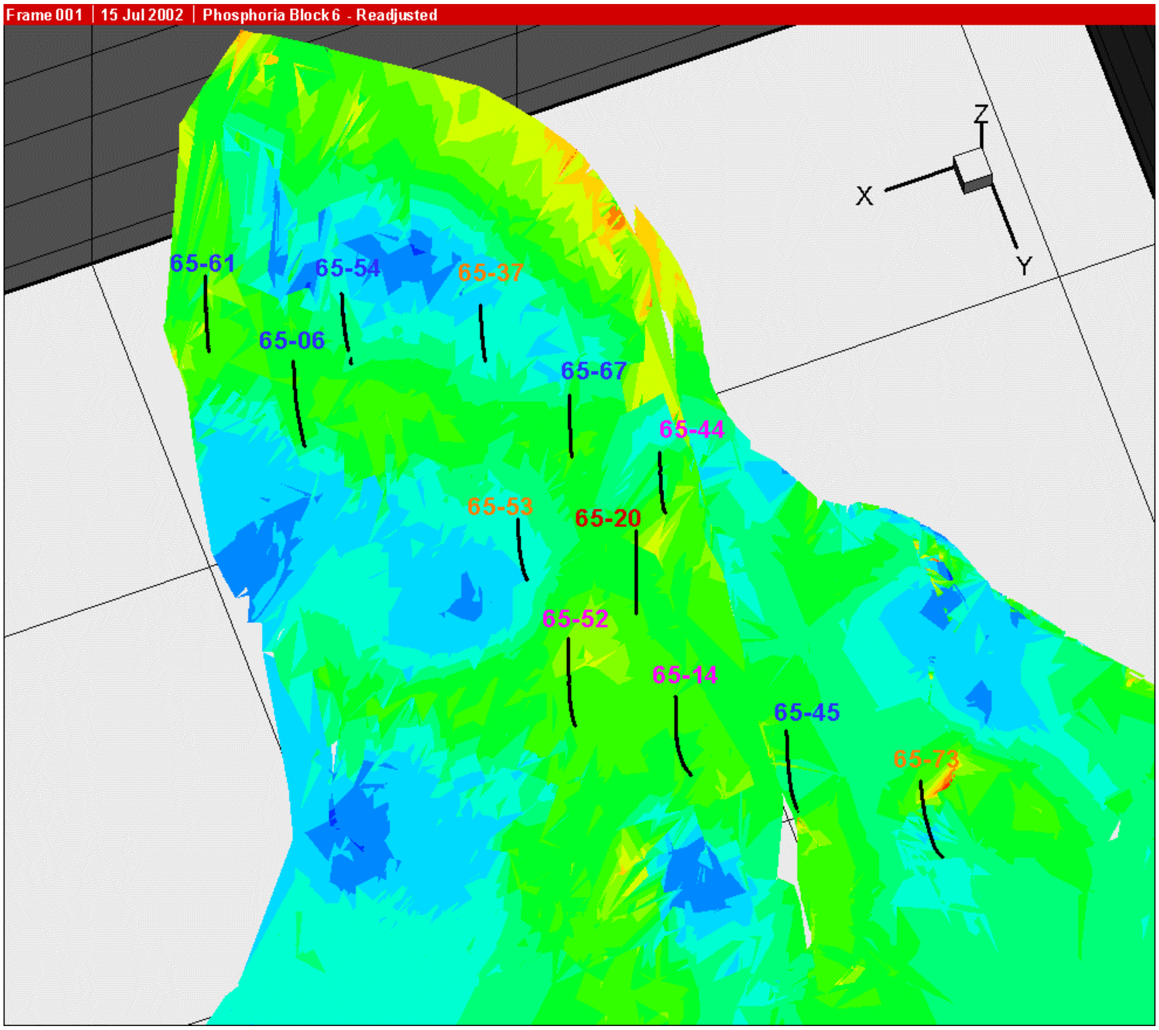

Figure 3-16. Bromide tracer test breakthrough pattern. The bromide was injected into Shoshone 65-20 (colored red). Large and nearly instantaneous breakthrough was seen in Shoshone 65-53; other strong breakthroughs were seen in Shoshone 65-37 (4 days) and in Shoshone 65-73 (20 hours). These wells are colored orange. The other wells (purple indicates a Tensleep completion with no Phosphoria completion; blue a Phosphoria completion) were monitored, but no large breakthroughs were seen.

Consider first the wells in Fault Block 6, the imbricate lying to the left of the Green Valley Fault in the figure. Shoshone 65-53 showed an almost immediate breakthrough, which is consistent with its close proximity to the injector, its presence in the same high strain region as the injector, and the strike of fractures that would provide a pathway from the injector to the well.

There are several corridors of higher strain that develop in all of the fault blacks, as shown by the green contours in Figure 3-16 and Figure 3-18. All of the Phosphoria wells lie in or near these corridors, however, breakthrough did not occur in all of them.

The explanation for the lack of breakthrough in Shoshone 65-06, Shoshone 65-54 and Shoshone 65-61 may be due to a fracture network "divide", as shown in Figure 3-18.

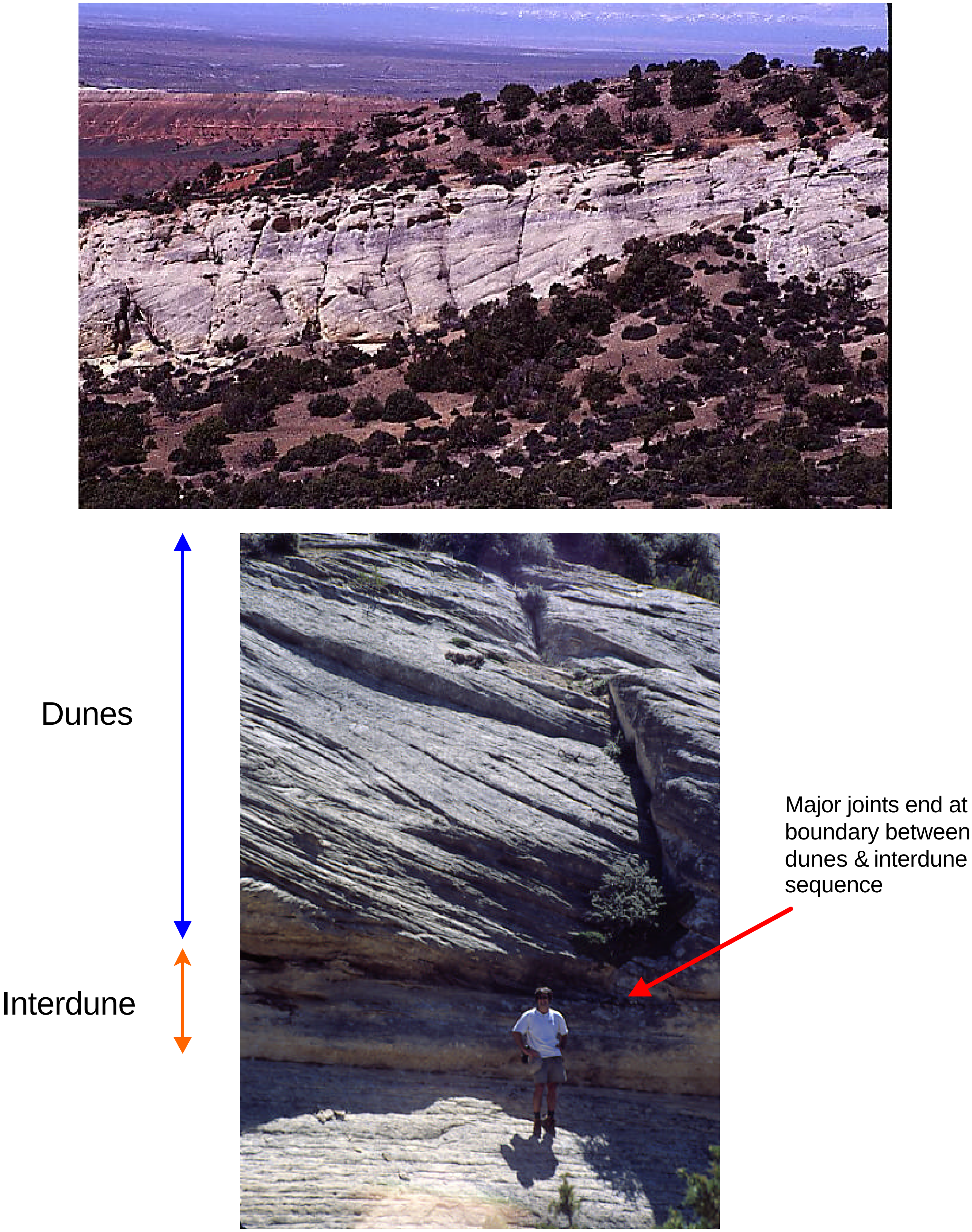

Figure 3-17. Large-scale fracturing in the upper Tensleep Formation at Zeisman dome. Upper photo shows large joints that extend from the top of the dune sequence to the bottom of the dune sequence, but consistently terminate at the boundaries of the dune sequence (lower photo).

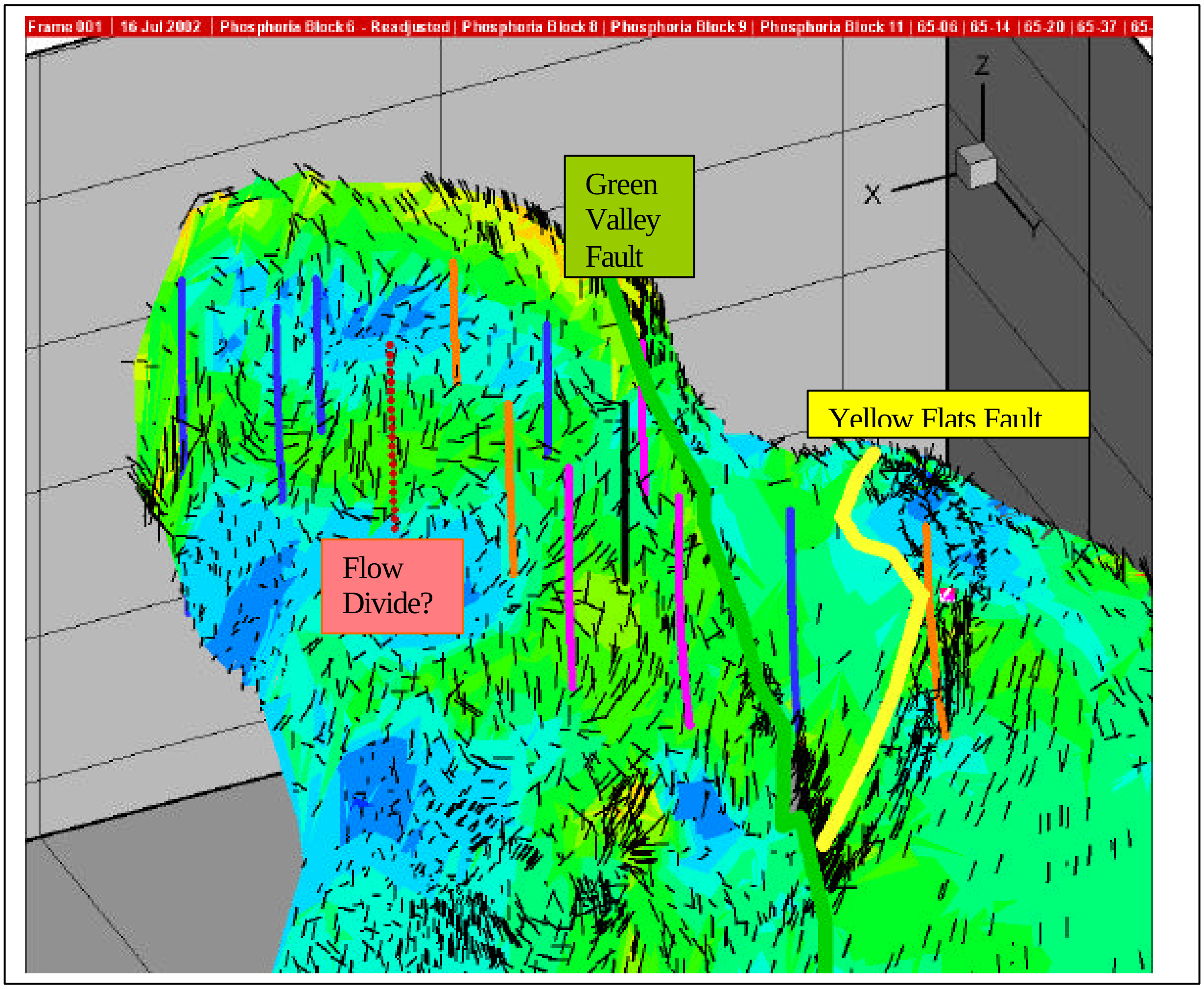

Figure 3-18. Fracture strikes inferred from strain field. Black lines indicate strike of dominant extensional fracture set, while length of line and color of contour indicates the magnitude of extensional strain. Wells are color-coded according to result and completion interval: black = injector; purple = Tensleep but no Phosphoria completion; blue = Phosphoria completion but no response; orange = Phosphoria completion and breakthrough observed.

The possible fracture network divide is shown as a red dotted line in the figure. Flow through the fracture system from right to left along this corridor might be inhibited by the orientations of the fractures at the divide: flow would have to occur perpendicular to the prevailing fracture direction. The remaining two wells, Shoshone 65-37 and Shoshone 65-67, lie in the same strain corridor as the injector and on the same side of the divide. Both should have shown tracer breakthrough according to the strain and fracture pattern. Shoshone 65-37 did show a breakthrough after about 4 days, but Shoshone 65-67 did not. The reason for this lack of response is not explained by the fracture strikes or strain pattern.

Shoshone 65-45 lies in Block 8, which is the imbricate between the Green Valley Fault and the Yellow Flats Fault. No response was seen in this well. This could be due to the hydraulic nature of the Green Valley Fault. At the surface, the Green Valley Fault is a significant erosional feature with enhanced vegetation growth, suggesting that the fault is a zone of higher fracturing and higher permeability than the rock on either side of the fault. This is in keeping with the high fracture intensity seen along the Green Valley Fault in Figure 3-18.

It is possible that this higher permeability zone diverts flow from Block 6 to Block 8. Evidence of this type of behavior has been documented for many faults. Shoshone 65-45 penetrates the Phosphoria near, but still some tens of meters away from the fault. It is possible that the reason for the lack of response is that tracer was diverted along the Green Valley Fault zone, and thus did not reach the well.

The other well, Shoshone 65-73, is in a much larger imbricate separated from Block 8 by the Yellow Flats Fault, and is in a large fracture zone following the footwall of the Yellow Flats Fault. This fault zone seems to be both wider, better connected and more intense than the Green Valley Fault zone, and perhaps explains why Shoshone 65-73 experienced breakthrough in less than a day.

One of the more noticeable features of the strain patterns in Figure 3-16 and Figure 3-18 are the horizontal and dip-parallel bands of higher strain (Figure 3-19 and Figure 3-20). These zones are hinges that formed during the initial folding of the field in the palinspastic restoration. They are zones of higher strain, and occur in both subhorizontal positions, relating to the upwarping and downwarping of the rock (Figure 3-20), and to the dip-parallel flexures that formed to accommodate the tight, doubly-plunging folding on each end of the field. These dip-parallel zones are particularly common in the northwestern end of the field where horizontal shortening is greater.

While these patterns exist in the palinspastic models, this does not necessarily guarantee that they exist in the Circle Ridge Field. Nor are such zones very easy to demonstrate from subsurface fracture data unless a number of wells were specifically located and logged for this purpose.

However, such first-order structural features are clearly significant enough that they should be seen in all of the formations involved in the folding of the Circle Ridge Field. This implies that they should be evident in surface outcrops in the Circle Ridge Field.

In fact, outcrop patterns in the Circle Ridge Field do substantiate the existence of horizontal and dip-parallel flexural hinge zones that are defined by zones a much higher fracturing, permeability and erosion, and separate blocks of more or less constantly-oriented strata from one another.

Figure 3-23 shows an example from the northwest end of the Field. This photograph shows a horizontal flexure zone. If rock were an elastic plate, then the beds would deform continuously without any discontinuities, as shown by the cyan-colored line in the photo. However, the rock actually deformed by breaking into blocks or panels. Within each block, the orientation of bedding is more or less constant, as shown by the

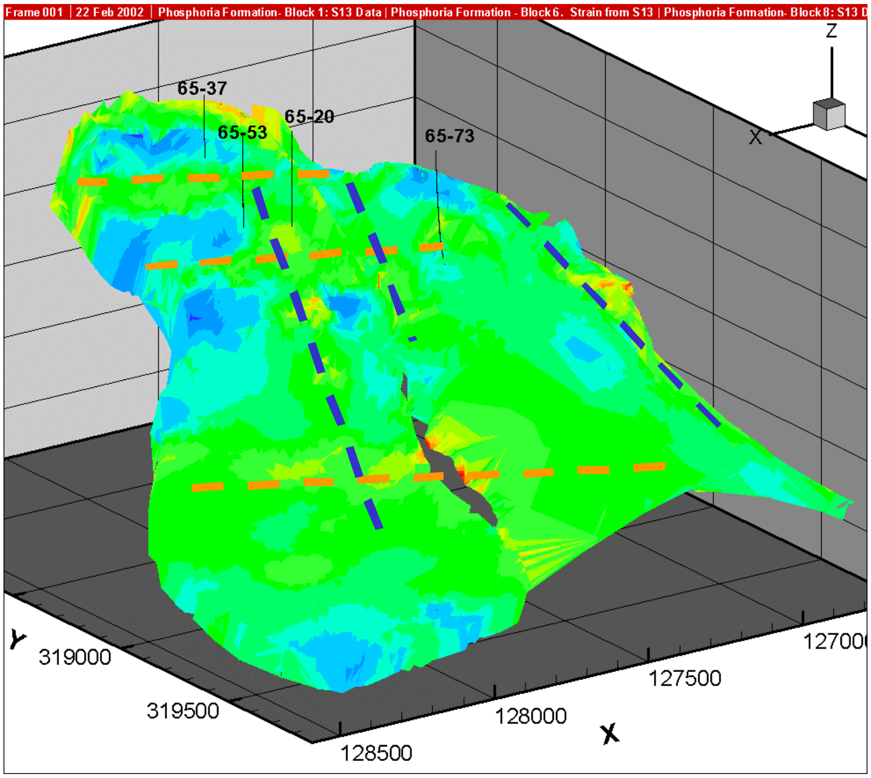

Figure 3-19. Map of strain in imbricate bloicks involved in the Bromide Trace Test, showing de velopment of horizontal (orange dashed line) and dip-parallel (blue dashed line) zones.

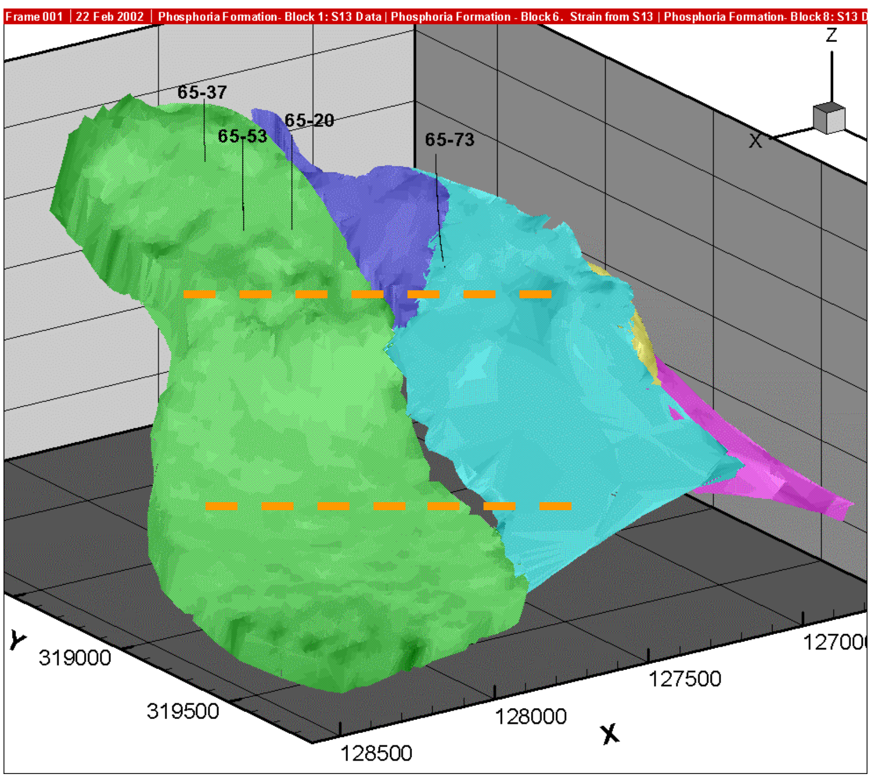

Figure 3-20. 3D view of imbricate blocks and illustration of two horizontal “hinges” or flexure zones (orange dashed lines) formed during the initial folding of the field.

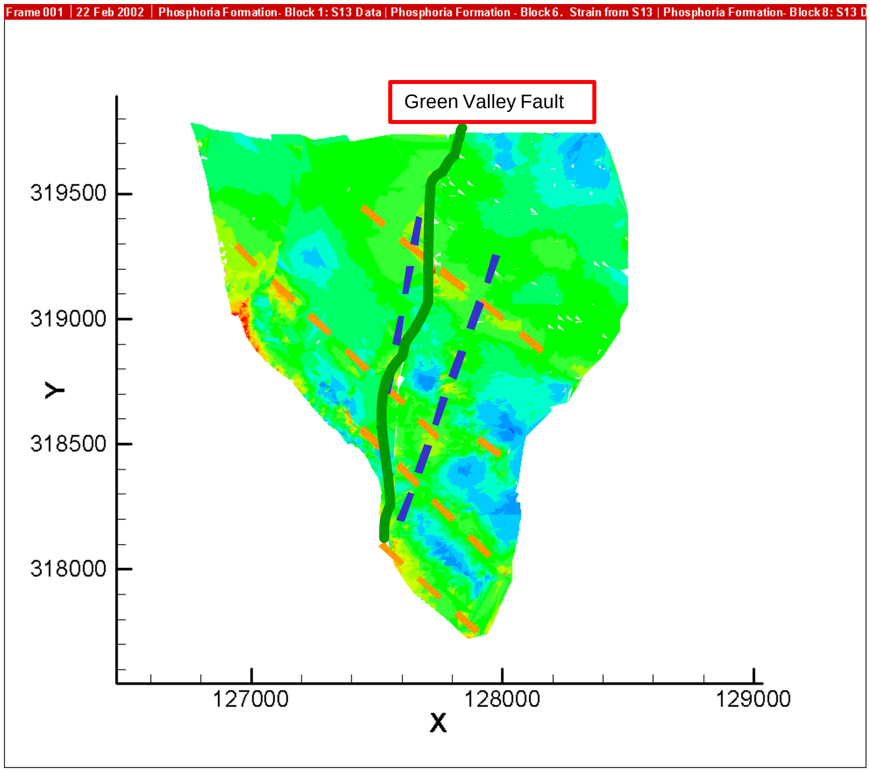

Figure 3-21. Delineation of flexural hinge zones in imbricate blocks, map view. The Green Valley Fault is shown for reference.

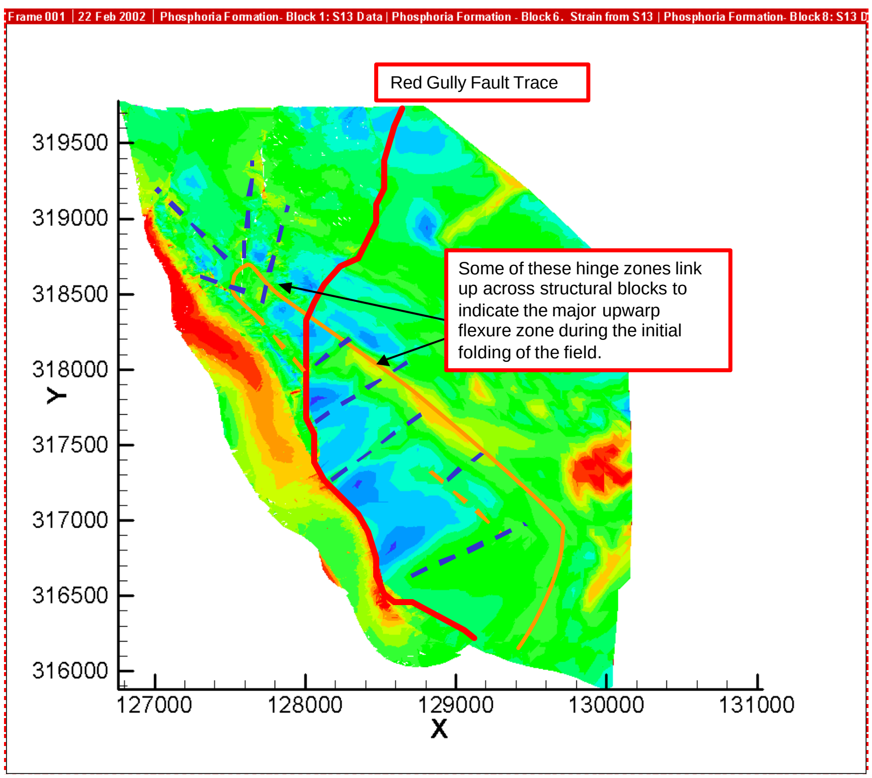

Figure 3-22. Map view of the Circle Ridge Field structural blocks and extensional strain contours, with major horizontal (downwarp) flexural hinge zone (orange solid line) and dip-parallel hinges (blue dashed lines) shown.

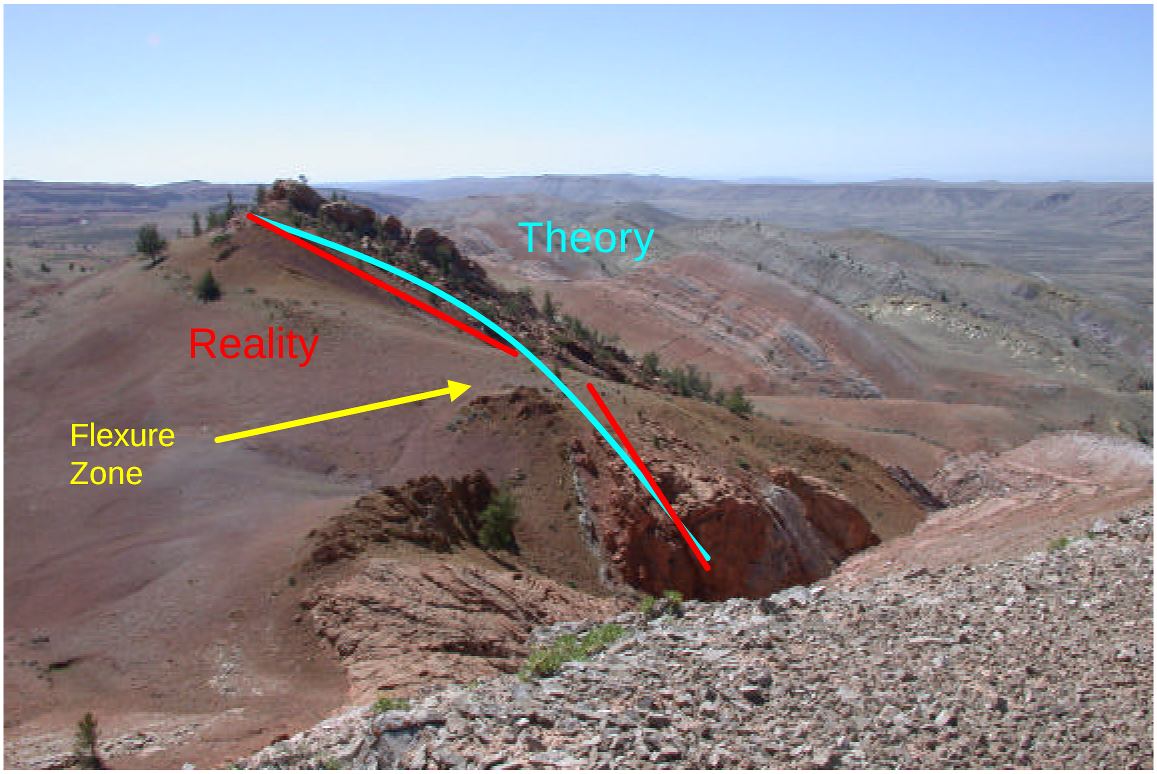

Figure 3-23. Example of a horizontal flexure zone. Most rock does not deform in a continuous curve (cyan-colored line), but rather as panels with more or less constant curvature that deform in zones of higher intensity fracturing or faulting between panels (red lines). The more highly fractured nature of these hinge zones typically leads to greater erosion on the surface.

red lines in the photo. The hinge zone separating these blocks is more highly fractured and eroded, and hence outcrops are rare or nonexistent.

Figure 3-24 shows a dip-parallel flexural hinge. This hinge occurs in the eastern portion of the field. Bedding orientation in the blocks on either side of the flexure zone strike more than 18° differently, and also have different amounts of dip on either side. In between these two blocks is a gully that delineates the flexure zone. in this zone, the rock is much more highly fractured, and as a result, eroded. Vegetation is also much more common in these gullies, probably due to a combination of the physical funneling of surface water through the gully, and the higher permeability of the rock.

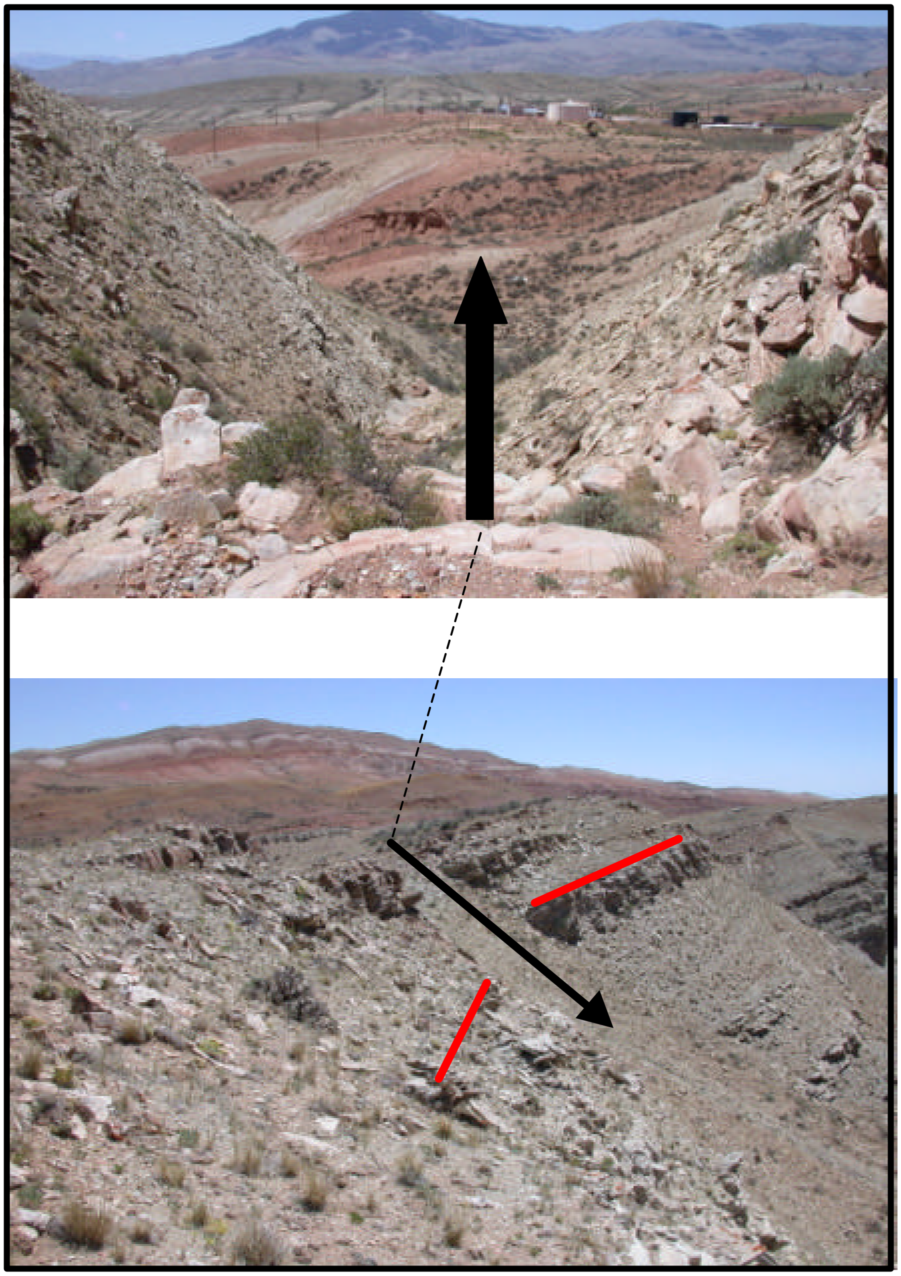

Figure 3-24. Example of a dip-parallel flexural hinge zone. The lower photo shows approximate bedding orientation for two blocks of Crow Mountain in the eastern portion of the Field. The difference in strike is over 18°, although the perspective of the photo makes this less obvious. The black arrow indicates the location of the flexural hinge, and as seen in both the top photo and the lower photo, this zone is much more highly fractured and eroded than the adjacent rock blocks. The top photo is taken at the top of the flexural hinge gully looking downward in the direction of the arrow in the lower photo.

3.2.4 FURTHER ANALYSIS OF THE NITROGEN INJECTION TEST

Some preliminary analyses of the nitrogen injection test, carried out in the Tensleep Formation in Block 1 (overthrust block), were reported in the third semi-annual report (La Pointe and others, 2001). The identification of the flexure zones in the bromide test analyses prompted a re-evaluation of the nitrogen injection test to further examine the relation between strain, the development of strain corridors, fracturing and flow conduits. The experimental details of this test can be found in La Pointe and others (2001).

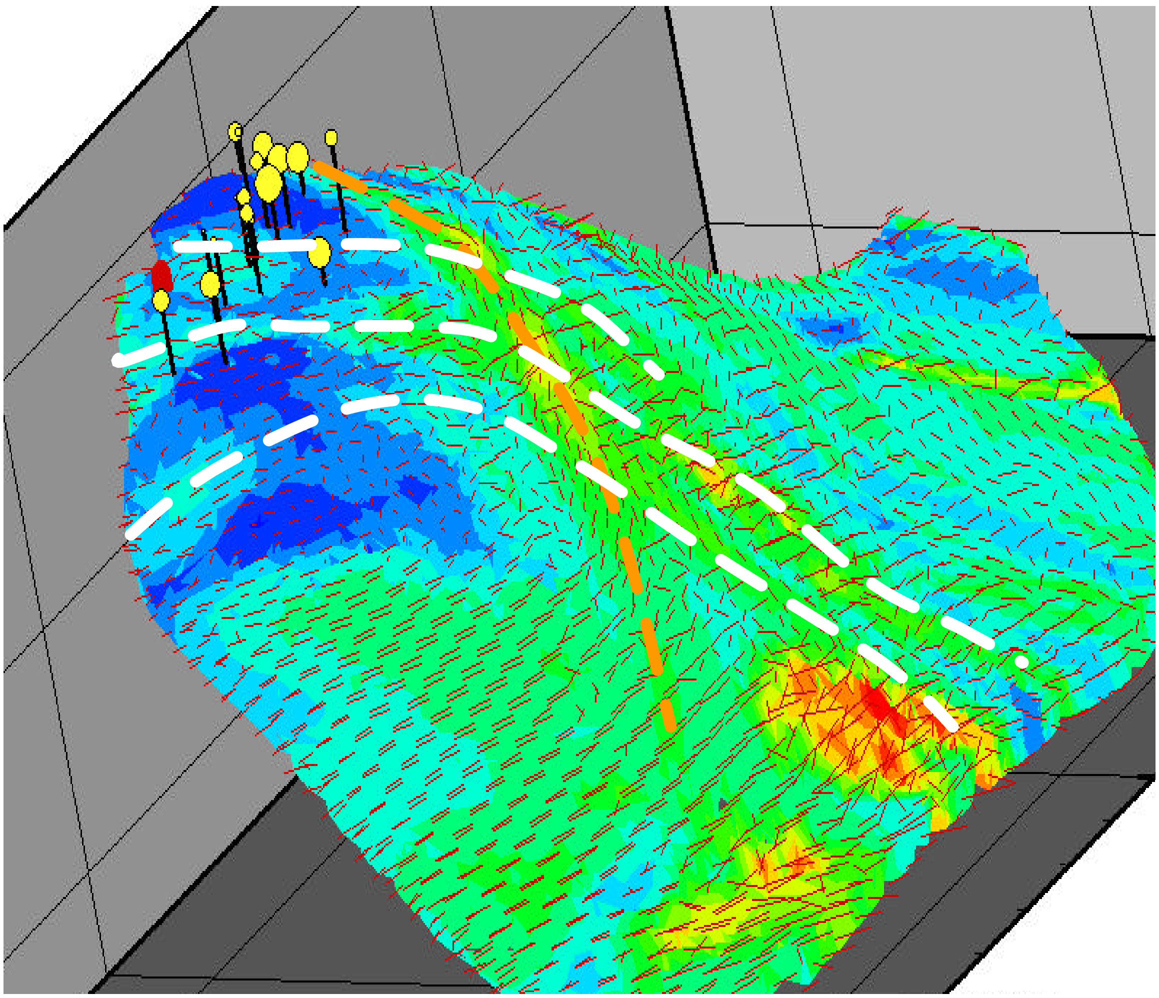

Figure 3-25. Overview of Nitrogen Injection tests results. The Overthrust Block is viewed looking from southeast to northwest. Contours indicate extensional strain magnitude, red lines indicate strike of fractures in response to extensional strain field. Wells where nitrogen breakthrough was indicated are shown; size of yellow circle at well top indicates the time of breakthrough (large circle indicate slow response; small circles indicate rapid response). Nitrogen test took place in upper portion of the structure where the reservoir tends to flatten.

Figure 3-25 shows an overview of the nitrogen injection test results. Most of the wells where nitrogen breakthrough was observed are located on the top, flatter portion of the structure. The inferred flexure zones are also shown. A number of wells that were also monitored, but where no nitrogen breakthrough was observed, occurred downdip from the responding wells.

This can be seen a little more clearly in Figure 3-26, which shows the results of the pressure magnitudes. In this figure, the size of the white circle atop the well is proportional to the pressure magnitude observed. Although there were many wells monitored downdip from the injection well, only those wells within the immediate cyan-colored contours (indicative of higher strains) showed pressure response.

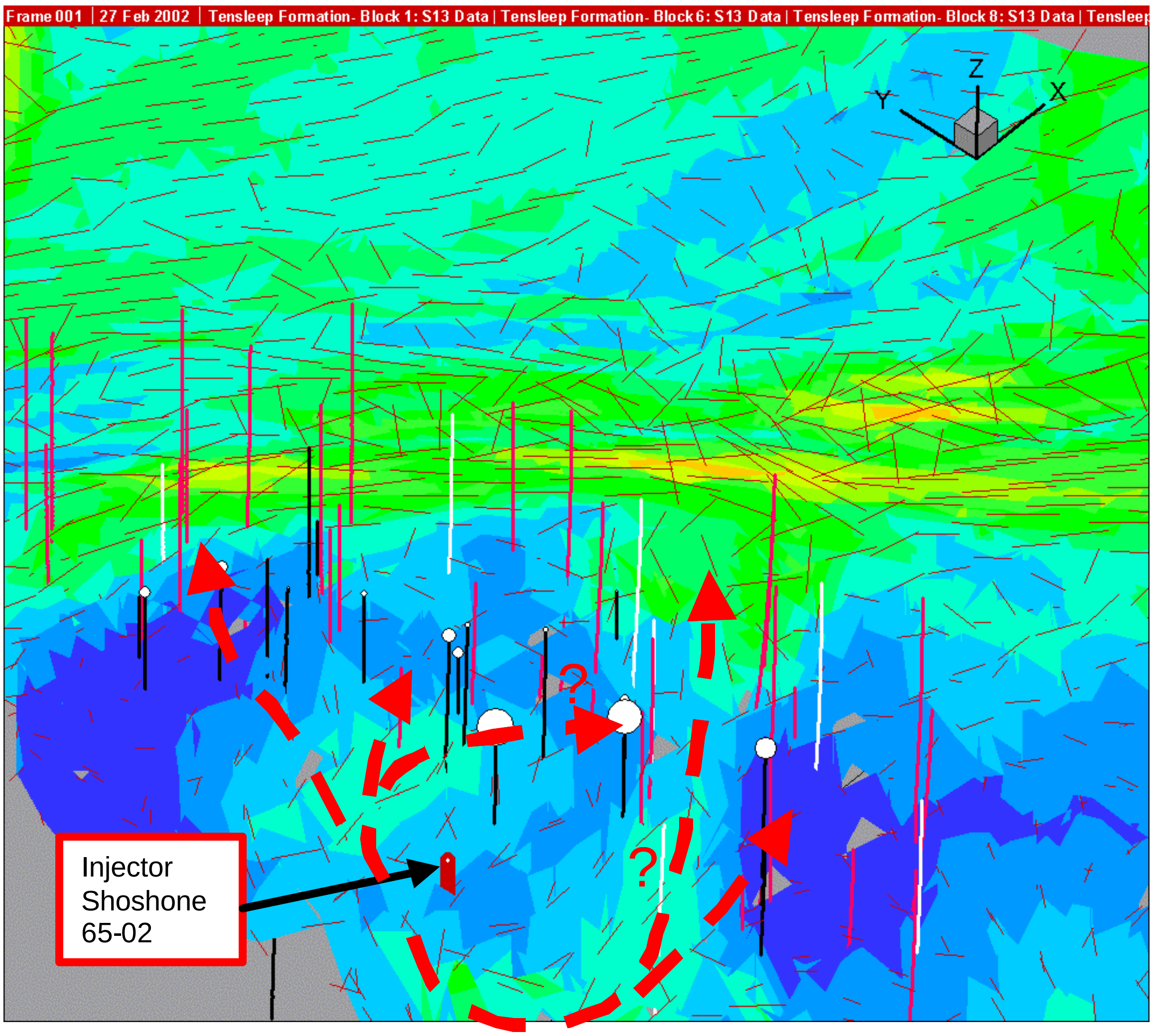

Figure 3-26. Pressure magnitudes and possible migration pathways for the nitrogen injection test. View is looking down on the structure from the southwest to the northeast. Size of circles indicates magnitude of pressure response. The largest responses were seen in two wells on flexure corridors close to the injector. Most of the responding wells are either in the cyan-colored pod above and left (northwest) of the injector, or along the downdip flexure corridor to the right (southeast) of the injector.

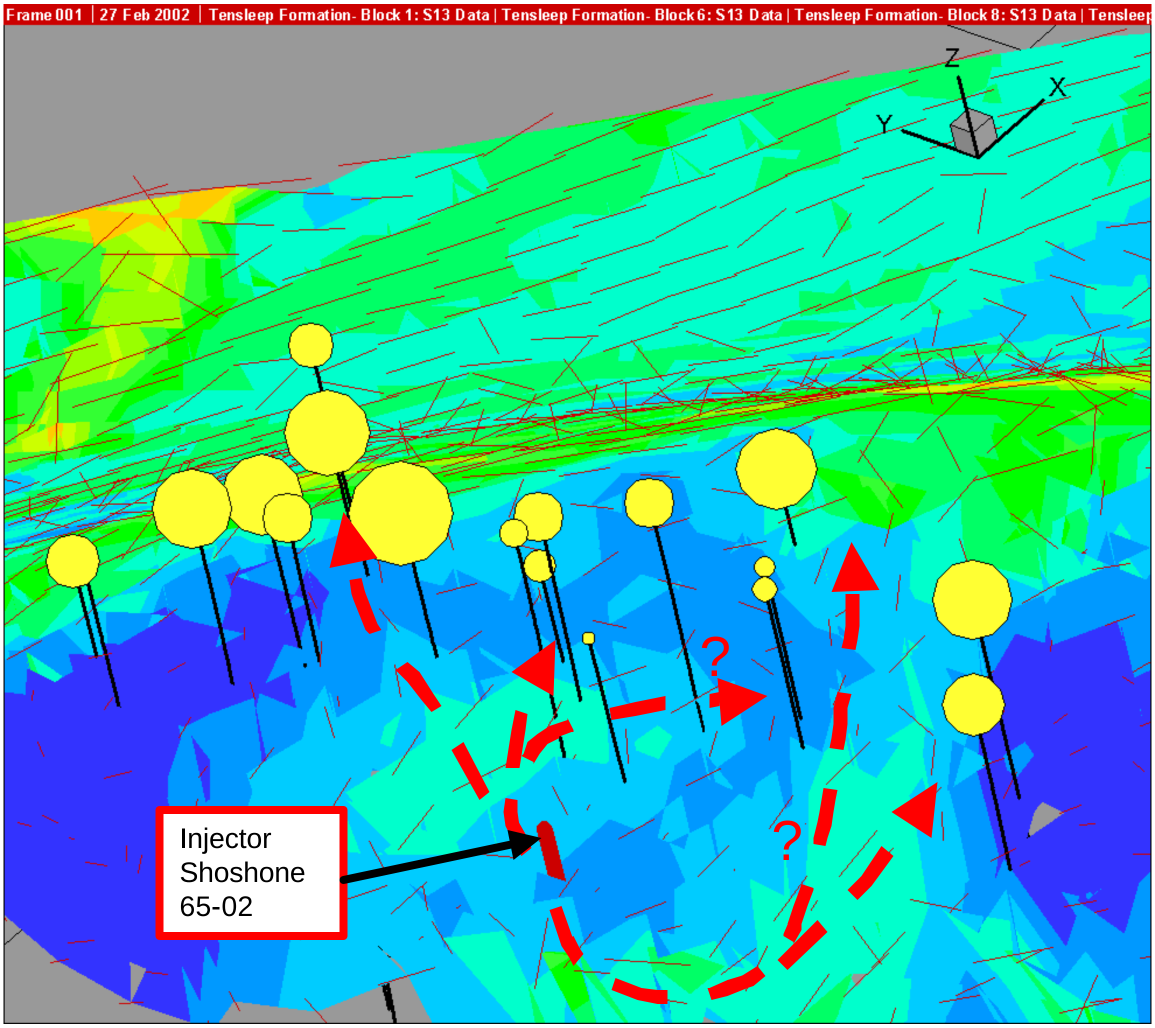

Figure 3-27. Time to breakthrough for only the wells in which a breakthrough response was observed. Radius of circle is proportional to time of breakthrough, so large circle indicate a longer time to breakthrough than smakll circles. Note that the responding wells tend to be in the high strain regions around the injector, and that the time to breakthrough is relatively short for the 5 wells in the center of the digram nearest the injector, and increases along the red-dashed fracture corridors as indicated in the figure.

Figure 3-27 shows a similar migration fairway in terms of time to breakthrough. Wells close in terms of path length along a fracture corridor from the injector tended to experience stronger and more rapid breakthrough. Wells at the distant ends of the corridors experienced slower and smaller magnitude breakthroughs. Monitoring wells separated from the fracture corridors by regions of low strain showed no breakthroughs. Essentially, the responding wells occur in one of two main strain "pods", or regions of higher strain (Figure 3-28). It is not clear why the monitoring wells down dip in the white-dashed flexure zone experienced no nitrogen breakthrough. It is possible that the portion of the zone where fracture intensity is much lower (shown in figure) may have led to a disconnect in the fracture network.

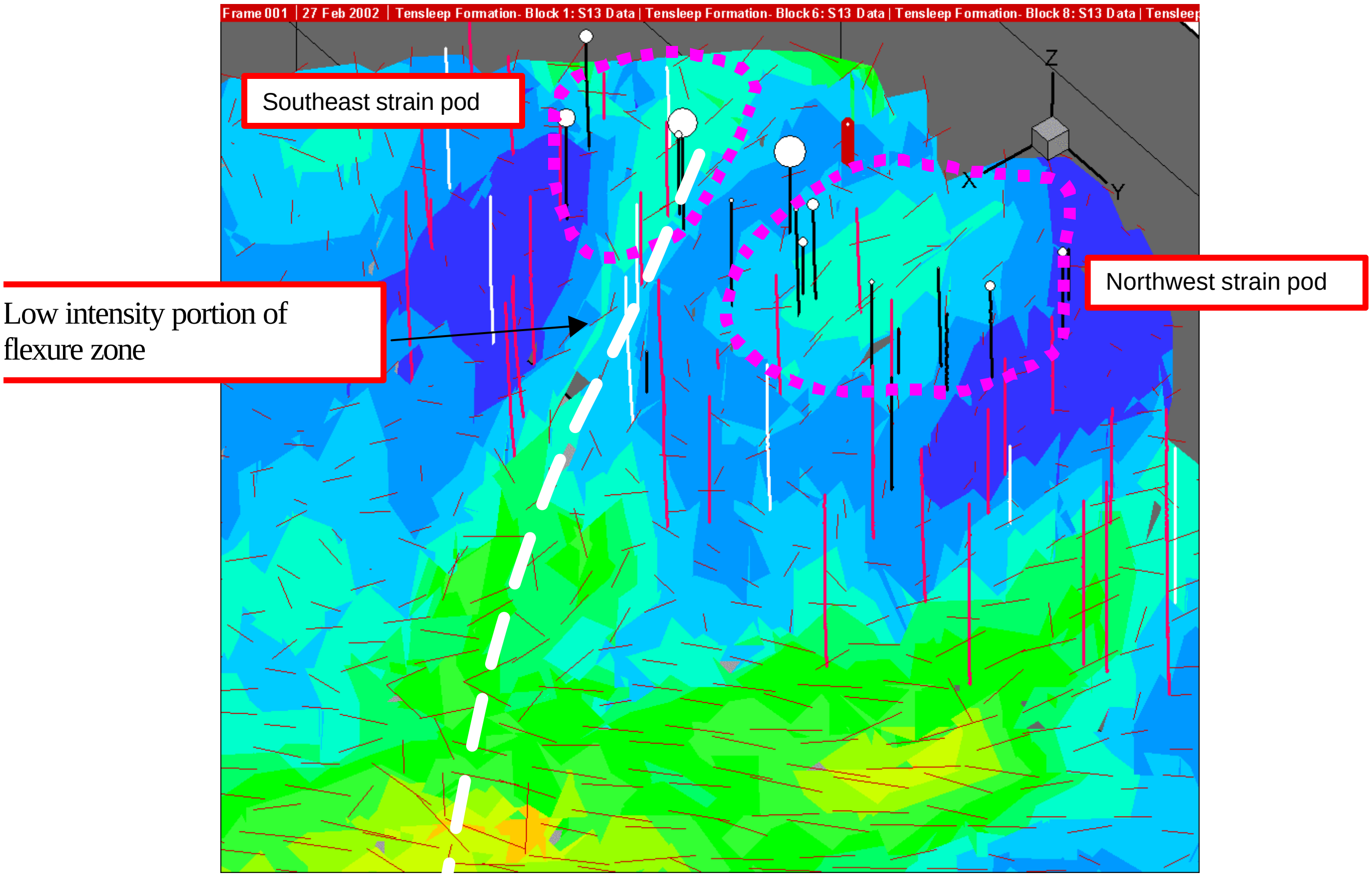

Figure 3-28. Delineation of strain pods. Most of the responding wells are in one of two strain "pods". Non-responding wells are typically not in these pods. They tend to be in low strain zones or in pods separated from the pods connected to the injector pods by areas of low strain. White dashed line indicates a dip-parallel flexure zone.

3.2.5 CONCLUSIONS REGARDING THE TRIBUTARY DRAINAGE/COMPARTMENTALIZATION CHARACTERISTICS OF THE RESERVOIR FROM THE TRACER EXPERIMENTAL RESULTS

The bromide and nitrogen injection tracer test results, combined with the strain patterns developed from the palinspastic reconstruction and comparison to outcrop evidence, suggests that the reservoir may be characterized by linear zones or corridors of high strain/high fracture network permeability. These zones are not randomly located or oriented, but rather occur in sub-horizontal and dip-parallel orientations. The horizontal zones formed during the initial folding of the field, and are features that accommodate the upwarping and downwarping of the field. The dip-parallel zones formed to accommodate the horizontal compression in the northwest and southeast portions of the field, particularly in the northwest, where horizontal shortening is much greater. Some of the this shortening was taken up by the imbricate faulting, but the formation of the doubly plunging fold also occurred along these flexural hinges that show little or no offset. Field evidence confirms the existence of these two types of zones.

While connectivity within these zones leads to enhanced fluid movement within the Tensleep or Phosphoria Formations, the bromide tracer test results indicate poor connection between the Phosphoria and Tensleep, at least for tracer injected into the Phosphoria and monitored in the Tensleep. The reason for this may be that the large extensional joints that form in the upper dune sequence of the Tensleep may terminate at the top of the sequence boundary, as they do in outcrops elsewhere in the Wind River and Bighorn Basins.

These results suggest that there is no “characteristic” tributary drainage radius from a well. Rather, the drainage area is a function of whether the well is situated in a strain corridor or not, and if it is in a corridor, how extensive and well connected the corridor is. Moreover, corridors should be much more extensive in the northwestern portion of the field where the greater horizontal shortening required more faulting and tighter folding.

These results also indicate that fracture network permeability is a second order effect compared to facture network connectivity patterns, and that a stochastic continuum representation of permeability in this reservoir using techniques such as Kriging would produce very different reservoir models than the one generated from the palinspastic reconstruction. Such structured corridors of high permeability are nearly impossible to characterize or simulate using stochastic field representations like Kriging that are commonly applied to matrix properties.

3.3 Calculation of Effective Properties

An important step in completing the reservoir model is to compute effective reservoir properties that reflect the porosity and permeability of the fracture system, and way in which fluids may transfer between the matrix and the fracture system.

The calculation of the effective properties is done for each grid cell based upon the fractures found in that grid cell in the model and the properties of the fractures. No upscaling of properties takes place, as is often done for matrix permeability values that have been established at a scale finer than the gridding.

The total number of data sets associated with the calculation of effective properties is large: 6 properties for each of 9 structural blocks for each of 2 formations, or 108 distinct files that were loaded into the final 3D integrated reservoir model. Figure 3-29 shows an example for Block 6, Phosphoria Formation.

The grid architecture has both a layer-parallel and a layer-orthogonal thickness. The six separate variables plotted in this Figure correspond to the six effective fracture parameters incorporated into the final model for all blocks and formations. The actual displays shown below are not from the final model; rather, they are displays of the parameters calculated within the discrete fracture network modeling code.

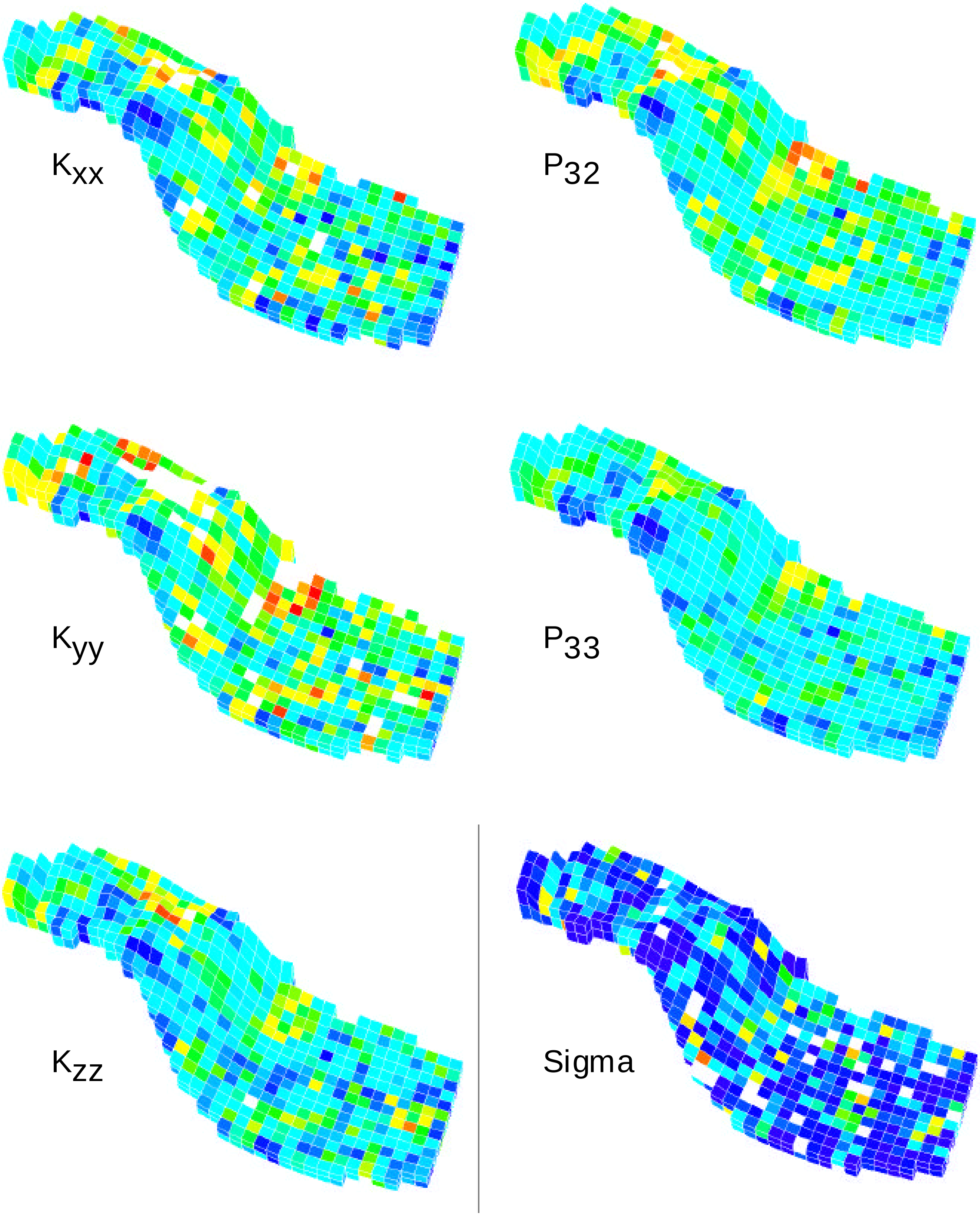

Figure 3-29. Example of effective fracture properties calculated for the Phosphoria Formation, Block 6. K_{xx}, K_{yy} and K_{zz} are directional fracture permeabilities; P_{32} is a measure of fracture intensity; P_{33} is the ratio of fracture pore volume to reservoir volume; and Sigma is the sigma factor.

3.4 3D Integrated Reservoir Model

This section shows aspects of the 3D integrated reservoir model using the GoCad® software.

Figure 3-30 shows the distribution of matrix porosity for both the Tensleep and Phosphoria Formations in the Overthrust Block. Wells in which the matrix porosity was calculated from the wireline logging suite are also shown, including wells that are outside of the immediate overthrust block itself. Matrix properties for structural blocks with well control are incorporated into the model. The fence display shown in the Figure is intended to help visualize the three-dimensional distribution of the matrix properties.

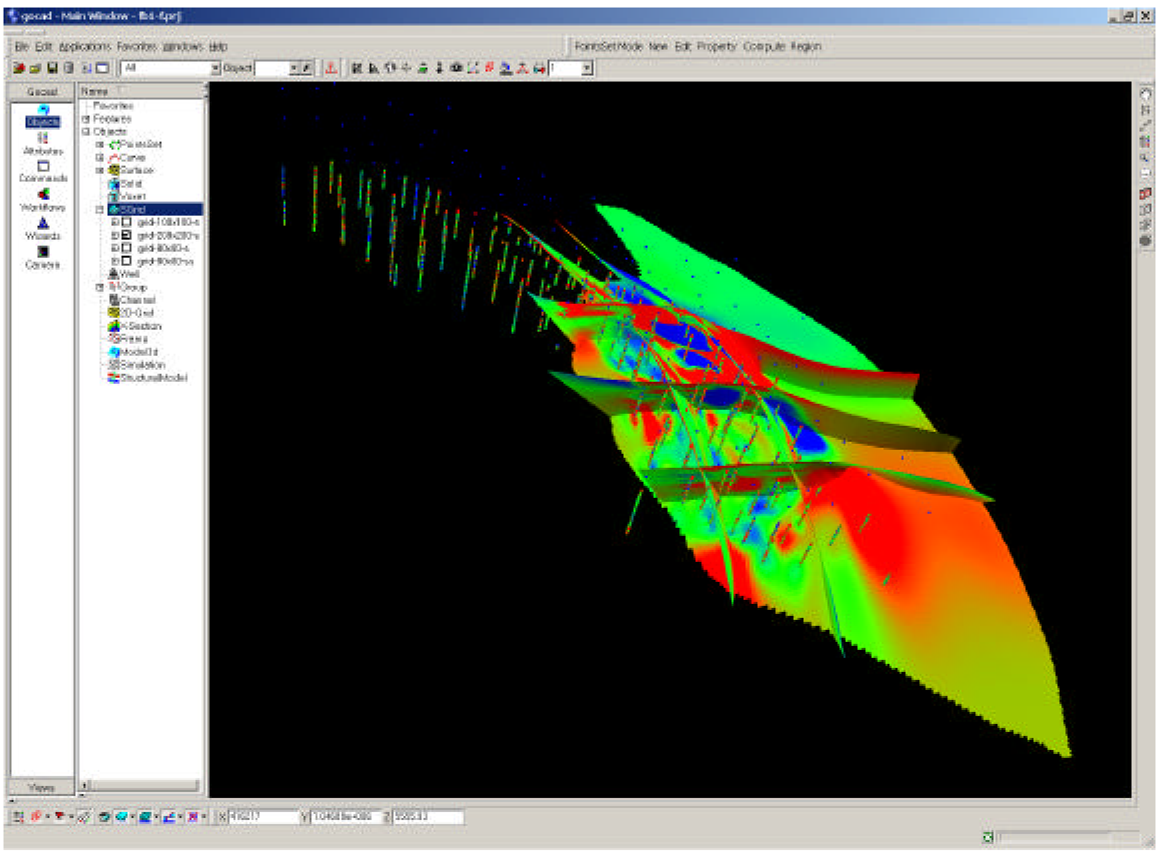

Figure 3-30. Matrix porosity distributed from well data in the Overthrust Block. The colors represent the value of the porosity. The wells used to create the model are also shown, and the colors in these wells indicate the value of matrix porosity calculated from the wireline log suite. The subvertical surfaces shown are not faults, but rather fence displays of the matrix porosity to help visualize the three-dimensional distribution of the data.

Figure 3-31 through Figure 3-35 show displays of the effective fracture properties. These include the directional fracture permeability values, fracture intensity, fracture porosity,

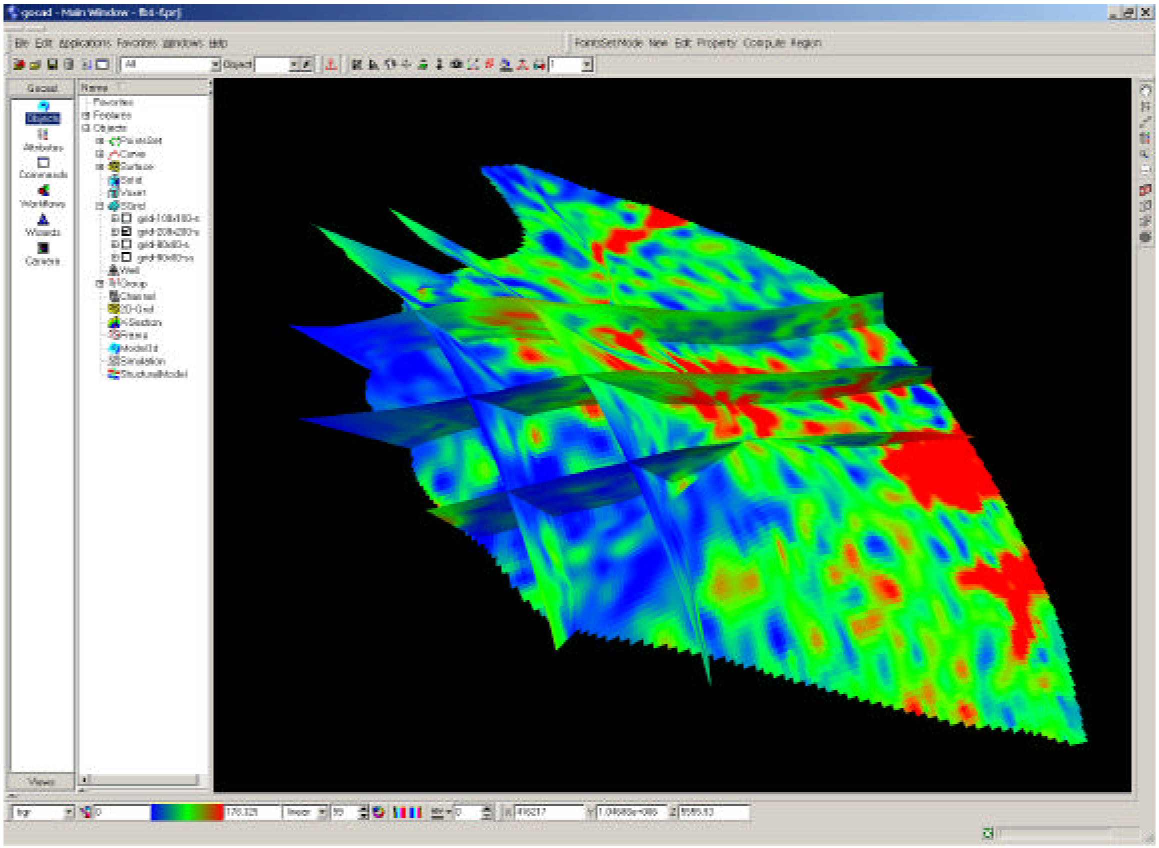

Figure 3-31. Distribution of fracture porosity in the Overthrust Block.

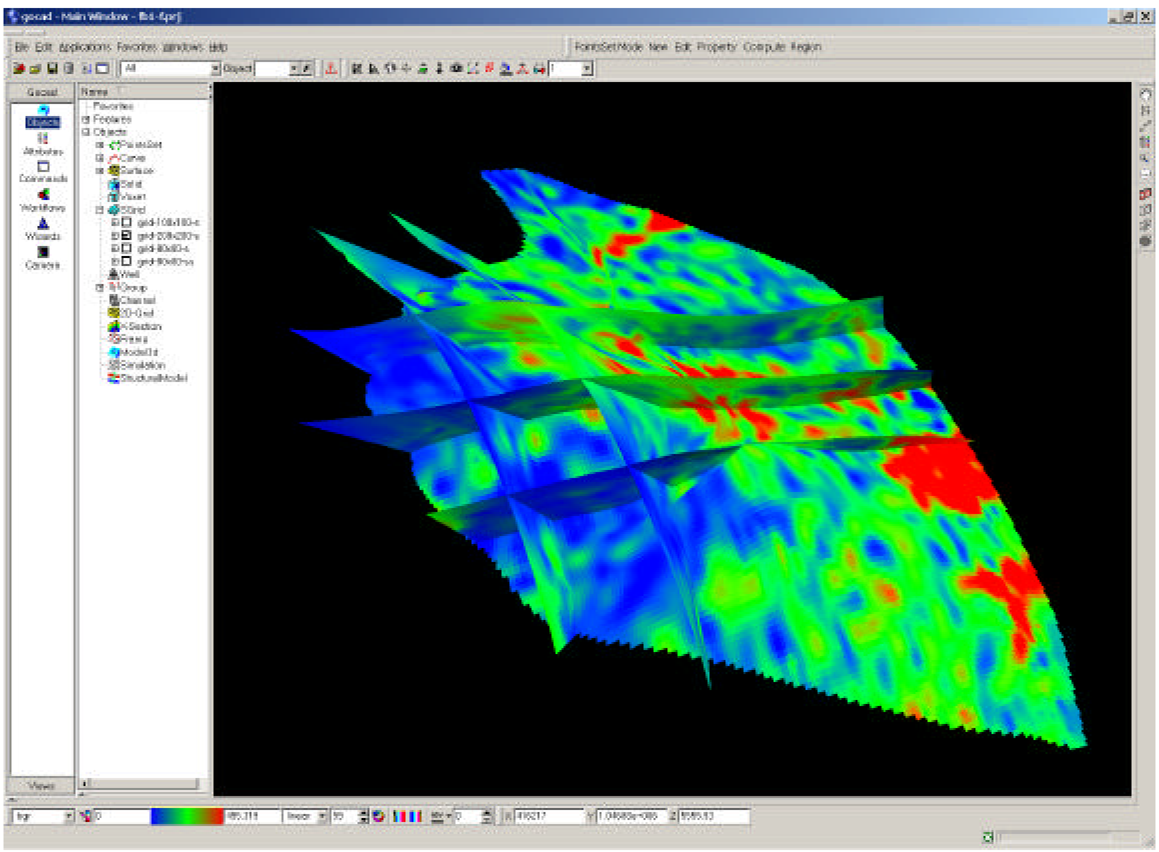

Figure 3-32. Distribution of fracture intensity in the Overthrust Block.

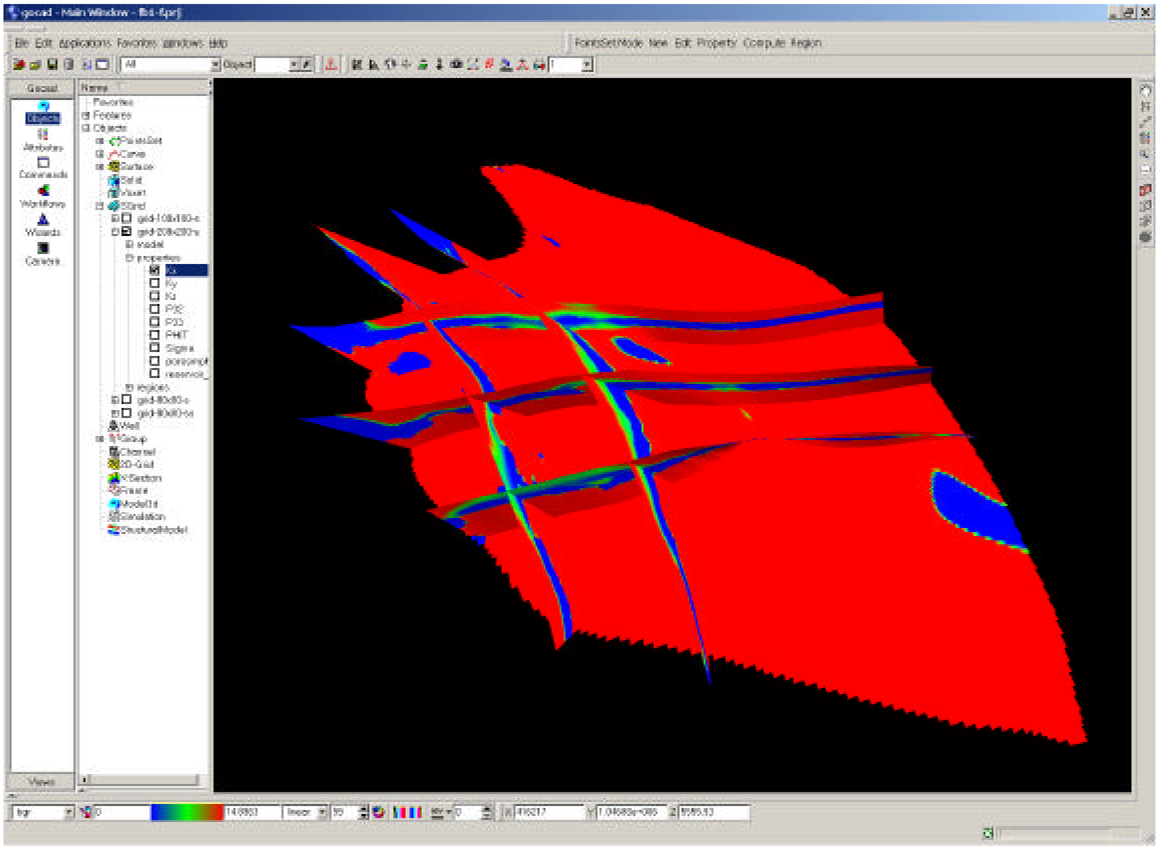

Figure 3-33. Distribution of effective fracture K_{xx} values in the Overthrust Block

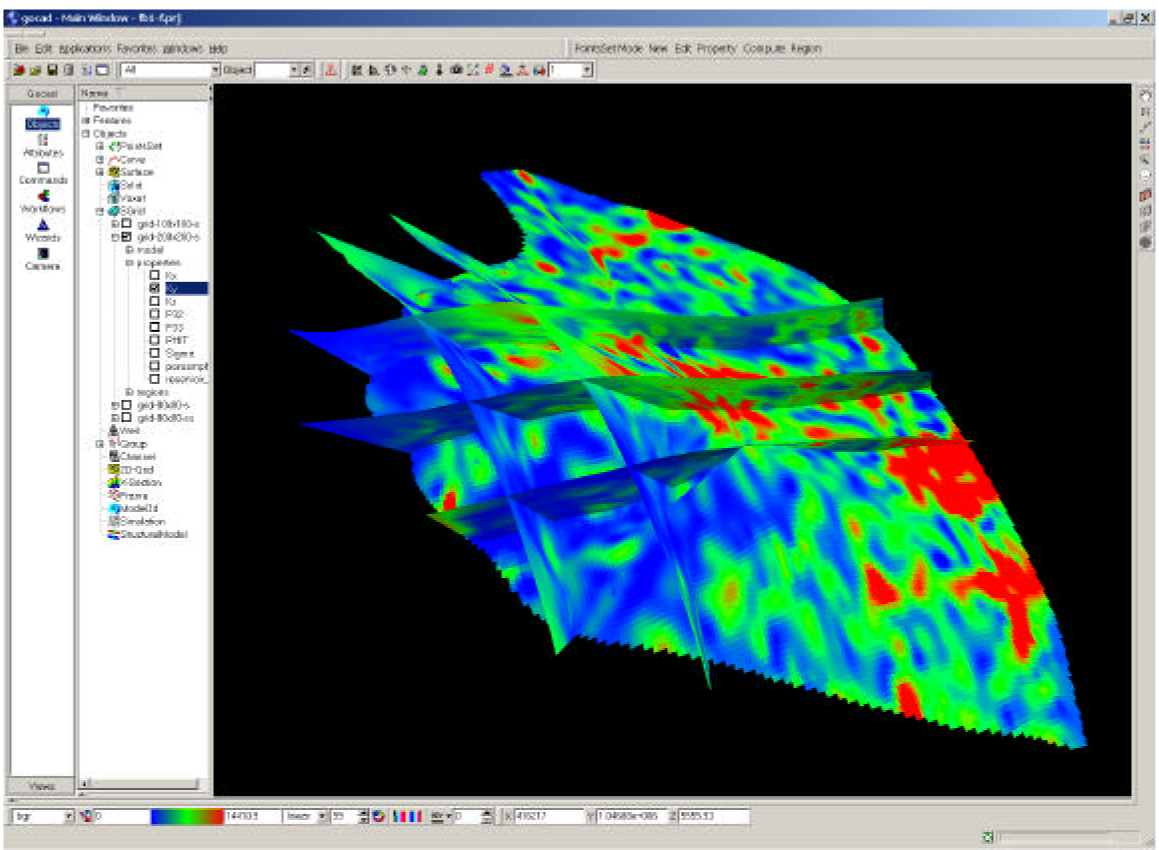

Figure 3-34. Distribution of effective fracture K_{yy} values in the Overthrust Block

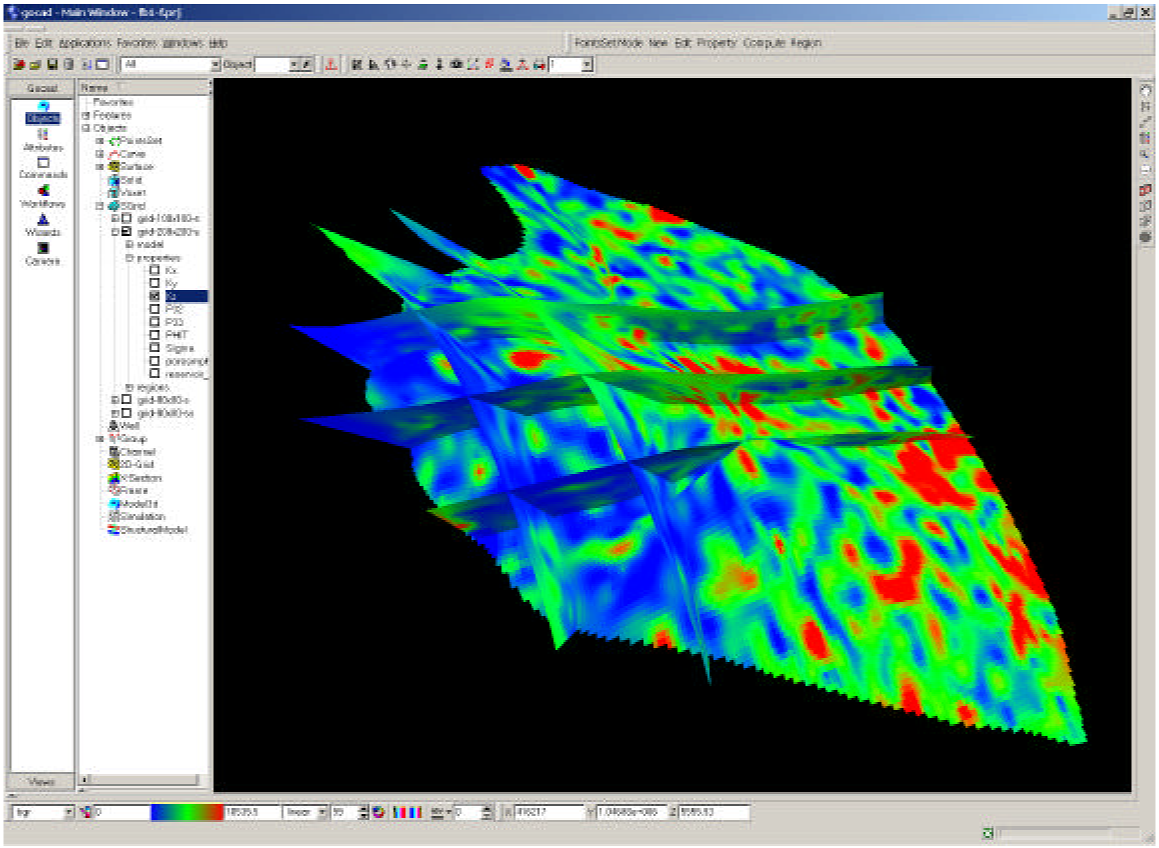

Figure 3-35. Distribution of effective fracture K_{zz} values in the Overthrust Block

and sigma factor for the Overthrust Block (structural Block 1).

3.5 Evaluation of Reservoir Management Strategies

Marathon Oil has been actively studying the economics of gas injection to improve the ultimate recovery of oil at Circle Ridge Field. The information contained within the final GOCAD model is all directly applicable to quantifying the economics of such a project. Marathon plans to high-grade their predictions concerning gas injection using the GOCAD model information, in conjunction with reservoir simulators and desktop calculations.

Due to the highly fractured nature of the Phosphoria and Tensleep in Circle Ridge, water flooding for secondary recovery operations has proved only marginally effective. In fact, Tensleep and Phosphoria water flooding has been suspended in the overthrust block, the major remaining reserve target for the field. In dual porosity fields like Circle Ridge, the drainage rates of oil from the matrix can be improved by filling the fractures with gas and driving the fracture gas-liquid contact down structure. This gas-oil gravity drainage mobilization process is described by the following Richardson and Blackwell (1971) equation:

$$\frac{(\Delta Z)_{So}}{\Delta t} = \frac{4.4X10^{-5} K_v \Delta r}{u_o q} \frac{dK_{ro}}{dS_o} \qquad \text{Equation 3-1}$$

where: K_{ro} = relative permeability to oil

K_v = matrix vertical permeability, in millidarcies

S_o = oil saturation, fraction of pore volume

Δ t = change in time in days

$\Delta\ r$ = difference in density between draining liquid and injected gas, in lb_m/ft^3

u_o = oil viscosity, in centipoises

q = porosity, fraction of bulk rock volume

$(\Delta Z)_{So}$ = vertical distance oil saturation moves in ft

As indicated by this equation, in order to predict the process, both matrix permeability and porosity, as well as current oil saturations, must be known. The petrophysical analysis of Circle Ridge logs performed under this project has allowed Marathon to update these critical components.

Equally as important as understanding these matrix properties, is an understanding of the fracturing in the field. The understanding of fracture porosity, in conjunction with the oil drainage rates and reservoir pressures, allows for the projection of gas requirements for gas-oil gravity drainage projects. This gas injection forecast is critical to the design and economics of the project. Additionally, Marathon's experience with gas injection projects has indicated the importance of fracture understanding in maximizing oil capture efficiency and in limiting the production of gas. Gas production is very undesirable, as it must be recompressed for reinjection or replaced by increased extraneous gas injection. Both of these cases result in higher costs for the project and a lowering of economic viability. The optimum placement of completions within highly productive fractures helps maximize the production of oil per completion, while limiting the potential for gas coning and production. An improved picture of fracture intensity and compartmentalization also aid in the placement of gas injectors. Ideal placement of injectors can help limit the number of injectors required and ensure that unnecessarily high completion pressure drops are not encountered.

In addition to studying the viability of gas injection at Circle Ridge, Marathon is also using information from this DOE project to evaluate the potential for dewatering the fracture system through increased withdrawals. This dewatering can create dual porosity gas-oil gravity drainage even with little or no extraneous gas injection. In conjunction with this dewatering, Marathon plans to investigate the use of horizontal drain holes to aid in the efficient capture of oil. Two Tensleep horizontal drain holes have been proposed for funding in 2003. Information from this project will aid the placement of the horizontal drain holes at or directly below the oil-water contact in the fracture system.

The orientation of the boreholes will be guided by the desire to intersect fractures and to produce areas of undrained oil-filled fractures (Figure 3-36). The red wellbore would be parallel to the dominant fracture orientation, and also be drilled into a region where lower than average fracture intensity is predicted. Alternatively, the yellow wellbore is oriented nearly perpendicular to the main fracture orientation, and into an area where the model predicts higher fracture intensity.

The improved structural visualization available from the GOCAD model is also expected to aid future recompletion attempts by Marathon oil. This visualization will also help quantify the potential for expanding any improved oil recovery process into the smaller fault blocks.

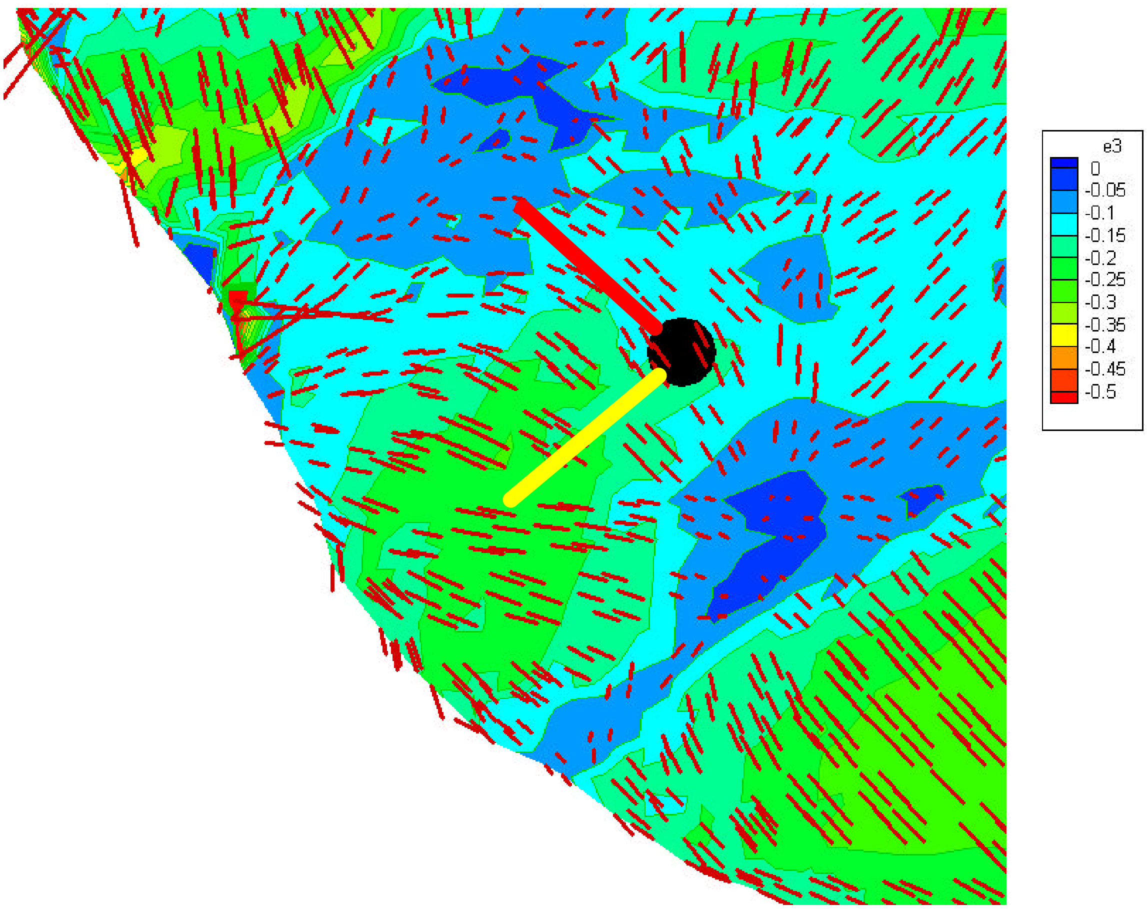

Figure 3-36. Example of fracture model for use in drainhole planning.

3.6 Technology Transfer

Technology transfer was accomplished in several different ways during the fourth semi-annual project period. These included meetings and presentations with the members of the tribal oil & gas commission and Marathon Oil, publications and additions and maintenance of the project web site.

3.6.1 MEETINGS AND WORKSHOPS

Two half-day meetings were held with members of the Tribal Oil & Gas Commission during this reporting period. Both meetings took place at Marathon Oil's offices in Cody, WY. The first meeting was held on January 24, 2002, while the second was held on July 11, 2002.

At each meeting, the progress that had been made and its overall importance to the project was reviewed with members of the Oil & Gas Commission, and problems or issues that had arisen were discussed.

At the July, 2002 meeting, it was agreed by the tribal commissioners, Marathon Oil and Golder that the final tribal workshop would be held in early September, 2002, at Marathon Oil's offices in Cody, Wyoming. The Tribe plans to videotape the presentations in order to be able to distribute project results and details more widely among the Northern Arapaho and Eastern Shoshone tribal members and organizations.

3.6.2 PUBLICATIONS/CONFERENCE PRESENTATIONS

During the fourth six-month period, an article on the Circle Ridge was published and a presentation at a professional society meeting was submitted and accepted. The article published is:

La Pointe, P. R., J. Hermanson, M. Dunleavy and R. Parney (2002). New tools for modeling and visualizing fractured reservoirs enhance engineering & reservoir development. Oil & Gas Journal, May, 2002.

The conference proceeding submitted and accepted is:

La Pointe, P. R. and J. Hermanson (2002). The Prediction of the Orientation and Intensity of Fractures in the Circle Ridge Field, Wind River Basin, WY, through the Geomechanical Reconstruction of the Palinspastic Strain Field. 2002 Oil Rock (SPE/ISRM Rock Mechanics Conference), 20-23 Oct., 2002, Irving, TX.

Additional manuscripts on various aspects of the project are underway, but have not been submitted.

3.6.3 PROJECT WEB SITE

3.6.3.1 Web Site Development

Website development consisted of adding new data in virtually all of the subcategories for the website, and also making substantial improvements to the *WorkFlow* portion of the website. Some of the new data added to the site are the results of the image log and high resolution spinner log for Shoshone 65- 37 and the tracer test data for the bromide tracer experiment, along with the 3rd semi-annual report and the Powerpoint presentations made at the tribal meetings in Cody described in Section 3.6.1..

In addition to adding data and reports, the project workflow module was considerably improved. Figure 3-37 shows the new interface for this module. The visitor is able to move the mouse over various portions of the diagram shown in the figure and to activate explanatory pages for most of the objects shown, as well as to go to the data or results that are related. For example, when “Field Reconnaissance” was selected (arrow in the

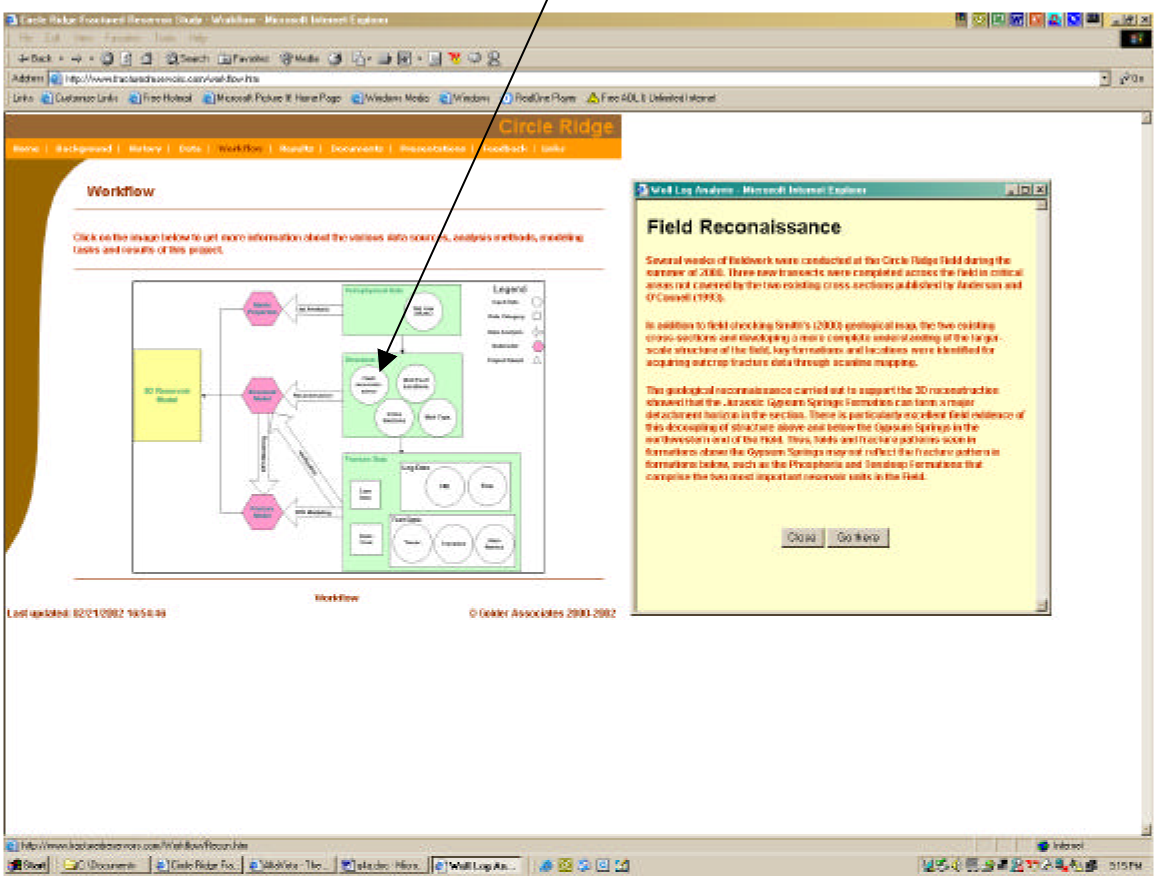

Figure 3-37. Screen grab showing new interface for *WorkFlow* module.

figure), a new frame appears that explains what this data was and how it fits into the overall workflow. If the visitor wishes to learn more, then clicking the “Go There” button takes the visitor to the section of the website containing photographs of the field reconnaissance. This feature helps the visitor to more readily understand why certain data has been collected, how it is analyzed or used, and how it fits into the overall project.

3.6.3.2 Web Site Statistics

From November 1, 2001 to July 31, 2001, there have been 688 visits to the project website. This translates into between two and three external visits a day. Figure 3-38 provides an overview of website activity, spanning the period August 17, 2000 through July 31, 2002 in order to provide context for the 4th semi-annual project period. This figure shows that the level of website activity has remained nearly constant since late November 2000, the time when the first project report was released.

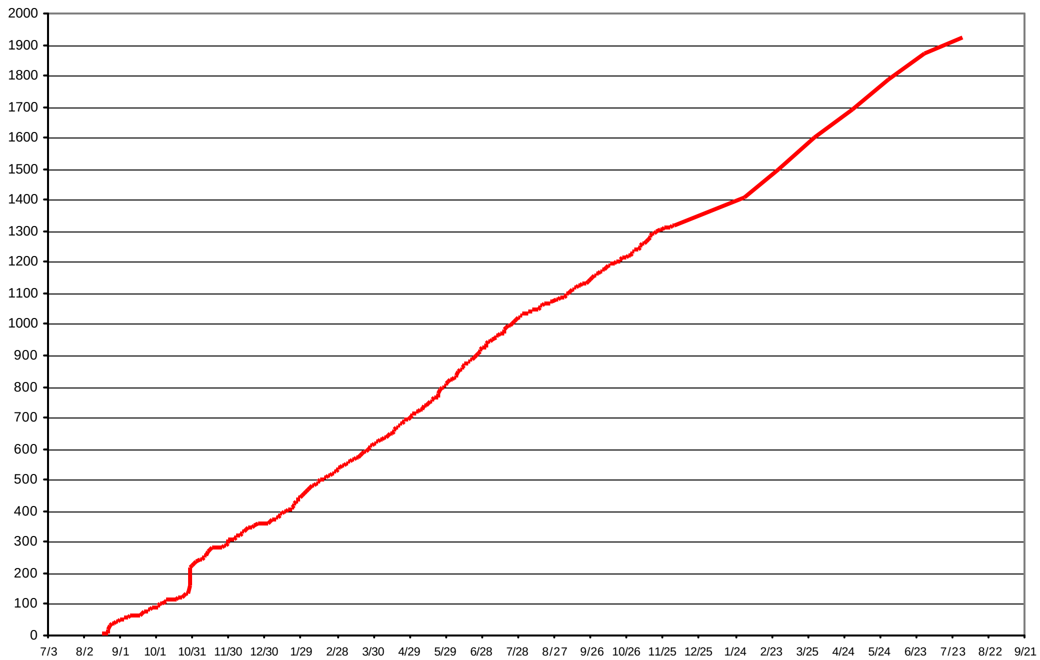

Figure 3-38. Web site activity, August 17, 2000 through July 31, 2002.

4 CONCLUSIONS

4.1 Overview

This section summarizes the most important results obtained in the project during the six-month reporting period, and discusses what implications they have for recovering additional oil from the Circle Ridge Field.

4.2 Validation of DFN Model

The fractures inferred from the strain pattern were compared to image log data for the third well, and also fracturing in outcrop near two of the well was compared to the orientations of fracture seen in the image logs.

The dominant fracture orientations seen in outcrop were approximately the same as the dominant orientations inferred from the image log data, supporting the use of outcrop data taken in the Crow Mountain and Red Peak Members for comparison to calculated strain data.

The orientation of the fractures in the third well followed the same relation to the strains seen in the outcrop data and the previous two wells; the dominant extension fracture (joint) set is typically orthogonal to the direction of maximum extensional strain calculated from the initial folding of the field. This further strengthens the conclusion reached in previous reports that most of the reservoir-scale fractures formed during the initial folding event, and that the strain calculated for this event can be used to infer fracture directions and intensity.

4.3 Investigation of Reservoir Connectivity, Compartmentalization & Tributary Drainage

The bromide tracer experiment showed several important features of the fracture network and its connectivity structure as it relates to reservoir compartmentalization and tributary drainage.

Tracer was injected into the Phosphoria, but the three monitoring wells that did not have Phosphoria completions did not show evidence of tracer breakthrough. This suggests that there may be poor connectivity between the Phosphoria and Tensleep Formations. This lack of connectivity was further investigated by examining outcrops of Tensleep elsewhere. These showed that the major joints in the top of the Tensleep typically terminated against the interface between the upper dune sequence and the interdune sequence below.

Of the remaining monitoring wells that had Phosphoria completions, only three showed evidence of breakthrough. These wells were well connected to the injection well by means of fracture corridors developed in the high strain regions of the reservoir blocks. Well that showed little evidence of breakthrough were either not in these higher strain corridors, or were isolated from the main corridors by "divides" of lower fracture intensity or unfavorable fracture orientations.

Moreover, the fracture corridors typically occurred along horizontal or dip-parallel flexure zones. These flexure zones formed during folding as the rock broke as panels, rather than as a continuous fold. Field reconnaissance of the overlying formations revealed evidence of both horizontal and dip-parallel flexure zones separating panels of rock.

Thus, the flexure zones are important geological features that control the fracture network connectivity and hence the compartmentalization and tributary drainage throughout the reservoir.

4.4 Determination of Properties for DFN Model

All properties for the DFN model were determined by the end of the 4th semi-annual period, making it possible to construct the DFN models for all nine major structural blocks and both the Phosphoria and Tensleep Formations.

4.5 Determination of Effective Fracture Reservoir Parameter Values

Once the DFN models for all of the blocks and formations were completed, the effective fracture-related parameter values were calculated. These properties included:

- Directional fracture permeability
- Fracture porosity
- Fracture intensity
- Sigma Factor

These properties were calculated for a grid that was created for each block and formation. The grid dimensions averaged 50 m by 50 m in horizontal extent, and 25 m in vertical extent. Where the formations thinned or thickened markedly, the vertical thickness of the grids changed accordingly.

4.6 Construction of Integrated Matrix/Fault-Block/Fracture Model

Effective fracture properties calculated on the grids, the major faults, the matrix properties and the wells were combined into a single numerical model using GoCad software.

4.7 Development of Reservoir Management Strategies

Marathon Oil has begun to use the project data for developing strategies to recover more oil from the Circle Ridge Field. Several strategies are being implemented. These include:

- Use of greatly enhanced knowledge of matrix properties to improve gas injection performance
- Identification of highly fractured areas will help to locate wells that have the desirable properties of maximizing oil production while reducing undesirable gas coning and injection
- Identification of fracture fairways and dominant fracture orientations is currently being used to design laterals from existing vertical wells. Budget requests have been made by Marathon engineers for two laterals in 2003 whose location and orientation takes into account the fracture intensity and orientations predicted in this project.

4.8 Technology Transfer

Technology transfer has been successfully accomplished in a variety of ways, including articles in major trade and professional society journals and proceedings; meetings with tribal members; reports and an updated and improved website.

5 REFERENCES

Dershowitz, W. S. and H. H. Herda (1992). Interpretation of fracture spacing and intensity. *In Rock Mechanics, Proceedings of the 33rd U.S. Symposium*, Santa Fe New Mexico, 3-5 June, 1992, A. A. Balkema/Rotterdam, 757 – 766.

Dershowitz, W., P. La Pointe, T. Eiben and L. Wei (2000). Integration of Discrete Feature Network Methods With Conventional Simulator Approaches. SPE Reservoir Evaluation & Engineering Journal, April, 2000

Horne, R. N., 2000. Modern Well Test Analysis (4th Printing). Petroway, Inc., Palo Alto, CA. 257p.

La Pointe, P. R. and J. A. Hudson (1985). Characterization and Interpretation of Rock Mass Joint Patterns. Geological Society of America, Special Paper 199, 37p.

La Pointe, P. R., P. C. Wallmann and W. S. Dershowitz, 1993. Stochastic estimation of fracture size through simulated sampling. International Journal of Rock Mechanics, Mining Sciences & Geomechanics Abstracts, vol. 30, no. 7, 1611-1617.

La Pointe, P. R., J. Hermanson and T. Eiben (2000). 3-D reservoir and stochastic fracture network modeling for enhanced oil recovery, Circle Ridge Phosphoria/Tensleep reservoir, Wind River Reservation, Arapaho and Shoshone tribes, Wyoming. Semi-Annual Technical Report – May 1, 2000 through October 31, 2000. DOE Award Number: DE-FG26-00BC15190

La Pointe, P. R., and J. Hermanson (2001). 3-D reservoir and stochastic fracture network modeling for enhanced oil recovery, Circle Ridge Phosphoria/Tensleep reservoir, Wind River Reservation, Arapaho and Shoshone tribes, Wyoming. Semi-Annual Technical Report – November 1, 2000 through April 31, 2001. DOE Award Number: DE-FG26-00BC15190

La Pointe, P. R., R. Parney, T. Eiben, M. Dunleavy, J. Whitney and D. Eubanks (2001). 3-D reservoir and stochastic fracture network modeling for enhanced oil recovery, Circle Ridge Phosphoria/Tensleep reservoir, Wind River Reservation, Arapaho and Shoshone tribes, Wyoming. Semi-Annual Technical Report – May 1, 2001 through November 30, 2001. DOE Award Number: DE-FG26-00BC15190

Richardson, J.G. and R. J. Blackwell, (1971). Use of simple mathematical models for predicting reservoir behavior, Journal Petrol. Tech. (JPT), Vol 251, 1145-1151.

Smith, V. (2000). Surface Geologic Map of the Circle Ridge Oil Field, Wyoming. B. S. Thesis, Baylor University, Waco, TX.